

Evaluation of nitrogen dynamics in high-order streams and rivers based on high-frequency monitoring

Kumulative Dissertation

zur Erlangung des akademischen Grades

"doctor rerum naturalium"

(Dr. rer. nat.)

in der Wissenschaftsdisziplin "Geoökologie"

eingereicht an der

Mathematisch-Naturwissenschaftlichen Fakultät

Institut für Umweltwissenschaften und Geographie

der Universität Potsdam

von

Xiaolin Zhang

Hauptbetreuer: Prof. Dr. Michael Rode, Universität Potsdam/Helmholtz-Zentrum für
Umweltforschung – UFZ, Deutschland

Betreuer: Prof. Dr. Andreas Lorke, Rheinland-Pfälzische Technische Universität
Kaiserslautern-Landau, Deutschland

Gutachter: Prof. Dr. Magdalena Bieroza, Swedish University of Agricultural Sciences,
Department of Soil and Environment, Uppsala, Sweden

Potsdam, den 04.09.2023

This work is protected by copyright and/or related rights. You are free to use this work in any way that is permitted by the copyright and related rights legislation that applies to your use. For other uses you need to obtain permission from the rights-holder(s).
<https://rightsstatements.org/page/InC/1.0/?language=en>

Published online on the
Publication Server of the University of Potsdam:
<https://doi.org/10.25932/publishup-60764>
<https://nbn-resolving.org/urn:nbn:de:kobv:517-opus4-607642>

Preface

This dissertation is prepared and submitted in accordance with the guidelines for the degree of Doctor rerum naturalium (Dr. rer. nat.) in Faculty of Science (Discipline Geoecology) at the University of Potsdam, Germany. This study was under the supervision of apl. Prof. Dr. Michael Rode (Helmholtz Centre for Environmental Research – UFZ) and Prof. Dr. Andreas Lorke (University of Kaiserslautern-Landau). The study was carried out at UFZ.

The study was mainly funded by the Chinese Scholarship Council (CSC) for a period of four years (No. 201804910588) and partially supported by the Department of Aquatic Ecosystem Analysis and Management (ASAM), UFZ.

The dissertation is presented as a cumulation of three peer-reviewed publications, including a general Introduction, a general Discussion and Summary as Chapter 1, Chapter 5 and Chapter 6, respectively. Chapters 2 – 4 present the three peer-reviewed manuscripts and are slightly modified from the original publication as detailed below:

- Chapter 2 **Zhang, X.**, Yang, X., Jomaa, S., Rode, M. (2020). Analyzing impacts of seasonality and landscape gradient on event-scale nitrate-discharge dynamics based on nested high-frequency monitoring. *Journal of Hydrology*, 591, 125585.
<https://doi.org/10.1016/j.jhydrol.2020.125585>
- Chapter 3 **Zhang, X.**, Yang, X., Hensley, R., Lorke, A., Rode, M. (2022). Disentangling in-stream nitrate uptake pathways based on two-station high-frequency monitoring in high-order streams. *Water Resources Research*, 2022, 59(3), e2022WR032329.
<https://doi.org/10.1029/2022WR032329>
- Chapter 4 Yang, X., **Zhang, X.**, Graeber, D., Hensley, R., Jarvie, H., Lorke, A., Borchardt, D., Li, Q., Rode, M. (2023). Large-stream nitrate retention patterns shift during droughts: Seasonal to sub-daily insights from high-frequency data-model fusion. *Water Research*, 243, 120347. <https://doi.org/10.1016/j.watres.2023.120347>

Declaration

I, *Xiaolin Zhang*, hereby declare that this dissertation entitled “Evaluation of nitrogen dynamics in high-order streams and rivers based on high-frequency monitoring” represents my own work. This dissertation has not been submitted to any other institution of higher education and has been prepared independently and exclusively with the specified resources.

Xiaolin Zhang

Magdeburg, January 11st 2023

Acknowledgement

The time is passing by quickly. After 4 years, it's almost the end of my doctoral period. Here I would like to thank all people who support me scientifically or spiritually during this period.

The most sincere thanks belong to my supervisor, Prof. Dr. Michael Rode, who offered me the opportunity to study in Germany. His professional knowledge and patience for dealing with my problems move me forward in completing my doctoral work. I learn a lot from his rigorous scientific practice. He also encourages me when I am not confident about my work. He is my supervisor not only in science but also in life.

Special thanks to my second supervisor, Prof. Dr. Andreas Lorke. He is very kind to offer helpful comments and raise new ideas about my work every time we discussed. Although it's pity that we didn't meet in person so many times due to the Covid-19. I would also like to thank Prof. Dr. Magdalena Bieroza for her review of this dissertation and the nice organization of workshop on high temporal resolution water quality monitoring and analysis.

I also thanks Prof. Dr. Gunnar Lischeid to become my committee chairman, as well as PD Dr. Katrin Wendt-Potthoff and Prof. Dr. Stefan Norra as my committee members.

In the last 4 years, I have received a lot of support from many UFZ colleagues, especially those in Haus 11. Dr. Seifeddine Jomaa and Dr. Xiaoqiang Yang are senior scientist and postdoc in our group, who guided me to get familiar with UFZ and Magdeburg, shared constructive ideas and helped me when I faced various problems. I also have spent nice time working with other members in the research group of Hydrological and Water Quality Modeling: Dr. Jingshui Huang, Salman Ghaffar, Xiangqian Zhou, Ghulam Abbas, Mufeng Chen and Yao Li. I express great gratitude to our technician, Uwe Kiwel. I cannot finish my field work without his help and I gained a lot of valuable experience in field work. I'm also grateful to the GEWANA group in UFZ, Magdeburg, especially Andrea Hoff, who assisted me in the laboratory. Although many of others I don't name them here, I owe my great gratitude to all colleagues in the Department of Aquatic Ecosystem Analysis and Management.

Finally, I would like to show my greatest gratitude to my family. During the Covid-19 period, it's difficult for us to get together. They always support and care for me from China. My parents always encourage and comfort me when I feel bad mentally. Last but not least, I am most grateful to my beloved, Xiaoqiang, who comes to my life in the right time. I cannot imagine to live through that difficult time of quarantine without him. I appreciate a lot for his care, understanding and support!

Contents

Preface	I
Declaration	III
Acknowledgement	IV
Contents	V
List of Tables	VII
List of Figures	VIII
Abstract	IX
Chapter 1: Introduction	1
1.1. Problem statement: Nitrogen enrichment	1
1.2. Background and the state-of-the-art	2
1.3. Objectives and questions	8
Chapter 2: Analyzing impacts of seasonality and landscape gradient on event-scale nitrate-discharge dynamics based on nested high-frequency monitoring	11
2.1. Abstract.....	11
2.2. Introduction.....	11
2.3. Data and methods	14
2.4. Results	17
2.5. Discussion.....	25
2.6. Conclusions.....	29
2.7. References.....	30
2.8. Supplementary Materials	34
Chapter 3: Disentangling in-stream nitrate uptake pathways based on two-station high-frequency monitoring in high-order streams	35
3.1. Abstract.....	35
3.2. Introduction.....	35
3.3. Data and methods	37
3.4. Results	42
3.5. Discussion.....	49
3.6. Conclusion	54
3.7. References.....	55
3.8. Supplementary Materials	59

Chapter 4: Large-stream nitrate retention patterns shift during droughts: seasonal to sub-daily insights from high-frequency data-model fusion	74
4.1. Abstract.....	74
4.2. Introduction.....	74
4.3. Method and Materials	76
4.4. Results	80
4.5. Discussion.....	83
4.6. Conclusion	88
4.7. References.....	89
4.8. Supplementary Materials	92
Chapter 5: Discussion.....	98
5.1. Evaluation of in-situ high-frequency monitoring	98
5.2. Scientific inspirations from field experiments and future work	101
5.3. Broader outlooks for water management.....	103
Chapter 6: Summary.....	105
References	106

List of Tables

Table 2.1. Number of storm events, mean duration, mean discharge (Q) and mean NO ₃ ⁻ -N concentration during each hydrological period at the SILB, MEIS and HAUS stations	19
Table 2.2. Statistics of events of four hysteresis types based on sign of the hysteresis index (<i>HI</i>) and concentration-change index (<i>CI</i>) at the SILB, MEIS and HAUS stations	24
Table 3.1. Morphological features of river reaches and overview of monitoring deployments.....	39
Table 3.2. Overview of high-frequency measurements and stream characteristics for the 11 campaigns	43
Table 3.3. Summary of daily mean whole-stream metabolism and in-stream N-uptake processes	44

List of Figures

Figure 2.1. Elevation and land use in the Selke catchment and locations of the three gauging stations ...	15
Figure 2.2. Boxplots of monthly discharge and NO_3^- -N concentrations at the three gauging stations	18
Figure 2.3. Discharge and NO_3^- -N concentrations from 2012-2017 at the three gauging stations	19
Figure 2.4. Boxplots of hysteresis index (<i>HI</i>) and concentration-change index (<i>CI</i>) of storm events	20
Figure 2.5. Examples of the four hysteresis types detected at the HAUS station	22
Figure 2.6. Hysteresis index (<i>HI</i>) and concentration-change index (<i>CI</i>) patterns at the three gauging stations during the wetting, wet, drying and dry periods.	23
Figure 2.7. Contribution of runoff volume and nitrate-N load from each subcatchment to the catchment outlet for shared events throughout the year.....	25
Figure 2.8. Conceptual interpretation of nitrate-discharge relationships	28
Figure 3.1. Locations of the five monitored stream reaches in Saxony-Anhalt, Germany	38
Figure 3.2. Time series of DO concentrations and gross primary production for all campaigns.....	45
Figure 3.3. Time series of NO_3^- -N concentrations and areal net NO_3^- -N uptake for all campaigns	46
Figure 3.4. Sub-daily time series of the disentangled NO_3^- -N uptake pathways.	48
Figure 3.5. Diel patterns of the subtracted U_D	49
Figure 4.1. (a) The Lower Bode river reach and the multi-parameter high-frequency monitoring scheme. (b) measurements of discharge, NO_3^- -N concentrations, dissolved oxygen and water temperature	77
Figure 4.2. The WASP simulations of discharge and NO_3^- -N tracer concentrations.....	80
Figure 4.3. (a) Daily total retention rate U_T and monthly counts of the four clusters of diel patterns. (b) Daily ratios of whole-stream gross primary production and respiration (i.e., P/R ratio).....	81
Figure 4.4. The four types of diel U_T patterns clustered and the corresponding hourly variations of retention rates.....	83

Abstract

Nutrient storage, transform and transport are important processes for achieving environmental and ecological health, as well as conducting water management plans. Nitrogen is one of the most noticeable elements due to its impacts on tremendous consequences of eutrophication in aquatic systems. Among all nitrogen components, researches on nitrate are blooming because of widespread deployments of in-situ high-frequency sensors. Monitoring and studying nitrate can become a paradigm for any other reactive substances that may damage environmental conditions and cause economic losses.

Identifying nitrate storage and its transport within a catchment are inspiring to the management of agricultural activities and municipal planning. Storm events are periods when hydrological dynamics activate the exchange between nitrate storage and flow pathways. In this dissertation, long-term high-frequency monitoring data at three gauging stations in the Selke river were used to quantify event-scale nitrate concentration-discharge (C-Q) hysteretic relationships. The Selke catchment is characterized into three nested subcatchments by heterogeneous physiographic conditions and land use. With quantified hysteresis indices, impacts of seasonality and landscape gradients on C-Q relationships are explored. For example, arable area has deep nitrate legacy and can be activated with high intensity precipitation during wetting/wet periods (i.e., the strong hydrological connectivity). Hence, specific shapes of C-Q relationships in river networks can identify targeted locations and periods for agricultural management actions within the catchment to decrease nitrate output into downstream aquatic systems like the ocean.

The capacity of streams for removing nitrate is of both scientific and social interest, which makes the quantification motivated. Although measurements of nitrate dynamics are advanced compared to other substances, the methodology to directly quantify nitrate uptake pathways is still limited spatiotemporally. The major problem is the complex convolution of hydrological and biogeochemical processes, which limits in-situ measurements (e.g., isotope addition) usually to small streams with steady flow conditions. This makes the extrapolation of nitrate dynamics to large streams highly uncertain. Hence, understanding of in-stream nitrate dynamic in large rivers is still necessary. High-frequency monitoring of nitrate mass balance between upstream and downstream measurement sites can quantitatively disentangle multi-path nitrate uptake dynamics at the reach scale (3-8 km). In this dissertation, we conducted this approach in large stream reaches with varying hydro-morphological and environmental conditions for several periods, confirming its success in disentangling nitrate uptake pathways and their temporal dynamics. Net nitrate uptake, autotrophic assimilation and heterotrophic uptake were disentangled, as well as their various diel and seasonal patterns. Natural streams generally can remove more nitrate under similar environmental conditions and heterotrophic

uptake becomes dominant during post-wet seasons. Such two-station monitoring provided novel insights into reach-scale nitrate uptake processes in large streams.

Long-term in-stream nitrate dynamics can also be evaluated with the application of water quality model. This is among the first time to use a data-model fusion approach to upscale the two-station methodology in large-streams with complex flow dynamics under long-term high-frequency monitoring, assessing the in-stream nitrate retention and its responses to drought disturbances from seasonal to sub-daily scale. Nitrate retention (both net uptake and net release) exhibited substantial seasonality, which also differed in the investigated normal and drought years. In the normal years, winter and early spring seasons exhibited extensive net releases, then general net uptake occurred after the annual high-flow season at later spring and early summer with autotrophic processes dominating and during later summer-autumn low-flow periods with heterotrophy-characteristics predominating. Net nitrate release occurred since late autumn until the next early spring. In the drought years, the late-autumn net releases were not so consistently persisted as in the normal years and the predominance of autotrophic processes occurred across seasons. Aforementioned comprehensive results of nitrate dynamics on stream scale facilitate the understanding of instream processes, as well as raise the importance of scientific monitoring schemes for hydrology and water quality parameters.

Chapter 1: Introduction

1.1. Problem statement: Nitrogen enrichment

Anthropogenic activities have put substantial pressure on the global environment. Among these, nitrogen (N) enrichment is gaining more concerns. The main reasons for N production by human are food and energy production (Galloway et al., 2004). Nitrogen inputs, largely from fertilizer application, are estimated to be 10-15 times higher than the turn of the twentieth century in many regions worldwide (Galloway et al., 2004; Howarth et al., 2012). Globally, the cultivation-induced N has increased from ca. 15 megatons (Mt, $\times 10^6$ tons) per year in 1980 to ca. 33 Mt per year in 2000 (Galloway et al., 2003). In the European Union (EU), agriculture contributes 50-80% of the total N load in most regions and catchments, and the total area-specific load (kg N/ha per year) increases with increasing human activities, in particular with more intensive agricultural production in the catchments (EEA, 2005). While anthropogenic N is fixed through the Haber-Bosch process for use as fertilizer in agriculture, most N is not converted to gas emission (i.e., dinitrogen, N_2) within agroecosystem but accumulates within soils or transports to water bodies via atmospheric and hydrological cycle (Galloway & Cowling, 2002; Howarth et al., 2012). Then what is the fate of these N into terrestrial water cycle?

The sharp acceleration of N within water bodies can cause severe water quality and ecological problems. Anthropogenic N is considered as the principle cause for eutrophication in costal marine ecosystems and one of the most limiting nutrients regulating the productivity in other terrestrial aquatic ecosystems (Howarth, 1988; Howarth & Marino, 2006). In EU, water stress is usually observed in areas with intensive agriculture activities, which are considered to be the diffusion source of N enrichment (EEA, 2021b; Grizzetti et al., 2008). In China, the anthropogenic N discharge in the water environment is well above threshold, with 14.5 Mt N per year during 2010-2014, of which the share from agricultural systems is 59% (Yu et al., 2019). In the United States, 41% of the river and stream length had a high level of N and around 4% were assessed as a high total nitrogen (TN) concentration ($> 5 \text{ mg l}^{-1}$) (Rashleigh et al., 2013). Many national and international directives have been adopted to reduce the water body pollution by nitrogen. For example, the Nitrate Directive in 1991 (91/676/EEC), the Urban Wastewater Treatment Directive in 1991 (91/271/EEC), the Water Framework Directive (WFD) in 2000 (2000/60/EC) and the National Water Strategy in 2021 (BMU). However, after 15 years implantation of WFD in Germany, only 8.2% of water bodies exhibited “good” or “high ecological status”, and N compounds still remain the main reason for “poor chemical status” of groundwater bodies (Arle et al., 2016). Among all water bodies, rivers and streams are important pathways to transport water and N from terrestrial sources to downstream aquatic sinks (e.g., lakes and estuaries). Although rivers and streams have long been seen as “inert conduits”, the in-

stream biogeochemical processes can remove N from river networks and play an important role in reducing downstream ecological impact (Jarvie et al., 2018; Seitzinger et al., 2002).

Nitrogen compounds can be divided into two groups: nonreactive N (i.e., N_2) and reactive N (Nr, including all biologically, photochemically, and radiatively active N compounds in Earth's atmosphere and biosphere, e.g., ammonium and nitrate). In N cycle, nitrate (NO_3^-) is the dominant form of N export and is highly related to anthropogenic activities (Caraco & Cole, 1990). Processes such as denitrification, organic matter burial in sediments, sediment sorption, and plant and microbial uptake can remove NO_3^- from the river networks (Seitzinger et al., 2002). Active in-stream biogeochemical processes of NO_3^- have gained much scientific attention now, e.g., autotrophic uptake and denitrification. However, it's difficult to quantify the in-stream NO_3^- uptake rates, relevant processes and influential factors due to methodologic restrictions. Tracer addition methods (e.g., ^{15}N addition and pulse injection) can either provide pathway-specific inferences or be applied in larger rivers, but both of them capture a snapshot of in-stream NO_3^- uptake process, which represent a single set of conditions without considering temporal dynamics (Covino et al., 2010; Hall et al., 2009; Mulholland et al., 2002; Tank et al., 2018). Hence, advanced methods (e.g., high-frequency monitoring for water chemical constituents) are emerging to have a more comprehensive view of links between the physical and chemical environment in a river system, as well as the process linkages between catchment hydrology and in-stream chemistry (Kirchner et al., 2004; Wade et al., 2012).

1.2. Background and the state-of-the-art

1.2.1. Development of online in-situ high-frequency water quality monitoring

There has long been a mismatch between water flux monitoring, which could be sub-hourly, and water quality monitoring, which were usually weekly, monthly or at best daily (Kirchner et al., 2004; Wade et al., 2012). Continuous online monitoring of pH and electrical conductivity were first available during the early 1990s (Robson et al., 1992, 1993), which provided a foresight of automated online high-frequency hydrochemistry observations. Later, monitoring for temperature, dissolved oxygen (DO) and chlorophyll (*Chl*) were available and used to assess the ecological status of surface water (Jarvie et al., 2001, 2003). Such in-situ high-frequency sensors have enabled monitoring at a higher temporal and spatial resolutions (Wade et al., 2012; Wollschläger et al., 2017) and connect disciplines of hydrology and biogeochemistry to have a deeper understand of hydrochemical, biological and ecological functions from catchment to in-stream scale (Jarvie et al., 2001, 2003; Kirchner et al., 2004; Rode, Wade, et al., 2016).

Continuous monitoring of NO_3^- has bloomed with different methods, e.g., nitrate-ion selective electrode (ISE) (Goff et al., 2002; Scholefield et al., 2005), wet chemical analyzers (Jannasch et al., 1994) and optical (UV) sensors (Finch et al., 1998; Johnson & Coletti, 2002). While optical sensors were first applied in ocean environment (Finch et al., 1998; Johnson & Coletti, 2002), they are now

most widespread because of its accuracy, in-situ convenience and low detection limits with specific instrument design (Pellerin et al., 2013, 2016). Continuous high-frequency NO_3^- monitoring can help identify nitrate sources and dominant transport pathways according to concentration-discharge relationships (Miller et al., 2017; Zhang et al., 2020), understand NO_3^- uptake pathways under a range of contrasting river and seasonal conditions (Kunz et al., 2017; Rode, Halbedel Née Angelstein, et al., 2016), and quantify coupled nitrate processes and metabolism (Heffernan & Cohen, 2010; Jarvie et al., 2018). Long-term high-frequency monitoring could even improve data analysis methods in water chemistry (e.g., wavelet techniques) which were limited by the record length of low-frequency samples. To date, the high-frequency NO_3^- measurement is a powerful tool to improve understanding of the hydrological and biogeochemical processes underlying long-term, episodic and diel stream NO_3^- dynamics (Burns et al., 2019).

1.2.2. Concentration-discharge (C-Q) relationship

Development of studying the C-Q relationship

Studies of solute concentration-discharge (C-Q) relationships that focus on storm or snowmelt events have a long history. Pioneering researchers described decrease in water quality constituents with increasing flow during snowmelt in western rivers during 1950s, which were based on daily manual sampling (Durum, 1953; Hem, 1948). With the deployment of automated water samplers in the 1970s (Walling & Teed, 1971), studies about C-Q relationships in surface water spurred. For example, complex solute response in high flow with peaks or troughs in concentrations that appeared ahead or lagged the discharge peak (Edwards, 1973; Walling & Foster, 1975), the hysteresis in solute response on the rising and falling hydrograph (Glover & Johnson, 1974), and the flushing behavior (Walling & Foster, 1975). The nitrate (NO_3^-) concentration-discharge analyses have been enhanced with the emergence of in-situ high-frequency water quality measurements during the last decade and further used to transform views of catchment processes with other water chemical solutes, allowing us to observe their hydrochemical evolution at temporal resolutions that are orders of magnitude finer than before (Kirchner et al., 2004).

Hysteresis and flushing behavior

Hysteresis is a commonly observed pattern of the C-Q relationship since the response of solute concentration to discharge rarely shows a simple linear or curvilinear form. In 1960s, early studies observed cyclical patterns between solute concentration and discharge that concentrations at a given discharge on the rising and falling limb are different (Hendrickson & Krieger, 1964; Toler, 1965). Such lagged solute response to discharge (C-Q hysteresis) could occur whenever there is a difference in the relative timing or form of solute and discharge responses and might be driven by early episode flushing of soluble materials (Evans & Davies, 1998; Walling & Foster, 1975). It's also recognized

that hysteresis could be caused by component mixing processes and later be tested by end-member mixing analysis (Hooper et al., 1990; Swistock et al., 1989).

Investigations applied hysteresis to explore nitrate (NO_3^-) concentration response to discharge have rapidly increased over the last decade partly due to the increasing availability of high-frequency measurements (Baker & Showers, 2019; Dupas et al., 2016; Vaughan et al., 2017; Zhang et al., 2020; Zimmer et al., 2019). These high-frequency data have allowed to detect every event within one catchment and quantify the hysteresis based by event-by-event normalization to produce a comparable hysteresis index (*HI*). The *HI* could reflect the relative magnitude and rotation direction of a C-Q hysteresis by incrementally using normalized NO_3^- on the rising limb minus that on the falling limb. For $HI > 0$, it more shows clockwise hysteresis; $HI < 0$, it more shows a counter-clockwise hysteresis (Lloyd et al., 2016). This method helps to classify the direction of hysteresis and is more easily to be quantified than determine manually. Varying hysteresis responses could be yielded by hydrological processes with various runoff sources and timings. Hence hysteresis patterns could provide insights to disentangle the movement of proximal and distal NO_3^- sources within a catchment (Baker & Showers, 2019; Butturini et al., 2008; Carey et al., 2014; Vaughan et al., 2017). For example, clockwise hysteresis usually indicates few or immobilized distal nitrate sources during the falling limb; counter-clockwise hysteresis indicates multiple or mobilized distal nitrate sources transported during the falling limbs.

Besides the direction, flushing behavior is often linked with hysteresis patterns. Flushing refers to the rapid transport of solutes to a stream during an event, which is usually controlled by solute accumulation on impermeable surfaces or in the shallow subsurface, and subsequently transported by surface or subsurface runoff generations (Burns, 2005). A similar flushing index (*FI*) is also used to characterize such behavior by calculating the difference between the normalized solute concentration at the point of peak discharge and the beginning of the event. For $FI > 0$, it indicates an increased concentration or so-called “accretion” effect on the rising limb; $FI < 0$, it indicated a decreased concentration or so-called “diluting” effect on the rising limb (Butturini et al., 2008; Vaughan et al., 2017; Zhang et al., 2020). Complex combinations between clockwise and counter-clockwise hysteresis or accretion and diluting effects at the gauging station can be caused by varying factors related with catchment characteristics. For example, complex distribution of NO_3^- sources due to heterogenous land use, the duration and magnitude of one precipitation event and the antecedent soil conditions. More details could be disentangled based on long-term high-frequency NO_3^- monitoring.

1.2.3. In-stream nitrate process

Total nitrogen (TN) compounds existing in the ecosystems are complex, including organic nitrogen (ON, i.e., protein, nucleic, amino sugars and urea) and inorganic nitrogen (IN, i.e., dinitrogen (N_2), ammonia/ammonium ($\text{NH}_3/\text{NH}_4^+$), nitrite (NO_2^-), nitrate (NO_3^-), nitric oxide (NO) and nitrous oxide

(N₂O)). Nitrogen exists in various oxidation states, ranging from +5 in the most oxidized forms to -3 in the most reduced forms (Reddy & DeLaune, 2008). In-stream biological processes related with NO₃⁻ mainly include:

Assimilation: It is an internal process that temporarily retaining dissolved N into particulate N, including assimilation by autotrophs and heterotrophs, with NO₃⁻ and NH₄⁺ as the main N demand (Imsande & Touraine, 1994; Tank et al., 2000). The in-stream autotrophic assimilation is highly related with photosynthetic activities, as a result of being proceeded by periphyton, phytoplankton and macrophytes. Hence, besides in-situ measurements, quantification of autotrophic assimilation can be coupled with stream metabolism (Heffernan et al., 2010; Jarvie et al., 2001; Lupon et al., 2016), or estimated by global radiation and riparian shading (Yang et al., 2019). Heterotrophic assimilation by bacteria often occurs when organic substrates do not contain sufficient N to support bacterial growth completely, and the rate can be high with high ambient NO₃⁻ concentration (Bernhardt et al., 2002; Middelburg & Nieuwenhuize, 2000)

Denitrification: This process is critical to regulate the removal of bioavailable N from natural and human-altered systems. In river networks, denitrification is the dominant dissimilatory way to remove NO₃⁻ from water permanently, which is usually linked to microbial respiration and can reduce eutrophication of downstream ecosystems (Mulholland et al., 2009; Seitzinger et al., 2006).

Denitrification tends to occur in anaerobic environment. One or both of ionic nitrogen oxides (i.e., NO₃⁻ and NO₂⁻) are used by facultative bacteria as electron acceptor during oxidation of organic matter (OM) and finally reduced into N₂, which is released into the atmosphere because of low solubility in water (Knowles, 1982; Reddy & DeLaune, 2008). Incomplete denitrification can result in N₂O, which is seen as a greenhouse gas but not closely relevant with aquatic nitrogen cycle. Hence, the process is influenced by the availability of OM and restricted in aquatic soils and sediments, e.g., the subsurface of the river bedforms (Gomez-Velez et al., 2015), or connected riverine wetlands (Reddy et al., 1989). Denitrification can account for 16% of total NO₃⁻ uptake in headwater stream. The rate is reported to become higher with higher NO₃⁻ concentration and ecosystem respiration rates (Mulholland et al., 2008).

Nitrification: This is a dissimilatory process to convert organic or inorganic N compound from reduced form to oxidized form, normally from NH₄⁺ to NO₂⁻ then to NO₃⁻. Nitrification can support denitrification by supplying heterotrophs with NO₃⁻ as the electron acceptor (Reddy & DeLaune, 2008). Factors regulating nitrification contains the availability of NH₄⁺, the supply of oxygen, alkalinity, inorganic carbon source, nitrifying population and pH (Sharma & Ahlert, 1977; Strauss et al., 2002). Temperature and pH were reported to cause diel variation of nitrification (Warwick, 1986).

Besides biological processes, there are other ways to remove NO₃⁻ from water, e.g., sorption to sediment and deposition of particulate ON. All these processes are bound with each other during the

downstream transport in the river networks. Nitrate is temporarily assimilated into particulate N, transported downstream, re-mineralized back into the water column and ultimately removed via coupled nitrification/denitrification (Seitzinger et al., 2006) or exported from the stream in remaining organic or inorganic forms (Arango et al., 2008). This process can be measured at the whole-stream level using the nutrient spiraling concept, which couples nutrient uptake and hydrological process (i.e., advection) along the downstream transport. The average distance traveled by total nitrogen during the completion of one spiral through these compartments is defined as the spiraling length (S , in *length*), which is dominated by the average downstream distance traveled by dissolved N in the water column before uptake by biota or sorption to particulate matter (i.e., uptake length, S_w , in *length*) (Newbold et al., 1982; Newbold et al., 1981; Stream Solute Workshop, 1990). The interconnections make the quantification of each NO_3^- uptake pathway challenging.

Traditional measurements of nitrate uptake at the reach scale

The uptake length is an important parameter to quantify N cycling in river networks and can be converted into areal uptake (U , in *mass area⁻² time⁻¹*) according to equations from Stream Solute Workshop (1990). The isotope tracer addition (e.g., radioisotopes such as ^{32}P , stable isotopes such as ^{15}N) is a preferred way to measure uptake length with maintaining ambient nutrient concentration. It was first used to measure the uptake length for phosphorus (P) by adding ^{32}P in a small woodland stream (Newbold et al., 1981). For nitrogen, the Lotic Intersite Nitrogen eXperiment (LINX) project and its subsequent LINX II project worked intensively on whole-stream N cycling using field ^{15}N stable isotope additions (Mulholland et al., 2002; Webster, 2000). The projects hypothesized that key hydrodynamic, chemical and metabolic characteristics can determine water retention and degree of N efficiency in stream ecosystems. Hence, numbers of streams with varying climatic and anthropogenic characteristics were selected to conduct the ^{15}N injection experiment, finding out the control of N export and different uptake pathways (Dodds et al., 2000; Hall et al., 2009; Mulholland et al., 2008, 2009; Peterson et al., 2001). In addition, the short-term nutrient addition is another common method to measure uptake length (e.g., a reactive solute (NO_3^- , NH_4^+) with a conservative tracer (chloride, Cl^-)), especially when the isotope tracer addition is difficult or expensive to conduct (Bernhardt et al., 2002; Munn & Meyer, 1990). This method can be used in large rivers but usually provide no pathway-specific inferences (Tank et al., 2008). Despite the importance of such addition experiments, there are still methodological limitations:

(1) The short-term nutrient addition can change ambient nutrient concentrations and influence the N biological processes, causing a longer uptake length compare with measurements by using isotope tracer addition. The ratio between the uptake length of short-term nutrient and isotope tracer addition should be a function of the increase in nutrient concentration during the addition and the degree of nutrient limitation (Mulholland et al., 2002).

(2) Both addition methods are usually conducted for a short period (e.g., few days) during low-flow periods, representing a single set of conditions without considering temporal dynamics. This makes uncertainty to extrapolate annual N processing rates (Mulholland et al., 2002; Tank et al., 2008).

(3) Due to the methodological difficulties in applying small-stream approaches to larger river systems, both addition methods are mainly limited to small streams. Research on the nitrate uptake in river networks is mainly related to models by scaling up site-specific experiments data from small streams to large streams and rivers, resulting in high degree of uncertainties. Considering the influence of large rivers on N exports, empirical measurements of N dynamics in large rivers are needed to understand its role of whole river networks (Tank et al., 2008; Wollheim et al., 2006; Ye et al., 2012).

To conclude, it's necessary to improve the methodology of quantifying N biogeochemical processes, which can provide empirical estimations for model simulation and fulfill the comprehensive concept of N processes from river networks to catchments to continents scale.

New methodology to measure reach-scale nitrate uptake: high-frequency monitoring

Recently, advances in high-frequency in-situ sensor technology have enabled continuous monitoring of in-stream water quality parameters (Burns et al., 2019; Pellerin et al., 2016; Rode, Wade, et al., 2016). Such passive approach can be applied across stream orders and over extended periods, improving the understanding of the spatiotemporal heterogeneity in the nitrate biogeochemical processes (Jarvie et al., 2018; Kunz et al., 2017; Rode, Halbedel Née Angelstein, et al., 2016; Yang et al., 2019).

Sub daily monitoring of nitrate concentration provides a brand-new vision of studying nitrate dynamics, which is commensurate with their physical, chemical and biological drivers at different temporal and spatial scales (Kirchner et al., 2004). The creation of diel variability is highly related to in-stream biogeochemical processes instead of hydraulic transport, and 70% of diel pattern are associated with autotrophic assimilation (Greiwe et al., 2021). In a steady spring-fed river, autotrophic assimilation and denitrification can be disentangled from diel process of nitrate concentration (Heffernan & Cohen, 2010). The methodology was later applied in other streams, showing the potential to allow better parameter constraints in watershed nutrient transport models (Rode, Halbedel Née Angelstein, et al., 2016; Yang et al., 2019).

Besides the improvement on temporal scale, the high frequency monitoring also upscales the size of study stream. The longitudinal profiling can assess nitrogen removal kinetics and reflect processes that vary in both space and time and over different scales in large streams and rivers (Hensley et al., 2014, 2020). The mass balance approaches have been applied in large stream reaches to quantify net nitrate uptake and uptake pathways (e.g., metabolism coupled autotrophic assimilation and denitrification), showing that seasonal variations in temperature and insolation affected the relative contribution of assimilatory versus dissimilatory uptake processes (Jarvie et al., 2018; Kunz et al.,

2017). Continuous in-situ high frequency monitoring offers new opportunities to deriving quantitative uptake estimates, even under dynamic inputs and lateral tributary inflow. These researches gradually fill in knowledge gaps in quantifying nitrate processes in higher order streams.

1.2.4. Data-model fusion

As mentioned in the previous section, high-frequency monitoring has improved our vision about in-stream nitrate cycle kinetics. Biochemical process-related information can be extracted directly from nitrate concentration series, but is often conducted under relative stable upstream boundary conditions (Heffernan & Cohen, 2010; Hensley & Cohen, 2016; Yang et al., 2019). For the more adaptive two-station method, the estimation accuracy highly relies on hydraulic transformations (Hensley & Cohen, 2016) and lateral inflow conditions (Zhang et al., 2022). For streams with more complex hydro-morphological conditions, inferences from purely high-frequency data can be difficult. Under such circumstances, river water quality modeling can assist in capturing varying river hydrodynamics (Huang et al., 2022).

Recently such data-model fusion gets increasing attraction in environmental science. On the one hand, smart monitoring technologies have seen a thriving development in the last decades. Earth observation is providing usable data at increasingly higher spatial and temporal resolution, from remote sensing images to high-frequency sensor developments (Boyd & Danson, 2005; Burns et al., 2019). On the other hand, low-cost computational power has supported the use of complex algorithms applications. Because of this, in general we are observing a shift of paradigm towards the development and application of data-driven models, which require data for their training and validation (Tsopanoglou & Jiménez del Val, 2021). Yang et al. (2019) developed a parsimonious approach for regionalizing the autotrophic uptake rate and integrated this method with a catchment hydrological model to investigate nitrate transport and in-stream uptake processes throughout river networks. Huang et al. (2022) used a hydrodynamic and river water quality to simulate 15 min-interval of discharge, DO and nitrate, estimating different in-stream nitrate uptake pathways and their seasonal variations. Such data-model fusion approach can relax the aforementioned methodological constrains and make the greatest use of high-frequency monitoring, bringing exciting novel research opportunities and applications like new analysis and data mining approaches.

1.3. Objectives and questions

This dissertation focuses on nitrogen dynamics (mainly nitrate, NO_3^-) in high-order streams based on high-frequency water quality monitoring. High-frequency datasets can reveal temporal dynamics that were obscured by traditional low-frequency sampling, which can offer new insights into biogeochemical processes of streams and their catchments. This can help governments set reasonable regulations of agricultural operations and WWTP activities. Moreover, high-frequency data motivate to transform our understanding of huge knowledge for fundamental aquatic processes, including

identifying NO_3^- sources and transport pathways in catchments, quantifying metabolism-coupled NO_3^- uptake processing and disentangling different NO_3^- uptake pathways, which are mostly studied in small streams and during short-time periods due to methodology limitations.

In this dissertation, firstly I analyzed long-term high-frequency monitoring data at three gauging stations in a 4th stream, the Selke stream, to evaluate NO_3^- sources and transport mechanisms in a nested catchment, as well as the influential factors (Chapter 2). Then I set up in-situ sensors to disentangle various reach-scale NO_3^- uptake pathways based on mass balance method in high-order streams (Chapter 3). A hydraulic model is used to further upscale the methodology for estimating long-term NO_3^- uptake in a longer reach, indicating the promising probability of long-term high-frequency data to understand cause-effect relationship of NO_3^- uptake by using time-series analysis approaches which before were limited due to the data length (Chapter 4). The dissertation covers three aspects and is intended for following objectives:

- I. Analyze event-scale nitrate-discharge (C-Q) relationships based on in-situ long-term high-frequency monitoring data:
 - 1) Analyze high-frequency data to quantify event-scale C-Q hysteresis and make it comparable among different events;
 - 2) Identify various NO_3^- sources and pathways at the catchment scale by interpreting different C-Q hysteresis pattern;
 - 3) Evaluate seasonality and landscape effects on C-Q relationships and its implications.
 - 4) Determine nitrate load from each subcatchment by analyzing shared events transported from upstream to downstream and its alterations related with seasonality and landscape variations.
- II. Quantify reach-scale in-stream NO_3^- uptake rates through mass balance methodology with multiple-parameter sensors:
 - 1) Estimate quantitative net NO_3^- uptake and metabolism rates based on two-station mass balance methodology in large streams with heterogenous river morphologies;
 - 2) Disentangle detailed NO_3^- uptake pathways using metabolism rates , e.g., GPP-based autotrophic assimilation;
 - 3) Explore the sub-daily pattern of each NO_3^- uptake pathway;
 - 4) Explain the change of NO_3^- uptake pathways under different monitoring conditions using multi-parameter monitoring;
 - 5) Assess the hydrological conditions (wet and dry) in terms of their influence on the fraction of each NO_3^- uptake pathway .

III. Upscale the mass balance method to quantify NO_3^- uptake in a longer stream via data-model fusion approach:

- 1) Use conservative tracer simulation in water quality modeling to simulate NO_3^- transport without biogeochemical processes;
- 2) Quantify continuous NO_3^- uptake based the tracer simulation during a long-term period and disentangle the NO_3^- overall retention and uptake pathways;
- 3) Compare variations of the net NO_3^- retention and uptake pathways between normal and drought years on the seasonal and sub-daily scales.

Chapter 2: Analyzing impacts of seasonality and landscape gradient on event-scale nitrate-discharge dynamics based on nested high-frequency monitoring

(An edited version of this paper was copyright by Elsevier Copyright (2023))

2.1. Abstract

Increasingly available high-frequency data during storm events, when hydrological dynamics most likely activate nitrate storage-flux exchanges, reveal insights into catchment nitrate dynamics. In this study, we explored impacts of seasonality and landscape gradients on nitrate concentration-discharge (C-Q) hysteresis patterns in the Selke catchment, central Germany, which has heterogeneous combinations of meteorological, hydrogeological and land use conditions. Three nested gauging stations established along the main Selke River captured flow and nitrate export dynamics from the uppermost subcatchment (mixed forest and arable land), middle subcatchment (pure steep forest) and lowermost subcatchment (arable and urban land). We collected continuous high-frequency (15-min) discharge and nitrate concentration data from 2012-2017 and analyzed the 223 events detected at all three stations. A dominant hysteresis pattern in the uppermost and middle subcatchments was counter-clockwise and combined with an accretion effect, indicating many proximal and mobilized distal nitrate sources. However, 66% of all events at the catchment outlet experienced a dilution effect, possibly due to mechanisms that vary seasonally. During wetting/wet periods (October-March), it was combined mainly with a counter-clockwise pattern due to the dominance of event runoff volume from the uppermost and middle subcatchments. During drying/dry periods (April-September), however, it was combined mainly with a clockwise pattern due to occasional quick surface flows from lowland near-stream urban areas. In addition, the clockwise hysteresis occurred mainly from May-October during mostly drying/dry periods at all three sites, indicating little distal nitrate transport in response to the low terrestrial hydrological connectivity, especially in the lowermost dry and flat subcatchment. This comprehensive analysis (i.e., clockwise vs. counter-clockwise, accretion vs. dilution) enables in-depth analysis of nitrate export mechanisms during certain periods under different landscape conditions. Specific combination of C-Q relationships could identify target locations for agricultural management actions that decrease nitrate output. Therefore, we strongly encourage long-term multisite and high-frequency monitoring strategies in heterogeneous nested catchment(s), which can help understand process mechanisms, generate data for physical-based water-quality modeling and provide guidance for water and agricultural management.

2.2. Introduction

Human activities (e.g., intensive agriculture, urbanization, deforestation) have altered the natural landscape extensively and hence influenced nitrogen (N) cycling greatly (Boyer et al., 2002; Howarth et al., 2012). The large external supplies of N clearly exceed terrestrial N demands for plant/crop growth and microbial transformation (Davidson et al., 2011). Driven by hydrological dynamics, the

excess terrestrial N has been exported to surface waters and redistributed spatially and temporally throughout fresh/coastal water systems (Reusch et al., 2018; Shields et al., 2008). Mitigation measures have been established according to guidelines of multiple government conventions (e.g., the European Union Water Framework Directive). Although diffuse nitrate pollution has been ameliorated, it remains a main cause of freshwater quality degradation (EEA, 2018). Pursuing more cost-effective measures requires better mechanistic understanding of catchment nitrate dynamics, especially in the context of contrasting landscape conditions (both natural and human) and strong seasonal variability.

Flow and nitrate dynamics during storm events are more active due to changes in storage-flux interactions and transport pathways, compared to those during hydrologically stable conditions (e.g., low flow, dry periods). Therefore, the event-scale relationship between nitrate concentration and discharge (C-Q relationship) has been investigated intensively to determine spatial and temporal variability in catchment nitrate functioning (Baker and Showers, 2019; Dupas et al., 2016; Zimmer et al., 2019). Hysteresis is the most commonly observed pattern of the C-Q relationship (Burns et al., 2019). Hysteresis patterns vary spatially and temporally due to variable combinations of nitrate sources (Bowes et al., 2015) and hydrological drivers (Vaughan et al., 2017). Celerity is well known to be faster than particle transport velocity in catchment hydrology (Cheraghi et al., 2016; McDonnell and Beven, 2014; Williams et al., 2018). Therefore, proximal nitrate storages generally respond faster than distal storages along the formation of hydrograph at the catchment scale, resulting in different hysteresis loops of the C-Q relationship (i.e., clockwise vs counter-clockwise). Meanwhile, nitrate storage varies vertically (along the soil profile) and horizontally under different landscape characteristics and anthropogenic conditions (Dupas et al., 2016; Musolff et al., 2016; Miller et al., 2017). Driven by flow generations, the mobilized terrestrial nitrate may further result in negative or positive hysteresis slopes for stream water, representing dilution or accretion effects, respectively. In turn, hysteresis analysis based on comprehensive monitoring data permits detailed explorations of the varying flow and nitrate dynamics. Continuous high-frequency data under various hydro-climatic conditions offers the opportunity to evaluate the changes of runoff partitioning and biogeochemical processes, as well as their impacts on nitrate mobilizations at multiple spatial scales (e.g., for the catchment-wide scale and the local near stream scale) (Carey et al., 2014; Vaughan et al., 2017). Intensive monitoring across contrasting landscape characteristics further enables detailed analysis of the interplay between heterogeneous landscape features and varying flow pathways (Fovet et al., 2018; Musolff et al., 2015; Williams et al., 2018).

Landscape characteristics reflect regional climate patterns, general pedological and geological properties and human impacts. Therefore, the spatial heterogeneity of landscape characteristics determines the spatial distribution of nitrate source areas and variable catchment mechanisms of hydrology and nutrient transport (Dupas et al., 2017; Poor and McDonnell, 2007). The long history of commercial fertilizer application has increased agricultural production but has also accumulated

excess N in terrestrial soils (Outram et al., 2016). N sources from agricultural lands have become one of the main pollution sources in most rivers and caused high risks to aquatic ecosystems (EEA, 2019). In forest areas, nitrate leaching likely depends on the amount of nitrate in throughfall and the C:N ratio of the organic soil horizon (Borken and Matzner, 2004; MacDonald et al., 2002). Therefore, a synchronous dynamic pattern between discharge and nitrate concentration is commonly observed in forest catchments. Artificial N is added mainly via atmospheric wet and dry deposition (e.g., ranging from 1-60 kg N ha⁻¹ yr⁻¹), which has also been increased greatly in the past few decades (MacDonald et al., 2002). In urban areas, extensive paved areas and artificial drainage networks can strongly alter natural processes of water movement and nitrate transport (Miller et al., 2014). For example, artificially drained flow easily bypasses the nitrate-rich soil and responds quickly, even under small precipitation events. Therefore, the process of N export can be misunderstood if the heterogeneity of catchment landscape characteristics is not considered, especially in nonuniform and nested catchments.

Driven by seasonal variations in meteorological and hydrological conditions, terrestrial export of nitrate always accompanies the changes of runoff components, and therefore, the surface nitrate C-Q relationship shows strong seasonality (Sickman et al., 2003). Different runoff components (i.e., surface flow, interflow and baseflow) usually have different nitrate concentrations due to their differing degrees of interactions with soil N sources (Miller et al., 2017). Therefore, the seasonally varying characteristic of runoff partitioning can alter the C-Q relationship of specific events considerably. Recent researches about C-Q relationship most focus on humid areas (Jacobs et al., 2018; Vaughan et al., 2017; Zimmer et al., 2019), where interflow plays an important role in transporting nitrate sources during events. Studies of process-based understanding of temporal nitrate dynamics in dry area are still rare (Dupas et al., 2016). For example, interflow and baseflow are considered the dominant runoff components during wet and dry periods, respectively, in the well-monitored Selke catchment in central Germany (Yang et al., 2018). However, quick surface flow from paved area and artificial drainage (both with relatively low nitrate concentrations) can also occur intermittently in the lowland arable/urban area during small events and cause different C-Q relationships at the outlet. The interplay among different runoff components and their effects on nitrate dynamics in dry area are hence in need of improved understanding. Moreover, seasonal biogeochemical processes can also influence the nitrate legacy at the catchment scale. In Western Europe, winter-spring high-flow periods experience high soil moisture, which activates hydrological connections between terrestrial and aquatic systems (Molenat et al., 2008; Strohmenger et al., 2020), and relatively low temperatures, which do not stimulate much biogeochemical turnover (Allen et al., 2002). In contrast, summer-autumn high-temperature growing seasons cause high soil evaporation and plant/crop transpiration, which result in low soil moisture that restricts hydrological connections (Bracken and Croke, 2007) and stimulates biogeochemical transformations of N in terrestrial and in-

stream phases (Racchetti et al., 2011; Rode et al., 2016a). Hence, these seasonal hydrological and biogeochemical processes can characterize the variation in the C-Q relationship.

Overall, the mechanistic interactions between flow and nitrate dynamics at the event scale vary spatially and temporally. Comprehensive monitoring datasets for highly heterogeneous catchments are rare, but they are essential to reveal effects of landscape heterogeneity and seasonality on C-Q relationships. In this study, we focused on the well-monitored Selke catchment (a subcatchment of the Terrestrial Environmental Observatories (TERENO) – Harz/Central German Lowland Observatory) (Wollschläger et al., 2016; Zacharias et al., 2011). Three nested gauging stations along the main Selke River capture the variety of catchment responses of flow and nitrate processes (Jiang et al., 2019; Yang et al., 2018). High-frequency multi-parameter sensors have been continuously deployed at each station, ranging from upper forest area to lowland agricultural area (Rode et al., 2016a). Here we collected discharge and nitrate-N concentration data that were continuously monitored during 2012-2017 at a 15-min interval. The objectives of this study were to (1) quantify event-scale C-Q relationships among heterogeneous conditions in the nested Selke catchment, (2) analyze impacts of deviating hydrological and landscape characteristics on hysteresis patterns based on subcatchments discrepancies, and (3) investigate seasonal variability of hysteresis patterns given the contrasting wet-dry conditions. With this study we show how nitrate fluxes are generated in heterogeneous subcatchments and how the interplay of these subcatchments can modulate C-Q relationships at varying seasonal conditions and event magnitudes at the whole catchment scale.

2.3. Data and methods

2.3.1. Study area and data collection

The Selke catchment (456 km²) is located in the transition area between the northern German plain and central German uplands. The elevation ranges from ca. 590 m in the upper Harz mountain region to ca. 100 m in the lowland region (Figure 2.1a), with mean annual precipitation decreasing from 790 to 450 mm, respectively (Yang et al., 2019). Three gauging stations set up from upstream to downstream (i.e., Silberhuetten (SILB), Meisdorf (MEIS) and Hausneindorf (HAUS)) (Figure 2.1a) capture responses of the heterogeneous catchments (Rode et al., 2016a). The drainage areas of the three stations are 99, 184, and 456 km², respectively. The uppermost and middle subcatchments lie in the Harz mountainous region, which is dominated by shallow and relatively impervious schist and claystone overlain mainly by cambisols. In contrast, the lowermost subcatchment lies in the unique central German loess-chernozem region, which has deep tertiary sedimentary rocks. Therefore, the catchment has high gradients of landscape characteristics, including meteorology, hydrology, biogeochemistry and anthropogenic impacts (Yang et al., 2019). The uppermost subcatchment is covered by well-mixed forest (60%) and agricultural (25%) areas, while most (85%) of the middle subcatchment is covered by pure steep forest (Figure 2.1b). Due to the high fertility of chernozems,

the lowermost subcatchment is extensively and intensively cultivated as arable land (ca. 80%) and contains considerable urban areas.

Both discharge and nitrate-N (NO_3^- -N) concentration are continuously measured at the three gauging stations. We collected high-frequency (15-min interval) data from 2012-2017 for the event-scale analysis. Discharge data were provided by the State Agency for Flood Protection and Water Management of Saxony-Anhalt (LHW). NO_3^- -N data were provided by the Helmholtz Center for Environmental Research-UFZ, using a TRIOS ProPS-UV sensor with an optical path length of 10 mm. The sensor data were validated by biweekly parallel grab samples. For more information about the high-frequency monitoring and maintenance, please refer to Rode et al. (2016b). In addition, long-term daily discharge and biweekly grab-sampled NO_3^- -N data (1994 - 2011) from LHW were also collected for a long-term overview of flow and NO_3^- -N concentration dynamics.

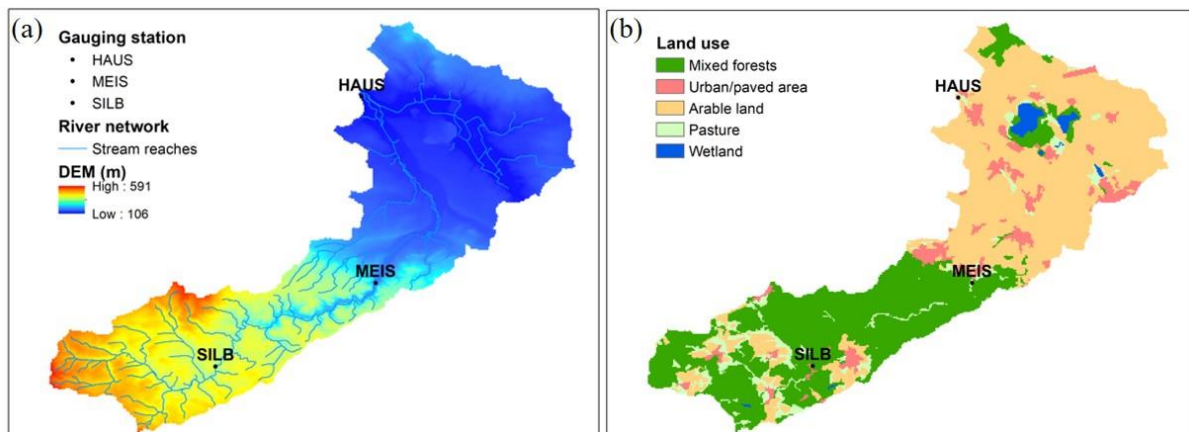


Figure 2.1. (a) Elevation and (b) land use in the Selke catchment and locations of the three gauging stations.

2.3.2. Variability in event-scale nitrate dynamics

2.3.2.1. Detecting storm events

Storm events were detected first based on automatic identification of all local maxima and minima of the discharge time series. Each local maximum was considered to be the discharge peak of each event, and the closest minima before and after the peak were selected as the preliminary start- and end-time of the event, respectively. Next, the final start- and end-times of each event were manually adjusted to ensure that they had a similar discharge. Successive events without a complete recession between them were merged into a single event with multiple peaks. Events with missing data ($> 10\%$) were excluded from further analysis. Events were detected using scripts in R software (R Core Team, 2020).

2.3.2.2. Calculation of hysteresis patterns

For each event, discharge and NO_3^- -N were normalized following Lloyd et al. (2016a):

$$Q_{t,norm} = \frac{Q_t - Q_{min}}{Q_{max} - Q_{min}} \quad (1)$$

$$N_{t,norm} = \frac{N_t - N_{min}}{N_{max} - N_{min}} \quad (2)$$

where Q_t and N_t are the discharge ($\text{m}^3 \text{s}^{-1}$) and $\text{NO}_3^- \text{-N}$ (mg l^{-1}) concentration measured at time t , $Q_{t,norm}$ and $N_{t,norm}$ are the normalized discharge and $\text{NO}_3^- \text{-N}$ concentration, and the subscripts ‘ $_{min}$ ’ and ‘ $_{max}$ ’ are the minimum and maximum values of each event.

To quantify the hysteresis pattern of the C-Q relationship, two indices were calculated from the normalized data. First, the non-dimensional hysteresis index (HI) was calculated as:

$$HI = \int N_{t,norm} \cdot dQ_{t,norm} \quad (3)$$

where HI equals the sum of hysteresis effects of the C-Q relationship during each event period (Zhang et al., 2017). HI ranges from -1 to 1 ($HI > 0$ indicates clockwise hysteresis, while $HI < 0$ indicates counter-clockwise hysteresis). Second, the concentration-changed index (CI), following Butturini et al. (2008), was calculated as:

$$CI = N_{tp,norm} - N_{ts,norm} \quad (4)$$

where $N_{tp,norm}$ and $N_{ts,norm}$ are the normalized $\text{NO}_3^- \text{-N}$ concentration at the discharge peak and start-time of each event, respectively. CI ranges from -1 to 1 ($CI > 0$ indicates an accretion effect of $\text{NO}_3^- \text{-N}$ concentration following flow dynamics, while $CI < 0$ indicates a dilution effect). Note that if the peak discharge lasted for more than one measured time point, the first time point $\text{NO}_3^- \text{-N}$ concentration was chosen as $N_{tp,norm}$.

2.3.2.3. Shared event analysis and statistic methods

Several “shared events” were specifically analyzed based on the start-, end- and discharge peak time points of each event at the SILB, MEIS, and HAUS stations. These events propagated from upstream to downstream and were detected simultaneously at all three stations. Then, the start- and end-times of each shared event were adjusted slightly to encompass the entire event duration at all three stations (i.e., using the latest start-time and the earliest end-time). Nitrate-N load (N_L , unit: kg) and runoff volume (R_V , unit: m^3) of each shared event at each station were calculated using the following two equations, respectively:

$$N_L = \int (Q_t \cdot N_t) \cdot dt \quad (5)$$

$$R_V = \int Q_t \cdot dt \quad (6)$$

where Q_t and N_t are the measured discharge ($\text{m}^3 \text{s}^{-1}$) and NO_3^- -N concentration (mg l^{-1}), respectively, during the shared period. Using values of N_L and R_V from the three nested stations, nitrate-N load and runoff volume were calculated for the uppermost subcatchment (subscript ‘ UP ’) as the values measured at the SILB station, for the middle subcatchment (subscript ‘ MID ’) as the values measured at the MEIS station minus those at the SILB station and for the lowermost subcatchment (subscript ‘ LOW ’) as the values measured at the HAUS station minus those at the MEIS station. In addition, nitrate-N load and runoff volume of the entire catchment (subscript ‘ ALL ’) were considered as the values measured at the HAUS station.

The nonparametric Wilcoxon signed rank test and Kruskal-Wallis test were used to detect significant differences in population medians of paired or multiple categories, respectively (Kruskal and Wallis, 1952; Wilcoxon, 1945). The distributions of samples were considered significantly different when the p -value was below the level of significance of 0.05.

2.4. Results

2.4.1. Overview of long-term dynamics

In the long-term data (1994-2017), runoff volume increased disproportionately from upstream to downstream stations; for example, although the uppermost subcatchment covered only 22% of the catchment, it contributed 64% of its total mean annual runoff volume (i.e., 3.31×10^7 and $5.15 \times 10^7 \text{ m}^3 \text{ yr}^{-1}$ at the SILB and HAUS stations, respectively). The spatial contribution of mean annual NO_3^- -N load generally followed that of flow volume (e.g., 68 t yr^{-1} at the SILB station was 43% of the total at the HAUS station). Differences in runoff volume and NO_3^- -N load among subcatchments were due to spatial variability in NO_3^- -N concentrations. From the SILB station to the HAUS station, median NO_3^- -N concentration increased significantly (from 1.01 to 2.68 mg l^{-1} , Wilcoxon signed rank test), while median specific runoff decreased significantly (from 169 to 67 mm yr^{-1} , Wilcoxon signed rank test).

Despite the high spatial variability, discharge and NO_3^- -N concentration showed strong seasonal patterns (Figure 2.2). Based on the general hydro-climatic cycling (Figure 2.2a), we categorized the hydrological year into four periods: wetting (October-December, with a continuous increase in mean monthly discharge from 0.90 to $1.80 \text{ m}^3 \text{ s}^{-1}$ at the HAUS station), wet (January-March, with high mean discharge of $2.96 \text{ m}^3 \text{ s}^{-1}$), drying (April-June, with mean monthly discharge decreasing from 2.42 to $0.99 \text{ m}^3 \text{ s}^{-1}$) and dry (July-September, with consistently low mean discharge of $0.58 \text{ m}^3 \text{ s}^{-1}$). The spatial distribution of flow varied greatly among the hydrological periods. The uppermost subcatchment generated most of the catchment’s runoff volume during the wet period but much less during the dry period (e.g., mean discharge in February and September was 70% and 53% that at HAUS, respectively) (Figure 2.2a). The seasonal pattern of NO_3^- -N was similar to that of discharge at

the SILB and MEIS stations, with high concentrations (e.g., $> 3 \text{ mg l}^{-1}$) during the wet period that gradually decreased during the drying period, and much lower concentrations (e.g., $< 1 \text{ mg l}^{-1}$) during the dry period (Figure 2.2b). However, $\text{NO}_3^- \text{-N}$ at the HAUS station had consistently high concentrations throughout the hydrological cycle (i.e., generally $> 2 \text{ mg l}^{-1}$). Mean $\text{NO}_3^- \text{-N}$ concentration during the dry period was significantly higher at HAUS (2.60 mg l^{-1}) than at SILB (0.58 mg l^{-1}). The high mean concentrations at HAUS, much higher than those at MEIS and SILB, were likely caused by urban point-source contributions before 2002 (Yang et al., 2018). Nonetheless, the mean monthly concentration decreased slightly from the beginning of the drying period but remained much higher than those at MEIS and SILB.

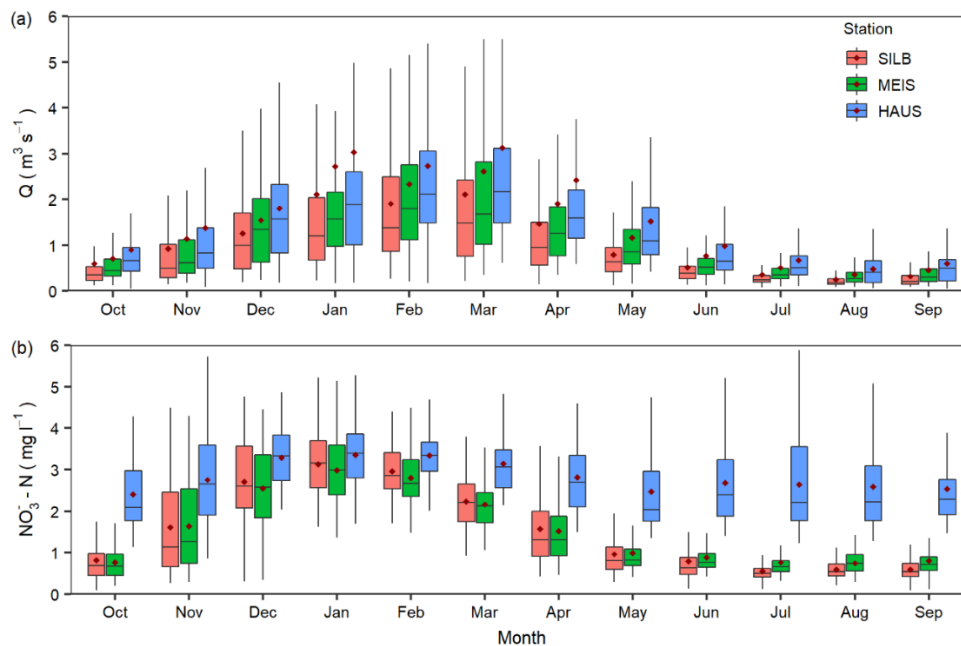


Figure 2.2. Boxplots of monthly (a) discharge and (b) nitrate-N concentrations at the SILB, MEIS and HAUS stations from 1994-2017. Outliers were omitted, and red diamond markers represent mean values. Whiskers represent 1.5 times the interquartile range.

2.4.2. Event detection

We analyzed 81, 72, and 70 detected events at the SILB, MEIS and HAUS stations, respectively, from 2012-2017 (Figure 2.3, Supplementary Table S2.1). Events were evenly distributed, while their magnitude and duration varied greatly during the four hydrological periods among the three stations (Table 2.1). Event durations were generally much longer during wetting/wet periods than during drying/dry periods (e.g., mean durations at the SILB station were 11.79 and 4.07 days during the wet and dry periods, respectively). Similarly, event-scale mean discharge and $\text{NO}_3^- \text{-N}$ had the highest values during the wet period and the lowest values during the dry period at the three stations (Table 2.1).

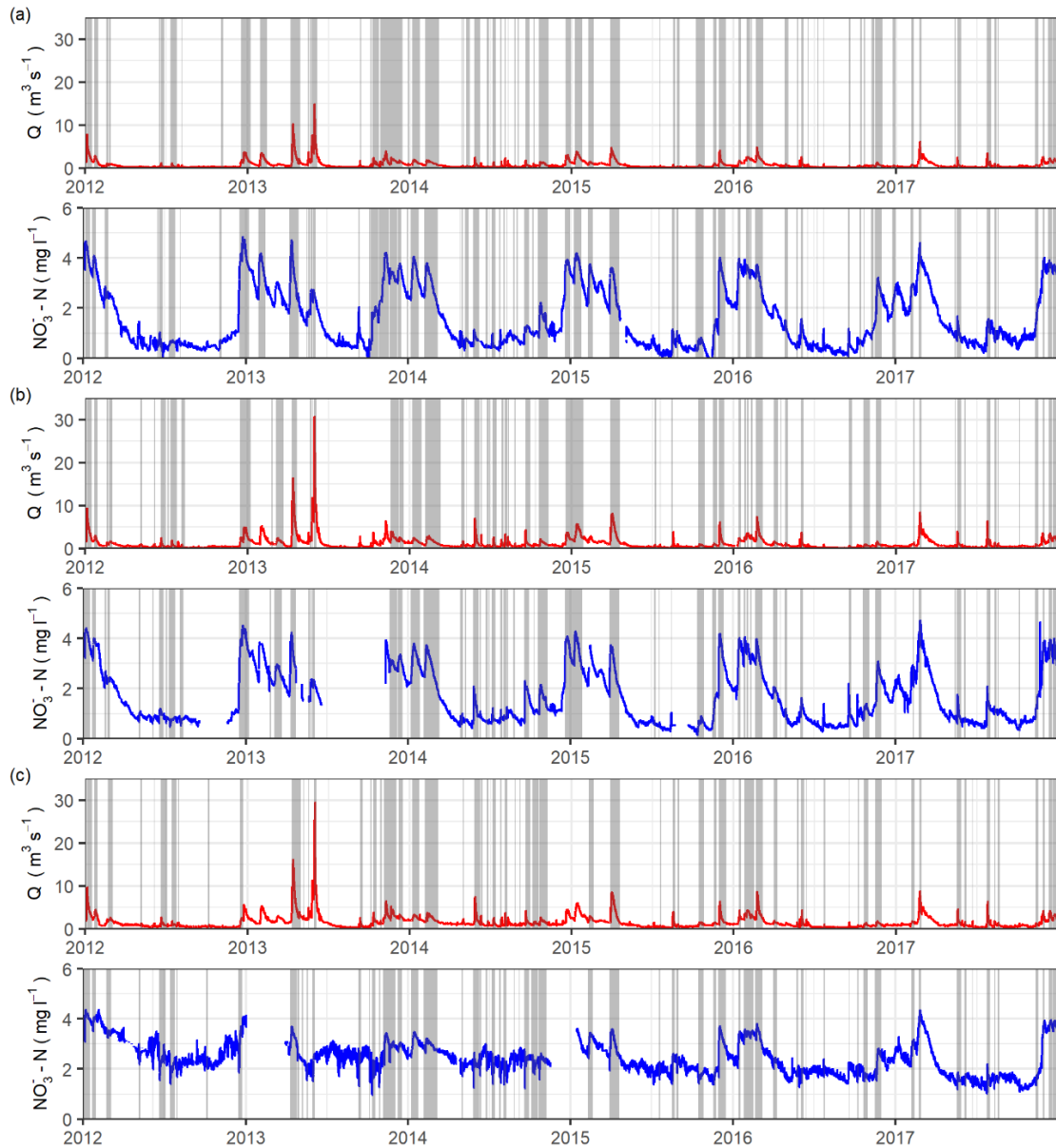


Figure 2.3. Discharge (Q) and NO_3^- -N concentrations at 15-minute intervals from 2012-2017 at the (a) SILB, (b) MEIS and (c) HAUS stations. A total of 81, 72, and 70 storm events (shaded areas) remained after manual adjustment, respectively.

Table 2.1. Number of storm events, mean duration, mean discharge (Q) and mean NO_3^- -N concentration during each hydrological period at the SILB, MEIS and HAUS stations.

Periods	SILB				MEIS				HAUS			
	Wetting	Wet	Drying	Dry	Wetting	Wet	Drying	Dry	Wetting	Wet	Drying	Dry
Number	25	16	20	20	17	18	20	17	20	15	18	17
Duration (days)	9.5	11.8	5.1	4.1	11.0	11.0	4.7	5.4	9.2	11.6	5.4	4.8
Q ($\text{m}^3 \text{s}^{-1}$)	1.12	1.95	1.42	0.56	1.73	2.56	2.42	0.85	1.93	3.29	2.69	1.21
NO_3^- -N (mg l^{-1})	2.29	3.38	1.30	0.85	2.42	3.15	1.24	0.98	2.49	3.33	2.16	2.04

2.4.3. Hysteresis pattern analysis

The patterns of HI and CI showed both spatial and seasonal variations. Negative HI (i.e., counter-clockwise hysteresis) dominated at the SILB, MEIS and HAUS stations (i.e., ca. 78%, 88% and 63% of all events, respectively) (Figure 2.4a). Most events with positive HI (i.e., clockwise hysteresis) occurred during drying/dry periods (78%, 67% and 88% at the SILB, MEIS and HAUS stations, respectively). The median HI was significantly different among four hydrological periods at each station (Kruskal-Wallis test). The trend for CI differed from that of HI . Positive CI (i.e., accretion effect) dominated in the uppermost and middle subcatchments (i.e., 89% and 79% of all events at the SILB and MEIS stations, respectively) (Figure 2.4b). However, 66% of events at the HAUS station had negative CI (i.e., dilution effect). The median CI between SILB and HAUS, and between MEIS and HAUS were significantly different (Wilcoxon signed rank test). Mean CI was positive during all four hydrological periods at the SILB and MEIS stations but was positive only during the wet period at the HAUS station (Figure 2.4b).

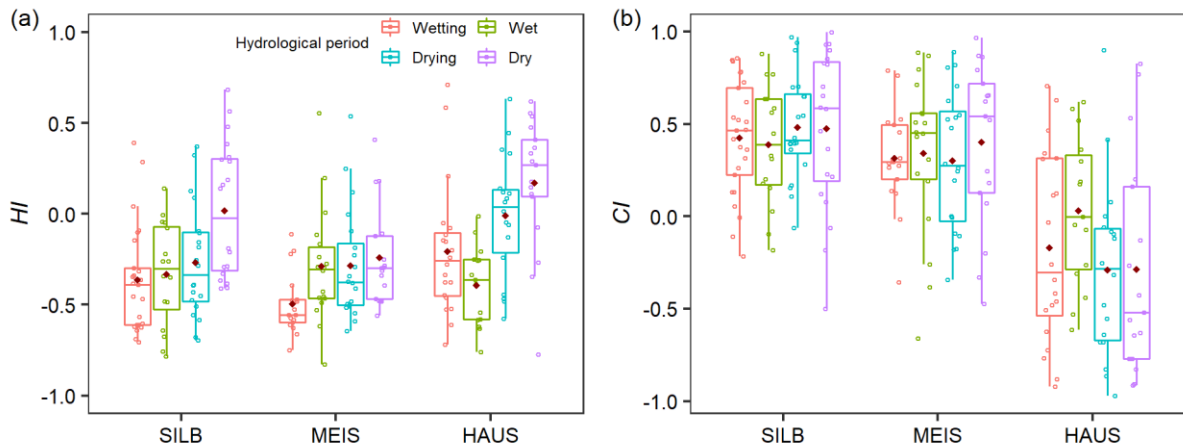


Figure 2.4. Boxplots of (a) hysteresis index (HI) and (b) concentration-change index (CI) of storm events during four hydrological periods at the SILB, MEIS and HAUS stations. Red points represent means. Whiskers represent 1.5 times the interquartile range.

We combined the two hysteresis indices and categorized all events into four categories (Figure 2.5). Event-scale hysteresis patterns varied greatly among the hydrological periods and landscape conditions (Figure 2.6). At the SILB station, the general hysteresis pattern was negative HI combined with positive CI (ca. 72%, Figure 2.6). The events in this category had the longest duration and highest total precipitation (Table 2.2). The pattern of positive HI combined with positive CI accounted for 17% of events at SILB, most of which occurred during drying/dry periods. Among events with negative CI , those combined with negative HI occurred during wetting/wet periods (Figure 2.6). In contrast, events with positive HI occurred during drying/dry periods and had the shortest duration, lowest total precipitation and lowest discharge and NO_3^- -N concentration (Table 2.2).

At the MEIS station, the general hysteresis pattern was the same as at the SILB station (i.e., 71% of events had negative *HI* with positive *CI*), but the percentage of positive *HI* with positive *CI* decreased to 8%, indicating an overall lower accretion effect (Table 2.2). Patterns of negative *HI* with negative *CI* increased to 17% of events at MEIS, with a relatively short duration and low discharge (Table 2.2). The pattern of positive *HI* with negative *CI* was least common and was evenly distributed among the wetting, drying and dry periods (Figure 2.6). Similarly, this pattern had the shortest duration and lowest total precipitation, discharge and NO_3^- -N concentration (Table 2.2).

The hysteresis pattern at the HAUS station differed strongly from those at the two upstream stations (Figure 2.6). The percentage of events with negative *HI* combined with positive *CI*, which dominated at upstream stations, decreased to only 27% at HAUS and had the longest duration, highest total precipitation and highest discharge and NO_3^- -N concentration (Table 2.2). The general pattern was negative *HI* with negative *CI*, which accounted for ca. 36% of all events. The pattern of positive *HI* with negative *CI* increased from < 5% at the upper two stations to 30% at the HAUS station. The pattern of positive *HI* with positive *CI* occurred only during drying/dry periods (Figure 2.6). Notably, regardless of *CI*, patterns with positive *HI* usually occurred during drying/dry periods (ca. 88%), with a short duration and low discharge and NO_3^- -N concentration, while patterns with negative *HI* occurred more during wetting/wet periods (ca. 73%), with a long duration and high discharge and NO_3^- -N concentration (Table 2.2).

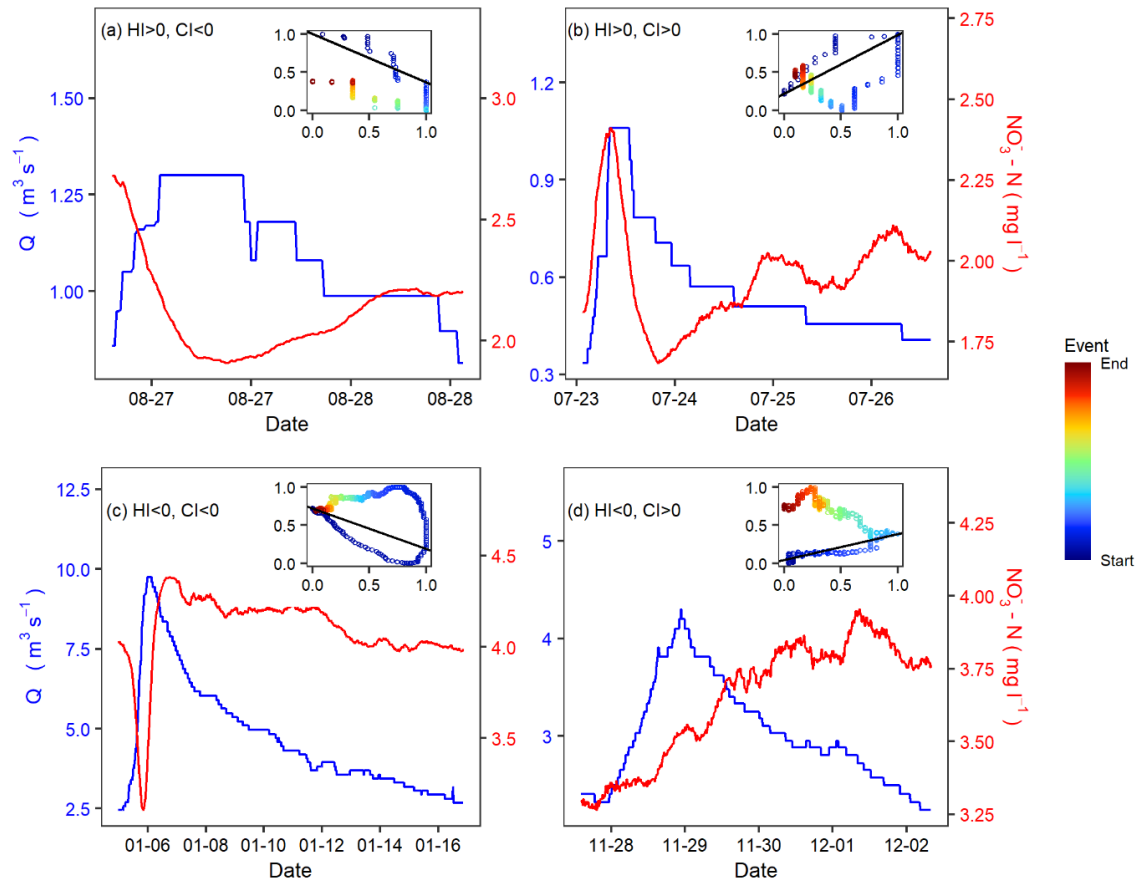


Figure 2.5. Examples of the four hysteresis types detected at the HAUS station: (a) an event in Aug. 2014 with a positive hysteresis index (HI) and positive concentration-change index (CI); (b) event in Jul. 2016 with a positive HI and negative CI ; (c) event in Jan. 2012 with a negative HI and positive CI ; and (d) event in Nov. 2017 with a negative HI and negative CI . Blue and red lines represent discharge and NO_3^- -N concentration, respectively. Inset plots show the corresponding hysteresis loops (from blue to red), in which the x-axis and y-axis are normalized values of discharge and NO_3^- -N concentration, respectively.

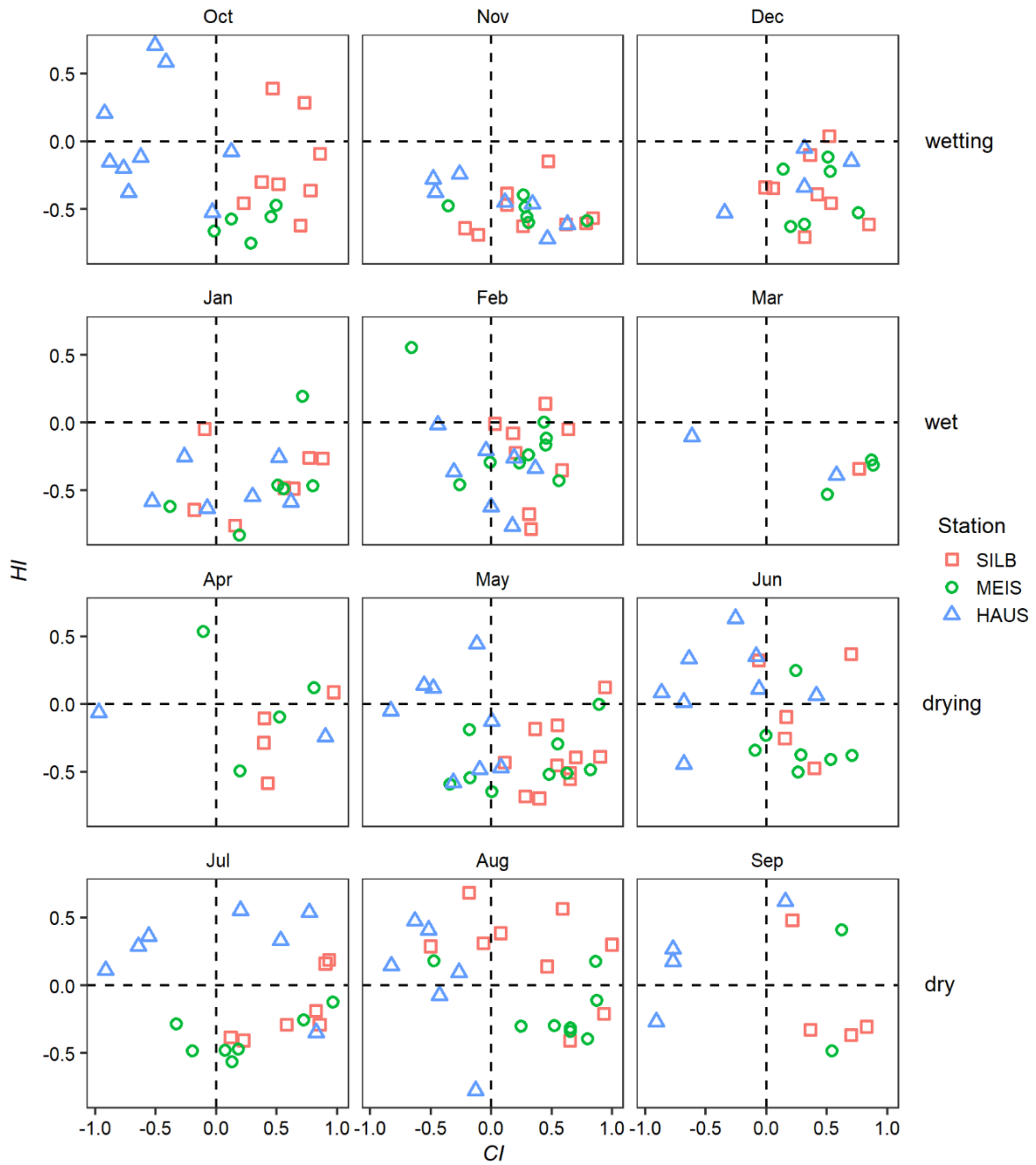


Figure 2.6. Hysteresis index (HI) and concentration-change index (CI) patterns at the SILB, MEIS and HAUS stations during the wetting, wet, drying and dry periods.

Table 2.2. Statistics of events of four hysteresis types based on sign of the hysteresis index (*HI*) and concentration-change index (*CI*) at the SILB, MEIS and HAUS stations (including number of storm events, mean duration, mean total precipitation (*P*), mean discharge (*Q*) and mean NO_3^- -N concentration).

<i>(HI/CI)</i>	SILB				MEIS				HAUS			
	(+/+)	(+/-)	(-/+)	(-/-)	(+/+)	(+/-)	(-/+)	(-/-)	(+/+)	(+/-)	(-/+)	(-/-)
Number	14	4	58	5	6	3	51	12	5	21	19	25
Duration (day)	4.6	2.5	8.7	6.7	14.0	4.4	8.0	5.4	2.1	4.8	10.2	9.3
Total P (mm)	18.70	4.17	27.66	20.00	27.60	7.52	23.78	20.26	12.32	20.45	22.64	19.28
Q ($\text{m}^3 \text{s}^{-1}$)	0.90	0.63	1.28	1.85	2.60	0.89	1.89	1.62	0.88	1.19	3.66	2.32
NO_3^- -N (mg l^{-1})	1.23	0.78	2.05	3.01	2.07	1.52	1.92	1.74	1.99	2.11	2.99	2.49

2.4.4. Shared events analysis

To investigate the influence of the landscape on seasonal flow and nitrate dynamics, we analyzed 24 catchment-wide shared events. Most shared events had negative *HI* at the SILB and MEIS stations, with only one event with positive *HI* at the MEIS station (Supplementary Table S2.2). Three shared events had positive *HI* during the dry period at the HAUS station, with a high contribution of NO_3^- -N load from the lowermost subcatchment (Table S2.2). The number of shared events with negative *CI* increased from upstream to downstream (i.e., 2, 3 and 12 at the SILB, MEIS and HAUS stations, respectively) (Table S2.2).

Runoff volume (R_V) and nitrate-N load (N_L) contributions from each subcatchment had strong seasonal variations at the event scale (Figure 2.7). During wetting/wet periods, $R_{V,UP}:R_{V,ALL}$ was significantly higher than $R_{V,MID}:R_{V,ALL}$ and $R_{V,LOW}:R_{V,ALL}$ (Kruskal-Wallis test). $R_{V,MID}:R_{V,ALL}$ and $R_{V,LOW}:R_{V,ALL}$ varied during the wetting period, but the former ratio increased and the latter one decreased during the wet period. During the drying period, $R_{V,UP}:R_{V,ALL}$ decreased quickly to a proportion similar to $R_{V,MID}:R_{V,ALL}$, while $R_{V,LOW}:R_{V,ALL}$ increased but remained lower than $R_{V,UP}:R_{V,ALL}$ and $R_{V,MID}:R_{V,ALL}$. During the dry period, contributions from the three subcatchments varied within a similar range, with slightly higher $R_{V,UP}:R_{V,ALL}$ than $R_{V,MID}:R_{V,ALL}$ and $R_{V,LOW}:R_{V,ALL}$.

Nitrate-N load contributions had a different seasonal pattern from runoff volume contributions (Figure 2.7b). During wetting/wet periods, nitrate-N load contributions from the three subcatchments generally followed runoff volume contributions (i.e., that from the uppermost subcatchment was significantly higher than that from the middle and lowermost subcatchments, Kruskal-Wallis test). Likewise, $N_{L,MID}:N_{L,ALL}$ and $N_{L,LOW}:N_{L,ALL}$ varied, with the former ratio increasing and the latter one decreasing. During the drying period, however, $N_{L,MID}:N_{L,ALL}$ increased quickly and ultimately

exceeded $N_{L,UP} : N_{L,ALL}$, while both $N_{L,UP} : N_{L,ALL}$ and $N_{L,MID} : N_{L,ALL}$ decreased to a similar low proportion. During the dry period, $N_{L,LOW} : N_{L,ALL}$ decreased. Thus, the subcatchment that contributed the most nitrate-N load varied among the four hydrological periods.

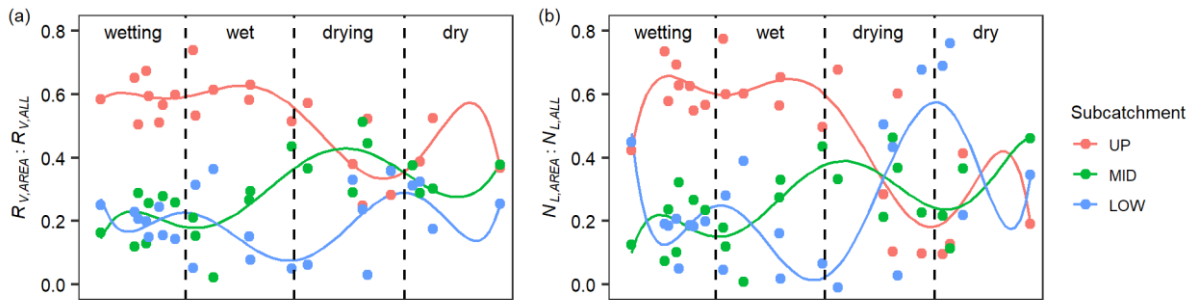


Figure 2.7. Contribution of (a) runoff volume (R_v) and (b) nitrate-N load (N_L) from each subcatchment to the catchment outlet for shared events throughout the year. Dashed lines separate the four hydrological periods. Solid lines indicate high-order polynomial regressions.

2.5. Discussion

Terrestrial nitrate transport at the catchment scale is strongly related to flow dynamics. In the Selke catchment, the land-to-stream transport has been identified as a key driven factor for surface water dynamics (Dupas et al., 2017). Due to the complex combination of meteorological, hydrological, geographical and pedological characteristics of each subcatchment, nitrate dynamics varied from upstream to downstream in the nested Selke catchment. Based on the hysteresis indices, four hysteresis patterns can be conceptualized (Figure 2.8). The driving factors of their occurrences in the Selke catchment (Figure 2.6) depend on the combinations of landscape features and hydrological conditions at the seasonal scale.

2.5.1. Characteristic patterns of flow and nitrate dynamics

The four hysteresis patterns varied strongly spatially and temporally. In the uppermost and forest-dominated middle subcatchments, the most common hysteresis pattern across different seasons was counter-clockwise hysteresis with an accretion effect during the rising limb (i.e., negative HI with positive CI , c.a. 70% at the SILB and MEIS stations). At the event scale, nitrate sources near stream reaches were flushed out quickly, which resulted in an accretion effect during the rising limb of the hydrograph, given the low ambient nitrate concentrations (Figure 2.8d). Although the uppermost mountainous regions contain considerable areas of agricultural land, nitrate cannot accumulate in the deeper subsurface due to the shallow impermeable bedrock and the consequently flashier flow pathways (Dupas et al., 2017; Yang et al., 2019). This feature results in higher nitrate concentrations in the interflow than in the baseflow. Consequently, a synchronous seasonal pattern of discharge and nitrate concentration was observed (i.e., generally high values during wetting/wet interflow-dominated periods and low values during drying/dry baseflow-dominated periods, Figure 2.2). Due to

sufficient precipitation during events and well-established hydrological connectivity, interflow can transport distal terrestrial nitrate sources to the stream, which further increases surface water nitrate concentrations. The time lag between hydrological celerity and solute transport velocity makes nitrate concentration normally peak after discharge do, which results in counter-clockwise hysteresis. However, this pattern decreased at the HAUS station, accounting for only 27 % and occurred more frequently during wetting/wet periods. Under high-flow and low-temperature conditions, the pattern at the catchment outlet was controlled more by the two upstream subcatchments due to their large contributions to both runoff volume and nitrate-N load (Figure 2.7) and low in-stream nitrate uptake (Rode et al., 2016a). Therefore, during wetting/wet periods, the hysteresis pattern at the HAUS station can depend more on upstream features than on those of the lowermost subcatchment.

The propagation effects also influenced the pattern of counter-clockwise hysteresis with a dilution effect at the three stations (Figure 2.8c). The uppermost and middle subcatchments had more saturation overland flow with lower nitrate concentration in forest areas (Zimmermann et al., 2006). Overland flow near streams can be generated quickly during wetting/wet periods with high discharge, causing a dilution effect at the beginning of events. The dominant runoff component of overland flow during the rising limb can be replaced by interflow quickly, with higher nitrate concentration, resulting in counter-clockwise hysteresis. This pattern was the most common pattern at the HAUS station. During wetting/wet periods, this hysteresis pattern at HAUS can be affected by the two upstream subcatchments as mentioned. Moreover, stream water routed from upstream subcatchments can also dilute nitrate concentration in the lowermost subcatchment, since the latter generally has higher nitrate concentration during low flow conditions (Figure 2.2), changing the hysteresis pattern from upstream accretion to downstream dilution across different seasons (Table S2.2). Besides influences from upstream subcatchments, features of the lowermost subcatchment can also cause a dilution effect. Urban/arable areas have been recognized to influence runoff generation in a catchment during storm events (Bronstert et al., 2002; Niehoff et al., 2002). Agricultural and municipal construction results in quick surface flow, which tends to decrease nitrate concentration. Dilution effects caused by surface flow during storm events were also observed in a mountainous agricultural catchment in California (USA) (Goodridge and Melack, 2012), mountainous agricultural catchments in the tropics (Jacobs et al., 2018) and urbanized catchments in North America (Barco et al., 2008). In this case, nitrate concentration decreased quickly at the beginning of the rising limb in the uppermost and lowermost subcatchments (Figure 2.5c), which both contain urban and arable areas (Figure 2.1). Interflow can then dominate quickly due to hydrological connectivity during wet periods, or baseflow can dominate again after quick flow during the dry period. In both situations, nitrate concentration increased after quick flow before the discharge peak, resulting in counter-clockwise hysteresis (Figure 2.8c). Therefore, this pattern dominated at the HAUS station not only due to events that propagated from upstream subcatchments, but also events generated in the lowermost subcatchment.

It was noticeable that clockwise hysteresis occurred more during drying/dry periods (Figure 2.6). Hydrological connectivity from land to stream can be limited by the higher temperature and lower soil moisture during drying/dry periods. Distal nitrate sources become immobilized and are not exported to the stream at low discharge, and thus resulted in clockwise hysteresis (Figure 2.5a). Our findings are in line with those of Baker and Showers (2019) who concluded that clockwise hysteresis was favored when antecedent soil moisture was low. In the uppermost subcatchment, the accretion effect was caused by plentiful proximal nitrate sources, as mentioned. In the middle subcatchment, atmospheric deposition is the main source of N in forest areas (MacDonald et al., 2002). Nitrate concentration has been reported to be higher in the topsoil than in groundwater due to uptake by deep-rooted vegetation and denitrification in deep soil layers (Chaves et al., 2009). Consequently, fewer distal nitrate sources can be transported to the stream during the baseflow-dominated dry period in the middle than in the uppermost subcatchment, which decreased the number of clockwise hysteresis at the MEIS station (Table 2.2). This pattern was the least common pattern at the HAUS station and occurred only during drying/dry periods (Figure 2.6). None of this pattern at HAUS belonged to shared event (Table S2.2). This indicated that this pattern could represent nitrate dynamics exclusively in the lowermost subcatchment. The lowermost subcatchment usually stores more nitrate due to mineral fertilizer and manure application. Saturated nitrate sources that are near the stream are easily flushed out when storm events occur, even at low discharge, leading to accretion effects (Figure 2.8b). Subsequently, nitrate concentration decreases quickly due to insufficient precipitation and low hydrological connectivity with distal nitrate sources, resulting in clockwise hysteresis.

The features of the lowermost subcatchment caused more clockwise hysteresis with the dilution effect (Figure 2.8a), which was the second-most common pattern at the HAUS station. This pattern appeared more during drying/dry periods when the lowermost subcatchment contributed considerable nitrate-N load and had substantial influence on nitrate export dynamics (Figure 2.7b). In this situation, the dilution effect at the HAUS station could be related to quick flow from paved areas in the lowermost subcatchment, as mentioned. Nitrate concentration followed a vertical gradient in the lowermost subcatchment: lower in the topsoil due to plant uptake and higher in deep soil due to legacy nitrate (Outram et al., 2016). Hydrological connectivity was low during drying/dry periods, and interflow could not increase enough to transport deep nitrate-rich sources to the stream, which results in the continued decrease in nitrate concentration during the falling limb. Therefore, clockwise hysteresis occurred more at the HAUS station than at the two upstream stations (i.e., only 4 and 3 times at SILB and MEIS, respectively).

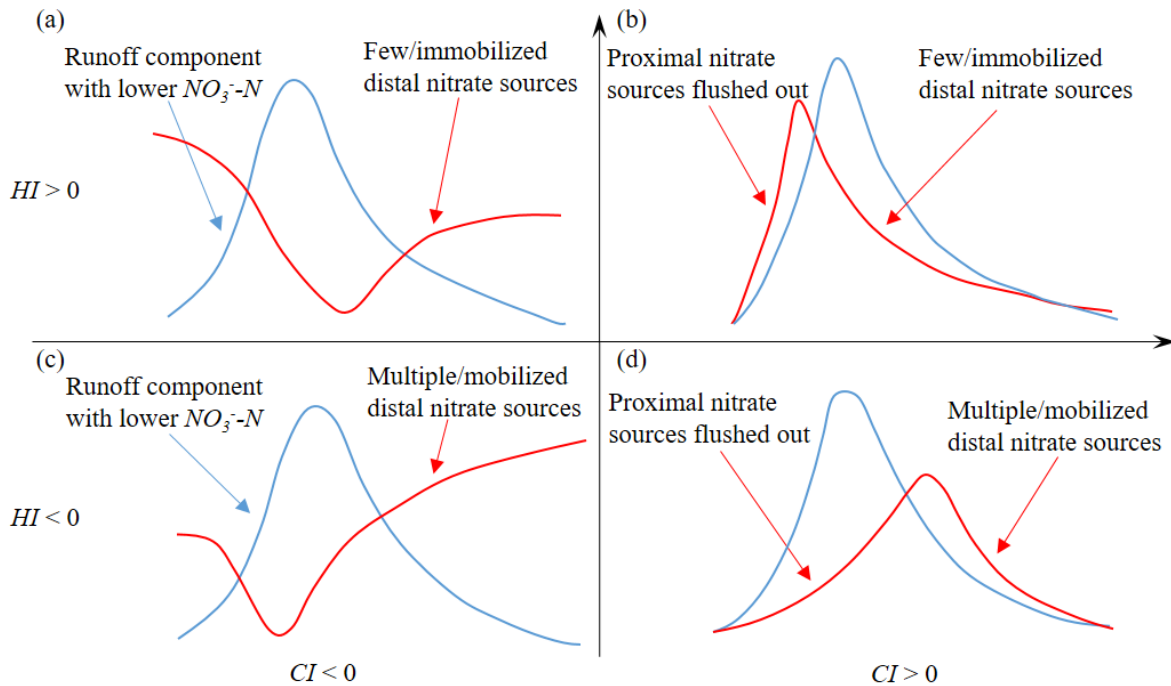


Figure 2.8. Conceptual interpretation of nitrate-discharge relationships during events for the four combinations of hysteresis index (HI) and concentration-change index (CI). Blue lines indicate flow behavior, and red lines indicate NO_3^- -N behavior. Arrows indicate dominant mechanisms during rising/falling limbs.

2.5.2. Implications and limits

Overall, the hysteresis pattern based on the C-Q relationship varied among landscapes, reflecting unique flow pathways and spatial nitrate storage. Due to different human activities (e.g., fertilizer application, drainage construction) and geological conditions, different patterns can dominate for a given dominant land use. For example, Carey et al. (2014) observed more clockwise hysteresis and a dilution effect in coastal catchments in which forest dominated. In contrast, we observed that counter-clockwise hysteresis with an accretion effect dominated in the upstream mountainous forest areas. This difference indicates that scientific monitoring should be set up according to meteorological, hydrological, geographical and pedological features rather than based only on land use. This is especially important in a nested catchment, where upstream subcatchment(s) can influence downstream subcatchment(s), and thus conceal nutrient export dynamics of the latter. Furthermore, differences in hydrological connectivity and biogeochemical processes due to seasonal variations can cause variable flow and nitrate dynamics (e.g., more clockwise hysteresis during drying/dry periods and more counter-clockwise hysteresis during wetting/wet periods). To disentangle seasonal effects, long-term high-frequency monitoring can provide reliable datasets. Our findings can be used to target mitigation measures when specific HI/CI combinations dominate in a given catchment. For example, when the C-Q relationship suggests that proximal nitrate sources dominate, management actions can

focus on agricultural land near streams, but when distal nitrate sources dominate, catchment-wide actions are required.

However, hysteresis analysis should also consider hydrographs with dual peaks or extremely long recession periods, which may influence the analysis (Lloyd et al., 2016b; Williams et al., 2018). Such hydrographs were rare in our study, but since they can improve understanding of process mechanisms during certain periods, they were not excluded. For example, the only shared event with positive *HI* at the MEIS station showed counter-clockwise hysteresis early in the event but was influenced by a dual peak and longer falling limb, which yielded a low positive value of *HI* (ca. 0.006). This analysis can improve understanding of the corresponding shared event at the SILB station that had negative *HI*: multiple distal sources can be consumed after a long period of flushing (e.g., during a large storm event) and cause lower nitrate concentrations during the late falling limb. This case requires catchment-wide management actions instead of focus on proximal streams, despite a positive *HI* at the MEIS station. Thus, events should be assessed carefully to avoid unreliable conclusions from statistical results, especially those with low values of *HI* or *CI*. Doing so may provide a detailed picture of variations in flow/nitrate dynamics.

Our comprehensive analysis of landscape and seasonality effects on flow and nitrate dynamics focused mainly on high-frequency monitoring data. Therefore, it is difficult to quantify the landscape effect in the three subcatchments of the Selke catchment, even when considering shared events. The landscape effect should be explored further using physical-based hydrological water-quality models. Current modeling is based mainly on daily data (Yang et al., 2018), which may bias detection of storm events and calculation of the nitrate-N load during storm events. Thus, future studies require high-frequency modeling, which can be used to quantify influential factors that result in different flow and nitrate dynamics and provide targeted advice for water management.

2.6. Conclusions

According to C-Q relationships, counter-clockwise hysteresis with an accretion effect dominated the catchment throughout the year; however, hysteresis was clockwise during specific periods in each subcatchment. Clockwise hysteresis occurred more during the dry period, indicating low hydrological connectivity from land to stream for export of distal nitrate sources. Dilution effects dominated in the lowermost catchment, which may have been influenced by flow propagating from upstream subcatchments during the wet period or generated by quick flow from paved areas.

When analyzing shared events, the uppermost subcatchment always dominated runoff volume and dominated nitrate-N load during all periods except the dry period, when the lowermost subcatchment dominated nitrate-N load, which indicates the substantial contribution of nitrate export regimes from the lower urban/arable area. At the event scale, this alternation suggests that high nitrate-loaded

interflow dominated in the upper mountainous subcatchments, while quick runoff (e.g., surface flow with low nitrate concentration) dominated in the lowermost subcatchment. This difference in nitrate export can increase during dry/hot seasons, when hydrological connectivity and biogeochemical processes change greatly.

These conclusions depend greatly on high-frequency data, which enabled events to be detected and nitrate-N load to be calculated more accurately. Although complex hydrographs may have influenced our results, the interpretation of the fundamental mechanism of variable C-Q relationships remains reliable. Water or agricultural management should be considered in complex conditions in which several mechanisms may coexist. Thus, a continuous and scientific monitoring strategy in a nested catchment is important to capture the nitrate export regime at the seasonal and catchment scale.

Acknowledgement

Xiaolin Zhang is funded by Chinese Scholarship Council (CSC). We would like to thank the Editor Huaming Guo, the Associate Editor Rafael Perez Lopez and the two anonymous Reviewers for their thoughtful comments. The high-frequency nitrate data are provided by TERENO (Terrestrial Environment Observatories) project. We thank the State Agency for Flood Protection and Water Management of Saxony-Anhalt (LHW) for providing high-frequency discharge data, German Weather Service (DWD) for providing precipitation data.

2.7. References

- Allen, A.P., Brown, J.H., Gillooly, J.F., 2002. Global biodiversity, biochemical kinetics, and the energetic-equivalence rule. *Science*. 297, 1545–1548. <https://doi.org/10.1126/science.1072380>.
- Baker, E.B., Showers, W.J., 2019. Hysteresis analysis of nitrate dynamics in the Neuse River, NC. *Sci. Total Environ.* 652, 889–899. <https://doi.org/10.1016/j.scitotenv.2018.10.254>.
- Barco, J., Hogue, T.S., Curto, V., Rademacher, L., 2008. Linking hydrology and stream geochemistry in urban fringe watersheds. *J. Hydrol.* 360, 31–47. <https://doi.org/10.1016/j.jhydrol.2008.07.011>.
- Borken, W., Matzner, E., 2004. Nitrate leaching in forest soils: an analysis of long-term monitoring sites in Germany. *J. Plant Nutr. Soil Sci.* 167, 277–283. <https://doi.org/10.1002/jpln.200421354>.
- Bowes, M.J., Jarvie, H.P., Halliday, S.J., Skeffington, R.A., Wade, A.J., Loewenthal, M., Gozzard, E., Newman, J.R., Palmer-Felgate, E.J., 2015. Characterising phosphorus and nitrate inputs to a rural river using high-frequency concentration–flow relationships. *Sci. Total Environ.* 511, 608–620. <https://doi.org/10.1016/j.scitotenv.2014.12.086>.
- Boyer, E.W., Goodale, C.L., Jaworski, N.A., Howarth, R.W., 2002. Anthropogenic nitrogen sources and relationships to riverine nitrogen export in the northeastern U.S.A. *Biogeochemistry* 57, 137–169. <https://doi.org/10.1023/A:1015709302073>.
- Bracken, L.J., Croke, J., 2007. The concept of hydrological connectivity and its contribution to understanding runoff-dominated geomorphic systems. *Hydrol. Process.* 21, 1749–1763. <https://doi.org/10.1002/hyp.6313>.
- Bronstert, A., Niehoff, D., Bürger, G., 2002. Effects of climate and land-use change on storm runoff generation: present knowledge and modelling capabilities. *Hydrol. Process.* 16, 509–529. <https://doi.org/10.1002/hyp.326>.

- Burns, D.A., Pellerin, B.A., Miller, M.P., Capel, P.D., Tesoriero, A.J., Duncan, J.M., 2019. Monitoring the riverine pulse: Applying high-frequency nitrate data to advance integrative understanding of biogeochemical and hydrological processes. *Wiley Interdiscip. Rev. Water* e1348. <https://doi.org/10.1002/wat2.1348>.
- Butturini, A., Alvarez, M., Bernal, S., Vazquez, E., Sabater, F., 2008. Diversity and temporal sequences of forms of DOC and NO₃-discharge responses in an intermittent stream: Predictable or random succession? *J. Geophys. Res.* 113. <https://doi.org/10.1029/2008jg000721>.
- Carey, R.O., Wollheim, W.M., Mulukutla, G.K., Mineau, M.M., 2014. Characterizing storm-event nitrate fluxes in a fifth order suburbanizing watershed using in situ sensors. *Env. Sci Technol.* 48, 7756–7765. <https://doi.org/10.1021/es500252j>.
- Chaves, J., Neill, C., Germer, S., Gouveia Neto, S., Krusche, A. V., Castellanos Bonilla, A., Elsenbeer, H., 2009. Nitrogen Transformations in Flowpaths Leading from Soils to Streams in Amazon Forest and Pasture. *Ecosystems* 12, 961–972. <https://doi.org/10.1007/s10021-009-9270-4>.
- Cheraghi, M., Jomaa, S., Sander, G.C., Barry, D.A., 2016. Hysteretic sediment fluxes in rainfall-driven soil erosion: Particle size effects. *Water Resour. Res.* 52, 8613–8629. <https://doi.org/10.1002/2016wr019314>.
- Davidson, E.A., David, M.B., Galloway, J.N., Goodale, C.L., Haeuber, R., Harrison, J.A., Howarth, R.W., Jaynes, D.B., Lowrance, R.R., Thomas Nolan, B., Peel, J.L., Pinder, R.W., Porter, E., Snyder, C.S., Townsend, A.R., Ward, M.H., 2011. Excess nitrogen in the U.S. environment: Trends, risks, and solutions. *Issues Ecol.* (available at <https://pubs.er.usgs.gov/publication/70032270>, last accessed on 9.6.2020)
- Dupas, R., Jomaa, S., Musolff, A., Borchardt, D., Rode, M., 2016. Disentangling the influence of hydroclimatic patterns and agricultural management on river nitrate dynamics from sub-hourly to decadal time scales. *Sci. Total Environ.* 571, 791–800. <https://doi.org/10.1016/j.scitotenv.2016.07.053>.
- Dupas, R., Musolff, A., Jawitz, J.W., Rao, P.S.C., Jäger, C.G., Fleckenstein, J.H., Rode, M., Borchardt, D., 2017. Carbon and nutrient export regimes from headwater catchments to downstream reaches. *Biogeosciences* 14, 4391–4407. <https://doi.org/10.5194/bg-14-4391-2017>.
- EEA, 2018. European waters -- Assessment of status and pressures 2018. European Environment Agency, Copenhagen, Denmark.
- EEA, 2019. Nutrients in freshwater in Europe. European Environment Agency, Copenhagen, Denmark.
- Fovet, O., Humbert, G., Dupas, R., Gascuel-Oudou, C., Gruau, G., Jaffrezic, A., Thelusma, G., Faucheux, M., Gilliet, N., Hamon, Y., Grimaldi, C., 2018. Seasonal variability of stream water quality response to storm events captured using high-frequency and multi-parameter data. *J. Hydrol.* 559, 282–293. <https://doi.org/10.1016/j.jhydrol.2018.02.040>
- Goodridge, B.M., Melack, J.M., 2012. Land use control of stream nitrate concentrations in mountainous coastal California watersheds. *J. Geophys. Res. Biogeosciences* 117, G02005. <https://doi.org/10.1029/2011JG001833>.
- Howarth, R., Swaney, D., Billen, G., Garnier, J., Hong, B., Humborg, C., Johnes, P., Mörth, C.-M., Marino, R., 2012. Nitrogen fluxes from the landscape are controlled by net anthropogenic nitrogen inputs and by climate. *Front. Ecol. Environ.* 10, 37–43. <https://doi.org/10.1890/100178>.
- Jacobs, S.R., Weeser, B., Guzha, A.C., Rufino, M.C., Butterbach-Bahl, K., Windhorst, D., Breuer, L., 2018. Using High-Resolution Data to Assess Land Use Impact on Nitrate Dynamics in East African Tropical Montane Catchments. *Water Resour. Res.* 54, 1812–1830. <https://doi.org/10.1002/2017wr021592>.

- Jiang, S.Y., Zhang, Q., Werner, A.D., Wellen, C., Jomaa, S., Zhu, Q.D., Büttner, O., Meon, G., Rode, M., 2019. Effects of stream nitrate data frequency on watershed model performance and prediction uncertainty. *J. Hydrol.* 569, 22–36. <https://doi.org/10.1016/j.jhydrol.2018.11.049>.
- Kruskal, W.H., Wallis, W.A., 1952. Use of Ranks in One-Criterion Variance Analysis. *J. Am. Stat. Assoc.* 47, 583–621. <https://doi.org/10.1080/01621459.1952.10483441>.
- Lloyd, C.E.M., Freer, J.E., Johnes, P.J., Collins, A.L., 2016a. Technical Note: Testing an improved index for analysing storm discharge-concentration hysteresis. *Hydrol. Earth Syst. Sci.* 20, 625–632. <https://doi.org/10.5194/hess-20-625-2016>.
- Lloyd, C.E.M., Freer, J.E., Johnes, P.J., Collins, A.L., 2016b. Using hysteresis analysis of high-resolution water quality monitoring data, including uncertainty, to infer controls on nutrient and sediment transfer in catchments. *Sci. Total Environ.* 543, 388–404. <https://doi.org/10.1016/j.scitotenv.2015.11.028>.
- MacDonald, J.A., Dise, N.B., Matzner, E., Armbruster, M., Gundersen, P., Forsius, M., 2002. Nitrogen input together with ecosystem nitrogen enrichment predict nitrate leaching from European forests. *Glob. Chang. Biol.* 8, 1028–1033. <https://doi.org/10.1046/j.1365-2486.2002.00532.x>.
- McDonnell, J.J., Beven, K., 2014. Debates—The future of hydrological sciences: A (common) path forward? A call to action aimed at understanding velocities, celerities and residence time distributions of the headwater hydrograph. *Water Resour. Res.* 50, 5342–5350. <https://doi.org/10.1002/2013WR015141>.
- Miller, J.D., Kim, H., Kjeldsen, T.R., Packman, J., Grebby, S., Dearden, R., 2014. Assessing the impact of urbanization on storm runoff in a peri-urban catchment using historical change in impervious cover. *J. Hydrol.* 515, 59–70. <https://doi.org/10.1016/j.jhydrol.2014.04.011>.
- Miller, M.P., Tesoriero, A.J., Hood, K., Terziotti, S., Wolock, D.M., 2017. Estimating Discharge and Nonpoint Source Nitrate Loading to Streams From Three End-Member Pathways Using High-Frequency Water Quality Data. *Water Resour. Res.* 53, 10201–10216. <https://doi.org/10.1002/2017wr021654>.
- Molenat, J., Gascuel-Oudou, C., Ruiz, L., Gruau, G., 2008. Role of water table dynamics on stream nitrate export and concentration in agricultural headwater catchment (France). *J. Hydrol.* 348, 363–378. <https://doi.org/10.1016/j.jhydrol.2007.10.005>.
- Musolff, A., Schmidt, C., Selle, B., Fleckenstein, J.H., 2015. Catchment controls on solute export. *Adv. Water Resour.* 86, 133–146. <https://doi.org/10.1016/j.advwatres.2015.09.026>.
- Musolff, A., Schmidt, C., Rode, M., Lischeid, G., Weise, S.M., Fleckenstein, J.H., 2016. Groundwater head controls nitrate export from an agricultural lowland catchment. *Adv. Water Resour.* 96, 95–107. <https://doi.org/10.1016/j.advwatres.2016.07.003>.
- Niehoff, D., Fritsch, U., Bronstert, A., 2002. Land-use impacts on storm-runoff generation: scenarios of land-use change and simulation of hydrological response in a meso-scale catchment in SW-Germany. *J. Hydrol.* 267, 80–93. [https://doi.org/10.1016/S0022-1694\(02\)00142-7](https://doi.org/10.1016/S0022-1694(02)00142-7).
- Outram, F.N., Cooper, R.J., Sünnerberg, G., Hiscock, K.M., Lovett, A.A., 2016. Antecedent conditions, hydrological connectivity and anthropogenic inputs: Factors affecting nitrate and phosphorus transfers to agricultural headwater streams. *Sci. Total Environ.* 545–546, 184–199. <https://doi.org/10.1016/j.scitotenv.2015.12.025>.
- Poor, C.J., McDonnell, J.J., 2007. The effects of land use on stream nitrate dynamics. *J. Hydrol.* 332, 54–68. <https://doi.org/10.1016/j.jhydrol.2006.06.022>.
- R Core Team, 2020. R: A language and environment for statistical computing. R Foundation for Statistical Computing, Vienna, Austria. <https://www.R-project.org/>.

- Racchetti, E., Bartoli, M., Soana, E., Longhi, D., Christian, R.R., Pinardi, M., Viaroli, P., 2011. Influence of hydrological connectivity of riverine wetlands on nitrogen removal via denitrification. *Biogeochemistry* 103, 335–354. <https://doi.org/10.1007/s10533-010-9477-7>.
- Reusch, T.B.H., Dierking, J., Andersson, H.C., Bonsdorff, E., Carstensen, J., Casini, M., Czajkowski, M., Hasler, B., Hinsby, K., Hyytiäinen, K., Johannesson, K., Jomaa, S., Jormalainen, V., Kuosa, H., Kurland, S., Laikre, L., MacKenzie, B.R., Margonski, P., Melzner, F., Oesterwind, D., Ojaveer, H., Refsgaard, J.C., Sandström, A., Schwarz, G., Tonderski, K., Winder, M., Zandersen, M., 2018. The Baltic Sea as a time machine for the future coastal ocean. *Sci. Adv.* 4, eaar8195. <https://doi.org/10.1126/sciadv.aar8195>.
- Rode, M., Halbedel Nee Angelstein, S., Anis, M.R., Borchardt, D., Weitere, M., 2016a. Continuous In-Stream Assimilatory Nitrate Uptake from High-Frequency Sensor Measurements. *Env. Sci Technol* 50, 5685–5694. <https://doi.org/10.1021/acs.est.6b00943>.
- Rode, M., Wade, A.J., Cohen, M.J., Hensley, R.T., Bowes, M.J., Kirchner, J.W., Arhonditsis, G.B., Jordan, P., Kronvang, B., Halliday, S.J., Skeffington, R.A., Rozemeijer, J.C., Aubert, A.H., Rinke, K., Jomaa, S., 2016b. Sensors in the Stream: The High-Frequency Wave of the Present. *Env. Sci Technol.* 50, 10297–10307. <https://doi.org/10.1021/acs.est.6b02155>.
- Shields, C.A., Band, L.E., Law, N., Groffman, P.M., Kaushal, S.S., Savvas, K., Fisher, G.T., Belt, K.T., 2008. Streamflow distribution of non-point source nitrogen export from urban-rural catchments in the Chesapeake Bay watershed. *Water Resour. Res.* 44, W09416. <https://doi.org/10.1029/2007wr006360>.
- Sickman, J.O., Leydecker, A., Chang, C.C.Y., Kendall, C., Melack, J.M., Lucero, D.M., Schimel, J., 2003. Mechanisms underlying export of N from high-elevation catchments during seasonal transitions. *Biogeochemistry* 64, 1–24. <https://doi.org/10.1023/A:1024928317057>.
- Strohmeier, L., Fovet, O., Akkal-Corfini, N., Dupas, R., Durand, P., Faucheux, M., Gruau, G., Hamon, Y., Jaffrezic, A., Minaudo, C., Petitjean, P., Gascuel-Oudou, C., 2020. Multi-temporal relationships between the hydro-climate and exports of carbon, nitrogen and phosphorus in a small agricultural watershed. *Water Resour. Res.* <https://doi.org/10.1029/2019wr026323>.
- Vaughan, M.C.H., Bowden, W.B., Shanley, J.B., Vermilyea, A., Sleeper, R., Gold, A.J., Pradhanang, S.M., Inamdar, S.P., Levia, D.F., Andres, A.S., Birgand, F., Schroth, A.W., 2017. High-frequency dissolved organic carbon and nitrate measurements reveal differences in storm hysteresis and loading in relation to land cover and seasonality. *Water Resour. Res.* 53, 5345–5363. <https://doi.org/10.1002/2017wr020491>.
- Wilcoxon, F., 1945. Individual Comparisons by Ranking Methods. *Biometrics Bull.* 1, 80–83. <https://doi.org/10.2307/3001968>.
- Williams, M.R., Livingston, S.J., Penn, C.J., Smith, D.R., King, K.W., Huang, C., 2018. Controls of event-based nutrient transport within nested headwater agricultural watersheds of the western Lake Erie basin. *J. Hydrol.* 559, 749–761. <https://doi.org/10.1016/j.jhydrol.2018.02.079>.
- Wollschläger, U., Attinger, S., Borchardt, D., Brauns, M., Cuntz, M., Dietrich, P., Fleckenstein, J.H., Friese, K., Friesen, J., Harpke, A., Hildebrandt, A., Jäckel, G., Kamjunke, N., Knöller, K., Kögler, S., Kolditz, O., Krieg, R., Kumar, R., Lausch, A., Liess, M., Marx, A., Merz, R., Mueller, C., Musolff, A., Norf, H., Oswald, S.E., Rebmann, C., Reinstorf, F., Rode, M., Rink, K., Rinke, K., Samaniego, L., Vieweg, M., Vogel, H.-J., Weitere, M., Werban, U., Zink, M., Zacharias, S., 2016. The Bode hydrological observatory: a platform for integrated, interdisciplinary hydro-ecological research within the TERENO Harz/Central German Lowland Observatory. *Environ. Earth Sci.* 76, 29. <https://doi.org/10.1007/s12665-016-6327-5>.
- Yang, X., Jomaa, S., Rode, M., 2019. Sensitivity Analysis of Fully Distributed Parameterization Reveals Insights Into Heterogeneous Catchment Responses for Water Quality Modeling. *Water Resour. Res.* 55, 10935–10953. <https://doi.org/10.1029/2019wr025575>.

- Yang, X., Jomaa, S., Zink, M., Fleckenstein, J.H., Borchardt, D., Rode, M., 2018. A New Fully Distributed Model of Nitrate Transport and Removal at Catchment Scale. *Water Resour. Res.* 54, 5856–5877. <https://doi.org/10.1029/2017wr022380>.
- Zacharias, S., Bogena, H., Samaniego, L., Mauder, M., Fuß, R., Pütz, T., Frenzel, M., Schwank, M., Baessler, C., Butterbach-Bahl, K., Bens, O., Borg, E., Brauer, A., Dietrich, P., Hajnsek, I., Helle, G., Kiese, R., Kunstmann, H., Klotz, S., Munch, J.C., Papen, H., Priesack, E., Schmid, H.P., Steinbrecher, R., Rosenbaum, U., Teutsch, G., Vereecken, H., 2011. A Network of Terrestrial Environmental Observatories in Germany. *Vadose Zo. J.* 10, 955–973. <https://doi.org/10.2136/vzj2010.0139>.
- Zhang, X.L., Zhang, Q., Werner, A.D., Tan, Z.Q., 2017. Characteristics and causal factors of hysteresis in the hydrodynamics of a large floodplain system: Poyang Lake (China). *J. Hydrol.* 553, 574–583. <https://doi.org/10.1016/j.jhydrol.2017.08.027>.
- Zimmer, M.A., Pellerin, B., Burns, D.A., Petrochenkov, G., 2019. Temporal Variability in Nitrate-Discharge Relationships in Large Rivers as Revealed by High-Frequency Data. *Water Resour. Res.* 55, 973–989. <https://doi.org/10.1029/2018wr023478>.
- Zimmermann, B., Elsenbeer, H., De Moraes, J.M., 2006. The influence of land-use changes on soil hydraulic properties: Implications for runoff generation. *For. Ecol. Manage.* 222, 29–38. <https://doi.org/10.1016/j.foreco.2005.10.070>.

2.8. Supplementary Materials

Please check the Supplementary Table S2.1 and S2.2 via the publication website (<https://doi.org/10.1016/j.jhydrol.2020.125585>).

Chapter 3: Disentangling in-stream nitrate uptake pathways based on two-station high-frequency monitoring in high-order streams

(This manuscript version is made available under the CC BY 4.0 license)

3.1. Abstract

In-stream nitrate (NO_3^-) uptake in rivers involves complex autotrophic and heterotrophic pathways, which often vary spatiotemporally due to stream hydraulic, biotic and abiotic variations. High-frequency monitoring of NO_3^- mass balance between upstream and downstream measurement sites can quantitatively disentangle multi-path NO_3^- uptake dynamics at the reach scale. However, this approach remains limited to a few river types and has not been fully explored for higher-order streams with varying hydro-morphological and biogeochemical conditions. We conducted two-station 15-min monitoring in five high-order stream reaches in central Germany, calculating the NO_3^- -N mass balance and whole-stream metabolism based on time series of NO_3^- -N and dissolved oxygen, respectively. With thorough considerations of lateral inputs, the calculated net NO_3^- -N uptake rates (U_{NET}) differed substantially among campaigns (ranging from -151.1 to 357.6 mg N m² d⁻¹, with cases of negative values representing net NO_3^- -N release), and exhibited higher positive values in the post-wet than in the dry period. Subtracting autotrophic assimilation (U_A , stoichiometrically coupled to stream metabolism) from U_{NET} , U_D represented net balance of heterotrophic NO_3^- -N uptake ($U_D > 0$, the dominance of denitrification and heterotrophic assimilation) and NO_3^- -N release ($U_D < 0$, the dominance of nitrification/mineralization). This rarely reported uptake pathway contributed substantially to U_{NET} patterns, especially during post-wet seasons; moreover, it appeared to exhibit various diel patterns, and for $U_D > 0$, diel minima occurred during the daytime. These findings advance understanding of complex reach-scale N-retention processes and can help develop future modeling concepts at the river-network scale.

3.2. Introduction

Excessive anthropogenic nitrogen (N) runoff from watersheds has been increasingly polluting aquatic ecosystems and causing eutrophication problems (Smith et al., 1999; Smith, 2003). One of the major diffuse-sources is fertilizers that have been applied intensively to increase agricultural production, and this anthropogenic N (mainly nitrate-nitrogen (NO_3^- -N)) has largely elevated N levels in river networks (Billen et al., 2013; Fowler et al., 2013). The capacity of stream biota to take up NO_3^- from the water column has attracted attention of environmental scientists and managers in the past few decades. Specifically, in-stream NO_3^- retention processes across headwaters and higher-order rivers are found to be able to buffer and mitigate significant NO_3^- pollution from further transporting to receiving waterbodies (Alexander et al., 2000; Zhao et al., 2015).

Despite this critical importance, accurately estimating rates of in-stream NO_3^- uptake at reach scales remains difficult, and partitioning it among different pathways (e.g., assimilation, denitrification) is even more difficult. Assimilation by photoautotrophs (U_A) is closely correlated with stream metabolism and, therefore, can be informed by gross primary production - GPP (Heffernan et al., 2010; Jarvie et al., 2018; Lupon et al., 2016). Heterotrophic uptake consists of assimilative uptake by heterotrophic microorganisms and dissimilatory denitrification (Jarvie et al., 2018). These uptake pathways are influenced by stream metabolism, stream morphology and ambient environmental conditions (Alberts et al., 2017; Heffernan et al., 2010; Kunz et al., 2017), and their complex convolution at the reach scale could result in high spatial and temporal variations in overall in-stream N dynamics. The seasonality of incoming solar radiation and riparian vegetation conditions can strongly influence GPP-related U_A (Alberts et al., 2017; Yang et al., 2019; Lupon et al., 2016). Agricultural and urban streams often exhibit high assimilatory NO_3^- uptake rates due to the elevated nutrient levels, but their N removal efficiency and relative N demand are much lower than forest streams (Arango et al., 2008). Restoring forest riparian buffers in these human-altered streams has been suggested as best management practice to help re-establish natural ranges of in-stream NO_3^- processing (Sobota et al., 2012; Sweeney et al., 2004). Therefore, river condition (e.g., riparian vegetation condition and sinuosity) is another important factor that influences denitrification efficiency, e.g., by affecting the water exchange with hyporheic zones (Gomez-Velez et al., 2015). NO_3^- uptake processes can also be strongly impacted by the seasonal variations of water temperature and flow conditions (Chamberlin et al., 2021; Hensley et al., 2015).

Several methods have been used to quantify NO_3^- uptake and partition its pathways, and each has inherent advantages and disadvantages. One approach is to add ^{15}N (Hall et al., 2009; Mulholland et al., 2002), but while it can provide pathway-specific inferences (Mulholland et al., 2009; Tank et al., 2018), its reliance on costly isotope addition logistically restricts its application to smaller streams. Pulse injections of unlabeled nutrients are an alternative approach (Covino et al., 2010) that can also be applied to larger rivers (Tank et al., 2018), but they usually provide no pathway-specific inferences. Moreover, these tracer-addition methods capture a snapshot of in-stream uptake processes, thus only representing a single set of conditions without considering temporal dynamics. More recently, advances in high-frequency in-situ sensor technology have enabled continuous monitoring of in-stream water quality parameters (Burns et al., 2019; Pellerin et al., 2012; Rode, Wade, et al., 2016). Because approaches based on in-situ monitoring are passive, they can be applied across stream orders and over extended periods, and can help to explore the spatiotemporal heterogeneity of NO_3^- uptake at sub-daily scales (Chamberlin et al., 2021; Rode, Halbedel Née Angelstein, et al., 2016).

Despite this advantage, several challenges remain, particularly regarding disentangling pathways. Heffernan and Cohen (2010) quantified NO_3^- assimilation and the sum of denitrification and heterotrophic assimilation based on diel variations in NO_3^- concentrations in a spring-fed river at a

single sampling station. For streams with dynamic upstream conditions, however, the one-station method is often limited to quantifying GPP-related autotrophic uptake during low-flow summer conditions (Rode, Halbedel Née Angelstein, et al., 2016; Yang et al., 2019). Alternatively, approaches based on two stations relax this constraint and have been successfully applied to investigate in-stream processes related to non-gaseous solutes such as NO_3^- (Hensley & Cohen, 2016; Kunz et al., 2017). Moreover, combining measurements of stream metabolism and NO_3^- mass balance help to disentangle and partition uptake pathways (Jarvie et al., 2018). In particular, this approach allows for subtracting assimilation uptake (U_A) from net uptake (U_{NET}) to quantify the rarely investigated remaining part (U_D), which represents heterotrophic uptake or NO_3^- release (Jarvie et al., 2018). Yet, the potential of multi-parameter two-station approaches has not been fully explored for describing dynamics of NO_3^- uptake patterns in high-order reaches with different stream conditions and under different seasons, nor for investigating detailed sub-daily patterns of pathway-specific NO_3^- uptake processes.

Here, we performed 11 campaigns of two-station high-frequency multi-parameter monitoring in five stream reaches in central Germany, which exhibit a variety of stream conditions in terms of morphological sinuosity and riparian and surrounding vegetation conditions. The objectives of this study were (1) to apply multi-parameter two-station approaches to disentangle NO_3^- uptake pathways (i.e., the net uptake U_{NET} , autotrophic assimilation U_A and their differences inferred heterotrophic uptake U_D) in heterogeneous high-order stream reaches under low-flow conditions, (2) to investigate pathway-specific uptake patterns and their variations between late spring (post-wet season) and summer (dry season) with varying stream conditions. and (3) to analyze the sub-daily pattern of U_D and its variability under different stream and seasonal conditions.

3.3. Data and methods

3.3.1. Study reaches

We selected two reaches (ca. 6 km each) in the 4th-order middle Weiße Elster River and three reaches (ranged 3-7 km) in the 6th-order middle and lower Bode River, all located in the lowland region of central Germany (Figure 3.1). These reaches exhibited substantial variation in stream morphological and surrounding landuse conditions (Table 3.1). The Weiße Elster River, ca. 250 km long, originates in the border region between the Czech Republic and Germany and flows north into the Saale River, Germany. In the middle Weiße Elster where the study reaches are located, NO_3^- -N concentrations have been increasing due to intensive agricultural activities and emissions from sewage-treatment plants (Wagenschein & Rode, 2008). The upstream reach (WE_1) (Figure 3.1a) and downstream reach (WE_2) (Figure 3.1b) have contrasting hydromorphological conditions (Table 3.1): WE_1 is artificially channelized and surrounded by arable land, whereas WE_2 conserves a highly sinuous morphology and passes through a patch of agricultural grassland. We stopped reach WE_2 ca. 100 m upstream of mining drainage to avoid the influence of groundwater discharge from the mine (Kunz et

al., 2017). The groundwater table in this area is low due to mining, which restricted interactions with groundwater during our measurements. Riparian deciduous trees surround the river corridor of both reaches, and the stream is partly shaded by broad leaves during the vegetation season.

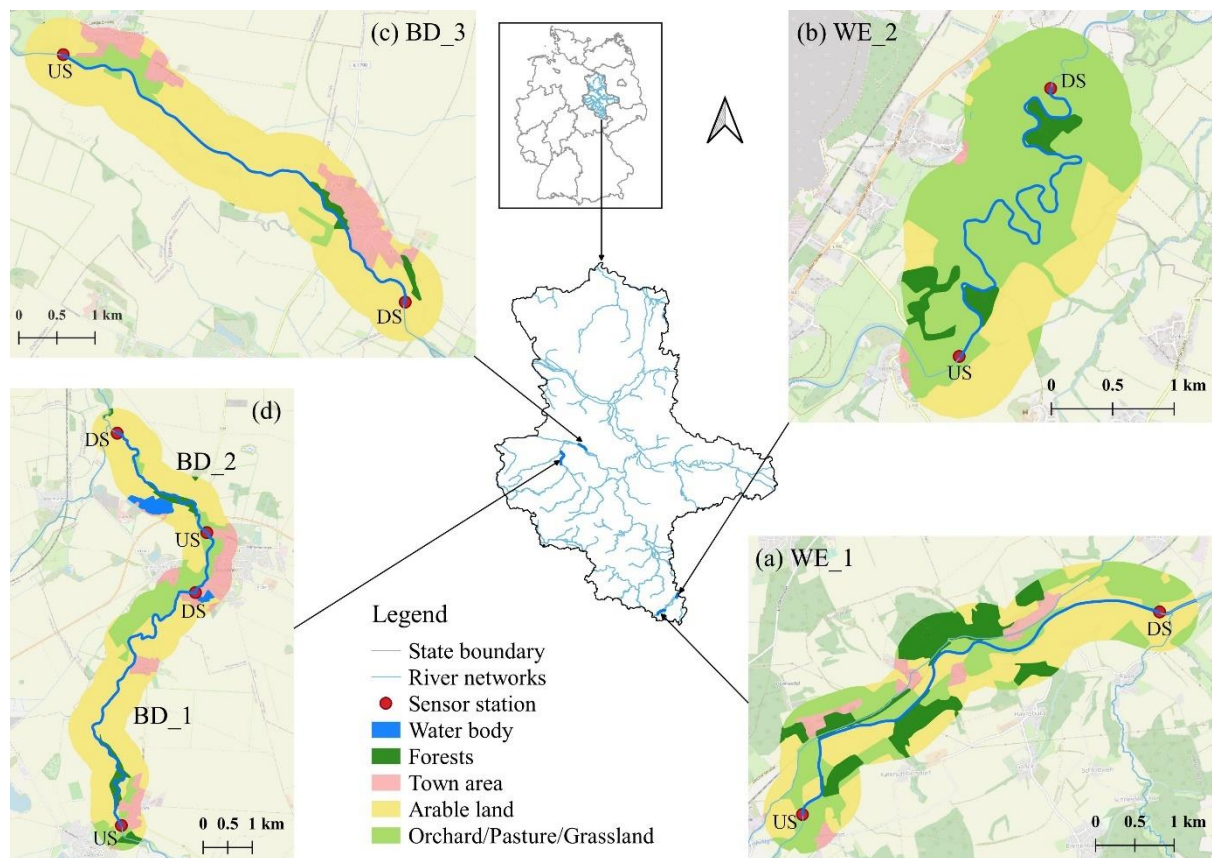


Figure 3.1. Locations of the five monitored stream reaches in Saxony-Anhalt, Germany, showing the two-station monitoring design (upstream station (US) and downstream station (DS)) and the riparian and morphological conditions of the reaches. The background map was taken from OpenStreetMap and riparian land uses (500 m on each side of the reaches) from CORINE (2018), from the Federal Agency for Cartography and Geodesy, BKG).

The Bode River, ca. 169 km long, originates in the Harz Mountain area and flows into the Saale River. The middle and lower Bode watershed has long been used for intensive agriculture due to its highly fertile Chernozem soils (Wollschläger et al., 2017). We chose two reaches (BD_1 and BD_2) in the middle Bode upstream of the confluence with the major tributary, the Holtemme, which is impacted greatly by urban effluent. Both reaches have relatively little sinuosity, indicating significant channel modification for surrounding agricultural use. Compared to BD_1 and BD_2, the lower Bode reach (BD_3) has a straighter river corridor (classified as “completely changed” by the State Agency for Flood Protection and Water Management of Saxony-Anhalt, Germany (LHW, 2022)) and is wider, with a gentler slope (Figure 3.1c and Table 3.1). In addition, more macrophytes were observed in BD_3 than in BD_1 and BD_2. Riparian vegetation, including deciduous trees, is extensive in all reaches, in addition to the varying surrounding land uses (Figure 3.1). The hydrology of the Bode

River corridor has also been altered by engineering structures. One weir is located between BD_1 and BD_2 and another is located ca. 700 m downstream of the BD_3 downstream station, both of which alter stream hydraulic characteristics and impound water upstream of the weirs.

Table 3.1. Morphological features of river reaches and overview of monitoring deployments.

Reach	River	Length (m)	Width (m)	Sinuosity	Slope (‰)	River morphology status ¹ & surrounding landscape ²	Deployment periods (start date - end date)	Campaigns (seasons)
WE_1	Weißer Elster	6280	23	1.20	0.5	Strongly modified and straightened; intensive arable land	2019/05/13-2019/05/16 2019/09/18-2019/09/23	2019-05 WE_1 (post-wet) 2019-09 WE_1 (dry)
WE_2	Weißer Elster	6100	23	2.65	0.89	Slightly modified and remains meandering; permanent grassland	2019/05/16-2019/05/20 2019/09/23-2019/09/26	2019-05 WE_2 (post-wet) 2019-09 WE_2 (dry)
BD_1	Middle Bode	7170	17	1.44	0.6	Slightly modified; considerable riparian forest and grassland	2019/06/17-2019/06/20 2020/08/03-2020/08/10	2019-06 BD_1 (post-wet) 2020-08 BD_1 (dry)
BD_2	Middle Bode	3360	17	1.24	0.6	Slightly to moderately modified; arable land with some forest	2019/06/20-2019/06/24 2020/08/12-2020/08/19 2021/07/19-2021/08/02	2019-06 BD_2 (post-wet) 2020-08 BD_2 (dry) 2021-07 BD_2 (transition)
BD_3	Lower Bode	6150	20	1.12	0.036	Completely changed; intensive arable land	2019/08/21-2019/08/26 2020/08/27-2020/09/03	2019-08 BD_3 (dry) 2020-08 BD_3 (dry)

Note: Sinuosity: the ratio of the curvilinear length (along the reach) to the Euclidean distance (straight line) between the end points of the reach. ¹ based on the “watercourse development status” classification of LHW (2022). ² CORINE (2018) from BKG

Discharge measurements were obtained from the nearest gauging stations operated by LHW: the Zeitz station (51°03'26"N, 12°08'37"E) for the Weißer Elster, the Wegeleben station (51°53'15"N, 11°11'22"E) for the middle Bode and the Hadmersleben station (52°00'20"N, 11°19'09"E) for the lower Bode, for which mean discharge from 2016-2020 was 11.99, 5.11 and 8.04 m³ s⁻¹, respectively. All campaigns were conducted during the low-flow period (May-September, see annual hydrographs Figure S3.1 in Text S3.2). Flow velocity ranged from 0.25-0.40 and 0.10-0.30 m s⁻¹ in the WE and BD reaches, respectively, estimated specifically for each campaign using the specific conductivity informed travel times (see Method 3.3.2).

3.3.2. Sensor deployment and data collection

For each reach selected, we set up in-situ sensors to monitor water chemistry at the upstream and downstream stations. At each station, an automated ultraviolet spectrophotometer (OPUS, ProPS WW, TriOS, Germany), with a precision of 0.03 mg l⁻¹ and accuracy of ± 2%, was deployed to measure NO₃⁻-N concentration. We used a sensor path length of 10 mm to measure absorption at wavelengths of 190-360 nm. Before each deployment, the sensors were calibrated and checked for measurement offsets by pre-running them side by side in the same stream water. A multi-parameter water-quality probe (EXO², YSI Environment, USA) was deployed to simultaneously measure water temperature (precision 0.001°C, accuracy ± 0.01°C), turbidity (precision 0.01 FNU, accuracy ± 2% FNU), pH (precision 0.01 units, accuracy ± 0.1), specific conductivity (precision 0.1 µS cm⁻¹, accuracy ± 0.5%), dissolved oxygen (DO, precision 0.01 mg l⁻¹, accuracy ± 1%) and *chlorophyll a* (*Chl-a*, precision 0.01 µg L⁻¹, linearity: R² > 0.999 for serial dilution of Rhodamine WT solution from 0-400 µg L⁻¹). The

two sensors were installed in a 20 cm diameter vented pipe to protect them from debris and other disturbances. The measurement frequency of both sensors was set to 15 minutes.

We conducted two or three campaigns per reach in different seasons, from May-June to August-September, representing post-wet and dry seasons, respectively, with an additional one conducted at BD_2 in July 2021 as transitional season (Table 3.1; Figure S3.1). The deployment length varied between 3 and 14 days, and the sensor built-in automatic cleaning wipers operated every one hour to prevent biofilm accumulation. During the 14-day campaign (2021-07 BD_2), we manually cleaned the pipes and probes at both stations after 7 days to ensure the data quality. We manually sampled water at both upstream and downstream stations on the first and last day of each campaign, and samples were prepared following the standard procedures in the Central Laboratory for Water Analytics & Chemometrics, Helmholtz Centre for Environmental Research – UFZ, Magdeburg, Germany. Detailed analytical descriptions can be found in Friese et al. (2014). NO_3^- -N, nitrite-N (NO_2^- -N), ammonium-N (NH_4^+ -N), total N (TN), soluble reactive phosphorus (SRP) and total phosphorus (TP) concentrations were measured. Concentrations of NH_4^+ -N were always low (with mean value 0.053 mg l^{-1}) in our study regions, therefore, we exclusively focused on NO_3^- -N uptake (Table S3.2). The laboratory analyses of grab sample NO_3^- -N concentrations were used as benchmarks for sensor verification, as instructed in the sensor manual. Finally, we performed longitudinal profiling (similar to Kunz et al., 2017) during the first campaign in each reach to identify potential inflows, e.g., small ditches and sewage pipes along the reach, during which we measured the same water chemistry parameters as we did at each station.

Sub-daily variations in specific conductivity were used as a natural tracer to estimate the mean travel time (τ) from upstream to downstream stations during each campaign by calculating the mean time lag between each corresponding peak and valley at upstream and downstream stations (for detailed information, see Text S3.1). Similar variations in NO_3^- -N concentrations were then used to cross-validate τ to ensure that it was estimated reasonably well.

3.3.3. Two-station method for assessing net nitrate uptake and stream metabolism

The two-station method was used to calculate reach-scale net NO_3^- -N uptake and stream metabolism. The areal net NO_3^- -N uptake (U_{NET}) was calculated as differences of inputs (from the upstream NO_3^- -N flux $Q_{US,t-\tau/2} \times [\text{NO}_3^- - N]_{US,t-\tau/2}$ and lateral seepage flux $Q_{L,t} \times [\text{NO}_3^- - N]_{L,t}$) and output of downstream flux $Q_{DS,t+\tau/2} \times [\text{NO}_3^- - N]_{DS,t+\tau/2}$, divided by total benthic area ($w \times L$):

$$U_{NET,t} = \frac{Q_{US,t-\frac{\tau}{2}} \times [\text{NO}_3^- - N]_{US,t-\frac{\tau}{2}} + Q_{L,t} \times [\text{NO}_3^- - N]_{L,t} - Q_{DS,t+\frac{\tau}{2}} \times [\text{NO}_3^- - N]_{DS,t+\frac{\tau}{2}}}{w \times L} \quad (1)$$

where Q_{US} and Q_{DS} denote upstream and downstream discharge, respectively (here we used the same values from nearby discharge gauging stations, Section 3.3.1); the width (w) was taken as the average

between upstream and downstream stations. Note that time-series of upstream and downstream fluxes were adjusted by $-\tau/2$ and $+\tau/2$, respectively, based on the estimated travel time τ between the two stations. Positive $U_{NET,t}$ indicates net NO_3^- -N uptake, whereas negative $U_{NET,t}$ indicates net NO_3^- -N release.

The lateral discharge inputs (Q_L) of three Bode reaches were estimated based on the drainage areas between the upstream and downstream stations and the daily runoff depth simulated using a grid-base catchment hydrological model. The NO_3^- -N concentration of the lateral seepage was roughly assigned as 2 mg l^{-1} for BD_1 and BD_2, 6.75 mg l^{-1} for BD_3 according to measurements from Bode lowland tributaries (from the state water authority-LHW). For the Weiße Elster reaches, we did not consider lateral inputs because of the small sub-areas and low groundwater levels. Further details of these lateral input considerations were provided in Supplementary Text S3.3.

Stream metabolism is typically measured using a one-station approach (Odum, 1956), but this method integrates over the entire upstream length required for reaeration to attenuate a diel signal (Chapra & Di Toro, 1991; Hensley & Cohen, 2016). This length ($3*v/k$) is much longer than that of our study reaches (Table S3.3). To estimate metabolism occurring within the same reach area as U_{NET} , we estimated areal net ecosystem production (NEP) using a two-station method. NEP was calculated from the mass-balance equation, which included measured DO concentrations and a reaeration term based on the Demars et al. (2011) method:

$$NEP_t = \frac{Q_{DS,t+\frac{\tau}{2}}[DO]_{DS,t+\frac{\tau}{2}} - Q_{US,t-\frac{\tau}{2}}[DO]_{US,t-\frac{\tau}{2}} - kQ_t[DO]_{def,t}}{w \times L} \quad (2)$$

where k denotes the reaeration coefficient that is determined by energy dissipation model (Tsvoglou & Neal, 1976) considering impacts of discharge and slope. $[DO]_{def}$ denotes the difference between saturation DO concentration and observed DO concentration over the entire reach (i.e., mean of $[DO]_{US,t-\frac{\tau}{2}}$ and $[DO]_{DS,t+\frac{\tau}{2}}$).

Nighttime ecosystem respiration (ER) is equivalent to nighttime NEP, assuming no primary production occurs at night. Daytime ER was calculated from mean nighttime NEP, and thus GPP was calculated as the sum of NEP and ER during the daytime (Bott, 2007; Roberts et al., 2007). Assuming that net primary production (NPP) equals half of GPP (Odum, 1957) and net photosynthetic quotient as one (i.e., 1 mol O_2 release with 1 mol CO_2 consumption), areal autotrophic assimilation uptake (U_A) was estimated from NPP and the stoichiometric C:N molar ratios of biofilm, which have been measured in each reach (Junge et al., 2005; Kamjunke et al., 2015) (eq. 3). The stoichiometric C:N molar ratios used were 7 and 9 for May and September in Weiße Elster, respectively, and 9.4 for the Bode. After subtracting the inferred U_A from U_{NET} , we interpreted the remaining part as heterotrophic uptake U_D , which reflects the inverse heterotrophic uptake (dissimilation via denitrification and

heterotrophic assimilation) and release (e.g., nitrification and remineralization) processes (eq. 4). Positive and negative U_D indicated the dominance of heterotrophic net NO_3^- -N uptake and net NO_3^- -N release, respectively.

$$U_{A,t} = \frac{GPP_t}{4.57 \times C:N} \quad (3)$$

$$U_{D,t} = U_{NET,t} - U_{A,t} \quad (4)$$

Because the original high-frequency measurements fluctuated greatly, we aggregated all data to hourly means for further analysis after all calculations. All calculations and statistical analyses (e.g., the ANOVA test) were performed using R software (Core Development Team, 2020).

3.4. Results

3.4.1. High-frequency measurements of stream water hydrological and physiochemical characteristics

The high-frequency measurements of water-quality parameters showed large variations across reaches, as well as across campaigns in each reach (Table 3.2 and S3.4). For the two reaches in the Weiße Elster (WE_1 and WE_2), although all campaigns were conducted during the low-flow period, Q in May 2019 was nearly two times higher than in September 2019. This likely contributed to the higher turbidity observed in May than in September. Within each reach, NO_3^- -N concentrations were similar in May and September, while between the two reaches, concentrations were slightly higher in the upstream reach WE_1 than the downstream reach WE_2. Water temperature in May was ca. 2°C lower than that in September for each reach, and that of WE_1 was generally lower than that of WE_2. DO concentrations were similar during all four campaigns (mean of ca. 10 mg l⁻¹), with slightly higher DO concentration and saturation percentage in May than in September for both reaches. Water pH and specific conductivity were significantly higher in WE_2 than in WE_1, and were significantly higher in September than in May for each reach. *Chl-a* was significantly higher in May than in September for WE_1, but the opposite for WE_2.

Water parameters had similar seasonal patterns during the five campaigns conducted over three years in the upper two reaches of the Bode River (BD_1 and BD_2). Discharge and associated turbidity decreased from June to August as the watershed continuously became dryer (Figure S3.1), and NO_3^- -N concentrations decreased slightly from June (> 1.60 mg l⁻¹) to August (< 1.34 mg l⁻¹). Water temperature was similar during all campaigns (17.0-21.7 °C). DO concentrations and saturation percentages were also similar, except for campaign 2020-08 BD_2, which had significantly lower values (ANOVA test, $p < 0.05$). The pH was higher in June than in August. Conversely, *Chl-a* was significantly lower in June than in August (means of 2.15 and 2.85 µg L⁻¹; ANOVA test, $p < 0.05$), except for the much lower concentrations (< 1.6 µg L⁻¹) during campaign 2021-07 BD_2.

The behavior of the downstream reach of the Bode River (BD_3) varied due to inputs from the upstream confluences of the Holtemme River and the lowland tributary Großer Graben (Figure 3.1), which are impacted greatly by urban wastewater and intensive lowland agriculture, respectively. Both campaigns were conducted in August, with similar environmental conditions for discharge, NO_3^- -N concentration, DO concentration and pH. However, water temperature and *Chl-a* concentration during the campaign in 2020 (16.18-17.03°C and 2.57 $\mu\text{g L}^{-1}$, respectively) were much lower than those in 2019 (17.49-20.04 and 4.46 $\mu\text{g L}^{-1}$, respectively).

Table 3.2. Overview of high-frequency measurements and stream characteristics for the 11 campaigns (i.e., means of upstream and downstream measurements).

Parameter	WE_1		WE_2		BD_1		BD_2		BD_3		
	2019-05	2019-09	2019-05	2019-09	2019-06	2020-08	2019-06	2020-08	2021-07	2019-08	2020-08
Q ($\text{m}^3 \text{s}^{-1}$)	9.06±0.38	4.55±0.18	8.58±0.44	4.75±0.26	2.5±0.11	1.57±0.08	2.34±0.17	1.65±0.31	1.93±0.17	1.98±0.11	2.2±0.06
T (°C)	11.84±0.97	13.09±0.5	13.29±2.1	15.17±0.41	19.52±0.7	19.3±1.39	19.35±0.47	20.65±0.64	18.54±1.11	18.56±0.78	16.74±0.24
N (mg l^{-1})	3.84±0.05	3.85±0.13	3.62±0.11	3.51±0.05	1.76±0.03	1.23±0.05	1.65±0.05	1.22±0.08	1.73±0.09	1.23±0.06	1.01±0.06
DO (mg l^{-1})	10.86±0.54	10.33±0.3	10.84±0.82	9.99±0.73	8.68±0.45	8.59±0.37	8.77±0.35	8.16±0.37	8.82±0.41	9.32±1.18	9.45±0.54
Turb (FNU)	1.91±0.23	1.53±0.16	1.78±0.11	1.52±0.17	3.84±0.17	1.8±0.22	4.21±0.44	2.11±0.58	4.05±0.61	1.2±0.14	1.2±0.11
pH	8.13±0.08	8.44±0.05	8.26±0.1	8.65±0.06	8.25±0.07	7.97±0.04	8.23±0.05	7.88±0.05	8.01±0.05	8.15±0.11	8.03±0.06
SpCond ($\mu\text{S cm}^{-1}$)	850.5±52.5	1224.4±39.0	1051.9±32.1	1337.6±16.1	727.5±6.5	733.0±23.5	822.6±21.6	789.0±48.6	768.6±32.9	1094.1±12.5	1169.9±31.6
<i>Chl-a</i> ($\mu\text{g L}^{-1}$)	4.19±0.57	2.72±0.47	2.63±0.45	3.2±0.26	2.12±0.15	2.84±0.58	2.19±0.13	2.8±0.6	1.35±0.13	4.46±0.85	2.57±0.13
τ (h)	5	7	4.5	6	8	14	3.5	4.5	4	14	15.5
v (m s^{-1})	0.35	0.25	0.38	0.28	0.25	0.14	0.27	0.21	0.23	0.12	0.11
k (10^{-5}s^{-1})	3.84	3.85	3.62	3.51	1.76	1.23	1.65	1.22	1.73	1.23	1.01

Note: Q: discharge. T: water temperature. N: NO_3^- -N concentration. DO: dissolved oxygen. Turb : turbidity.

SpCond: specific conductivity. *Chl-a*: *chlorophyll a*. τ : travel time from upstream to downstream stations. v : velocity, calculated by dividing river length by τ .

3.4.2. Whole-stream metabolism and NO_3^- -N uptake processes across reaches

Among all 11 campaigns, GPP showed consistent diel patterns, but with large variations across campaigns (Table 3.3; Figure 3.2). For the two reaches in the Weiße Elster (WE_1 and WE_2), GPP in May was significantly higher than that in September, whereas the absolute value of ER was significantly lower (ANOVA test, $p < 0.05$). For the middle Bode reach BD_1, GPP was similar during the campaigns in June 2019 and August 2020 (ca. 0.7 $\text{g O}_2 \text{ m}^{-2} \text{ d}^{-1}$), while the absolute ER of the former was twice as high as that of the latter (3.3 vs 1.6 $\text{g O}_2 \text{ m}^{-2} \text{ d}^{-1}$). In BD_2, mean GPP was the lowest in August 2020 and was similar in June 2019 and July 2021 (1.1-1.8 $\text{g O}_2 \text{ m}^{-2} \text{ d}^{-1}$). Mean ER was also the lowest in August 2020 and the highest in June 2019 (2.0-3.7 $\text{g O}_2 \text{ m}^{-2} \text{ d}^{-1}$). For the most downstream reach (BD_3), GPP of the two August campaigns in 2019 and 2020 was similar and among the highest of all campaigns.

Patterns of NO_3^- -N concentrations and net NO_3^- -N uptake (U_{NET}) in the 11 campaigns differed significantly across reaches, as well as among campaigns in the same reach (Table 3.3; Figure 3.3). In

the Weiße Elster River, mean autotrophic assimilation uptake (U_A) in May was higher than that in September in both reaches. Reach WE_2 showed continuously positive U_{NET} during both campaigns, but only the campaign in May 2019 showed positive U_D . In the Bode River, the two campaigns in BD_1 showed negative U_{NET} . In BD_2, the campaigns in June 2019 and July 2021 showed continuously positive U_{NET} , while in August 2020, U_{NET} was lowest and negative for several mid-day hours (with mean value $53.6 \text{ mg N m}^{-2} \text{ d}^{-1}$). In the most downstream reach (BD_3), continuously positive U_{NET} was observed during the two August campaigns; however, only the campaign in 2019 had positive U_D .

Table 3.3. Summary of daily mean whole-stream metabolism and in-stream N-uptake processes.

Processes	Units	WE_1		WE_2		BD_1		BD_2			BD_3	
		2019-05	2019-09	2019-05	2019-09	2019-06	2020-08	2019-06	2020-08	2021-07	2019-08	2020-08
GPP	$\text{g O}_2 \text{ m}^{-2} \text{ d}^{-1}$	2.7	1.7	2.8	2.2	0.8	0.7	1.6	1.1	1.8	4.1	4.6
ER	$\text{g O}_2 \text{ m}^{-2} \text{ d}^{-1}$	-1.6	-2.5	-1.2	-3.6	-3.3	-1.6	-3.7	-2.0	-2.5	-2.3	-3.2
U_{NET}	$\text{mg N m}^{-2} \text{ d}^{-1}$	-151.1	-30.5	319.6	33.7	-100.8	-61.2	357.8	53.6	130.9	133.7	86.8
U_A	$\text{mg N m}^{-2} \text{ d}^{-1}$	83.9	41.1	86.4	53.0	18.6	16.4	37.1	24.7	40.9	95.2	106.1
U_D	$\text{mg N m}^{-2} \text{ d}^{-1}$	-235.0	-71.5	233.2	-19.3	-119.4	-77.6	320.7	28.8	90.0	38.5	-19.3

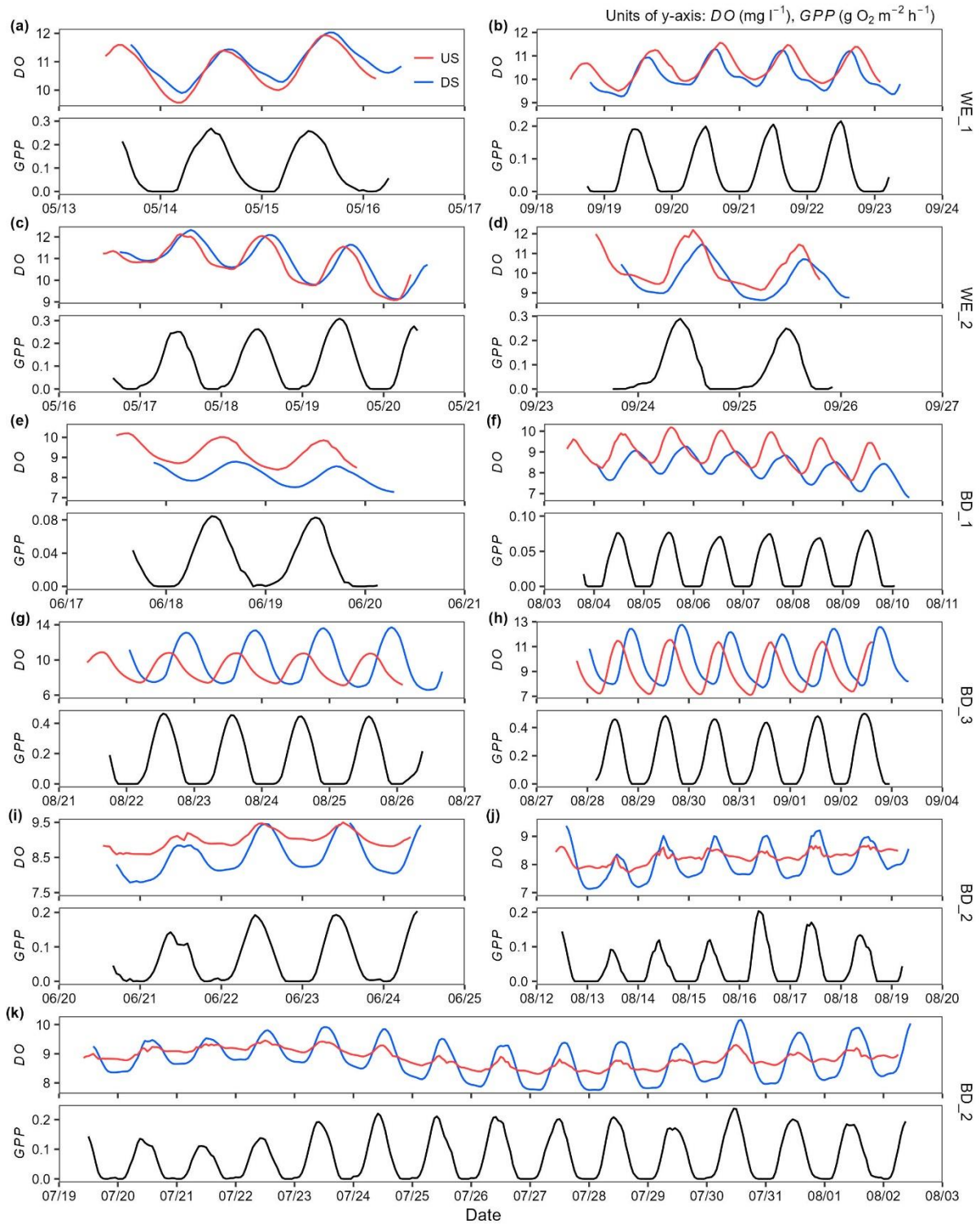


Figure 3.2. Time series of DO concentrations (mg l^{-1} , the upper panel of each subplot) at the upstream (US) and downstream (DS) stations, and the two-station based gross primary production (GPP, $\text{g O}_2 \text{ m}^{-2} \text{ h}^{-1}$, the lower panel of each subplot) for each of all campaigns at reaches WE_1 (a and b), WE_2 (c and d), BD_1 (e and f), BD_3 (g and h) and BD_2 (i-k).

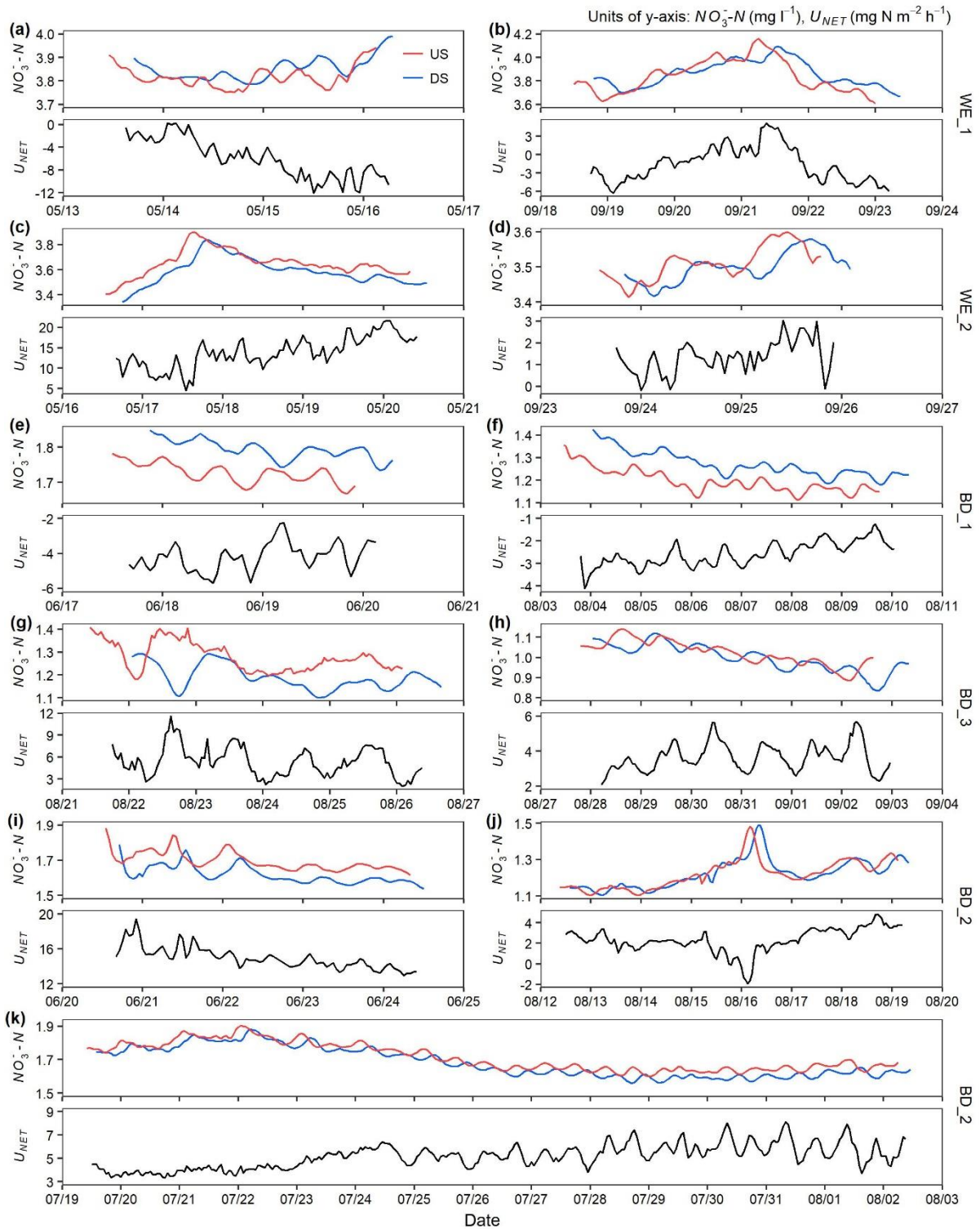


Figure 3.3. Time series of the measured $\text{NO}_3^- \text{-N}$ concentrations (mg l^{-1} , the upper panel of each subplot) at the US and DS stations and the two-station based areal net $\text{NO}_3^- \text{-N}$ uptake (U_{NET} , $\text{mg N m}^{-2} \text{h}^{-1}$, the lower panel of each subplot) for each of all campaigns at reaches WE_1 (a and b), WE_2 (c and d), BD_1 (e and f), BD_3 (g and h) and BD_2 (i-k).

3.4.3. NO₃⁻-N uptake pathways and their diel variations

The mass-balance based U_{NET} were partitioned into U_A and U_D at the sub-daily scale (Figure 3.4). Except for campaigns in WE_1 and BD_1, most campaigns exhibited $U_{NET} > 0$ (i.e., net NO₃⁻-N uptake), while their net uptake rates varied greatly (the daily mean U_{NET} ranged from 33.7 mg N m⁻² d⁻¹ during the 2019-09 WE_2 campaign to 357.8 mg N m⁻² d⁻¹ during the 2019-06 BD_2 campaign). In general, the net uptake was the highest in May-June post-wet season campaigns (Figure 3.4c and i), with generally much lower values in July-August campaigns (Figure 3.4g, j and k) and the lowest in late August and September dry season campaigns (Figure 3.4d and h). Moreover, U_{NET} was dominated mainly by U_D rather than U_A during the post-wet seasons, with U_D accounting for 90% and 73% of U_{NET} throughout the 2019-06 BD_2 and 2019-05 WE_2 campaigns, respectively. Interestingly, for the three campaigns in BD_2, U_{NET} decreased substantially from June to August, associated with decreasing U_D uptake (mostly > 0) proportions and increasing U_A proportions (Figure 3.4i-k). The absolute uptake rates of U_A were similar, while U_{NET} was significantly lower in July and August (i.e., 53.6 and 130.9 mg N m⁻² d⁻¹, respectively), resulting in dramatical decreases of U_D uptake rates, with even few negative values occurred during the mid-day hours in August (indicating net N release). Such decreased U_D and its further diurnal shift between uptake and release (U_D cross zero) were ubiquitously observed in our campaigns that have been conducted in dry seasons (see most of August and September campaigns in Figure 3.4).

The four campaigns conducted in WE_1 and BD_1 reaches (Figure 3.4a-b and e-f, respectively) showed ubiquitous negative U_{NET} (i.e., net NO₃⁻-N release), and the releasing rate of campaigns during post-wet seasons was generally higher than that of campaigns during dry seasons for the same reach.

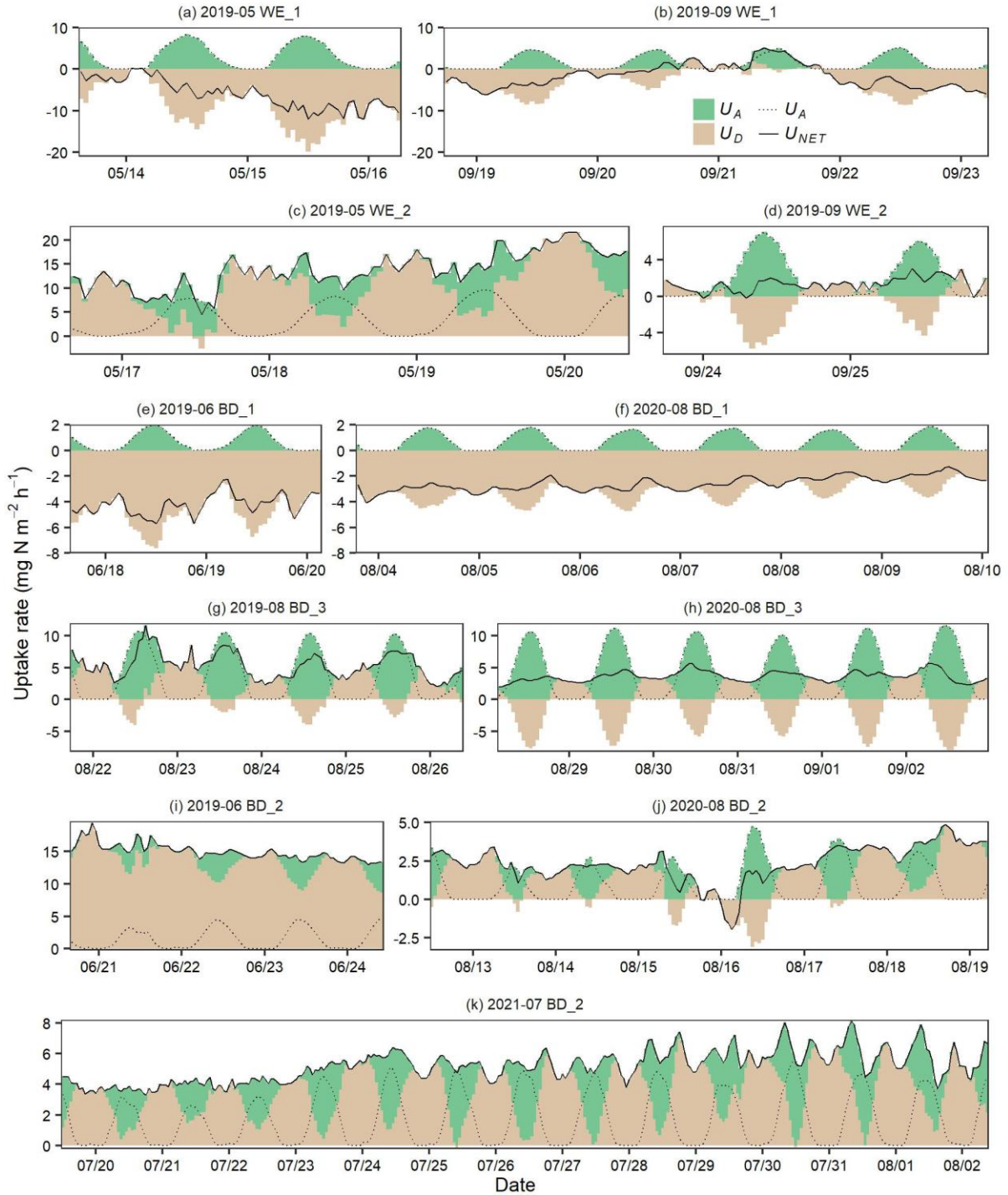


Figure 3.4. Sub-daily time series of the disentangled NO_3^- -N uptake pathways in all eleven campaigns. The overall net NO_3^- -N uptake (U_{NET}) rates were partitioned into autotrophic assimilation uptake (U_A , green colored area) and heterotrophic uptake (U_D , brown colored area). Note that negative U_{NET} indicates net NO_3^- -N release within the monitored reach, and negative U_D represents.

In addition to the seasonal and cross-reach variations, U_{NET} also showed various diel patterns among campaigns. For instance, during the daytime, U_{NET} decreased to its diurnal minima in campaigns 2019-05 WE_2 and 2021-07 BD_2 (Figure 3.4c and k) while increased to diurnal maxima during the

2019-08 BD_3 campaign (Figure 3.4g). For campaigns with $U_{NET} < 0$, the net NO_3^- -N release also varied diurnally, likely increasing during the daytime (e.g., Figure 3.4a and e). As the remaining part of subtracting U_A from U_{NET} , U_D exhibited distinct diel signals (Figure 3.5). For campaigns with consistent $U_D > 0$ in Figure 3.5a, the heterotrophic NO_3^- -N uptake exhibited obvious decreasing diel pattern (i.e., the minima occurred during the daytime) because U_{NET} did not increase equally with the increases of U_A and sometimes even decreased significantly. In contrast, for campaigns with consistent $U_D < 0$ in Figure 3.5b, the nitrification N release increased during the daytime, accompanied with higher day-time net release (i.e., higher values of $|U_{NET}|$ shown in Figure 3.4). Interestingly, despite of the large variability of U_D , the relative degrees of its diel variations (i.e., hourly U_D rescaled by the mean of each day) were largely consistent within a campaign duration (Figure 3.5), and similar across reaches (e.g., campaigns 2019-08 WE_2 and 2021-07 BD_2) and seasons (e.g., the June and August campaigns in BD_1). Also, it is worth noting that such diel variations could be largely masked when net uptake rates were very high (e.g., up to ca. $357 \text{ mg N m}^{-2} \text{ d}^{-1}$ in campaign 2019-06 BD_2, right after a moderate flow event, Figure S3.2) or be affected by dramatic changes of stream environments (e.g., water temperature decreased by $2 \text{ }^\circ\text{C}$ and specific conductivity increased by $100 \text{ } \mu\text{S cm}^{-1}$ during the second day of campaign 2019-05 WE_1, Figure S3.5a).

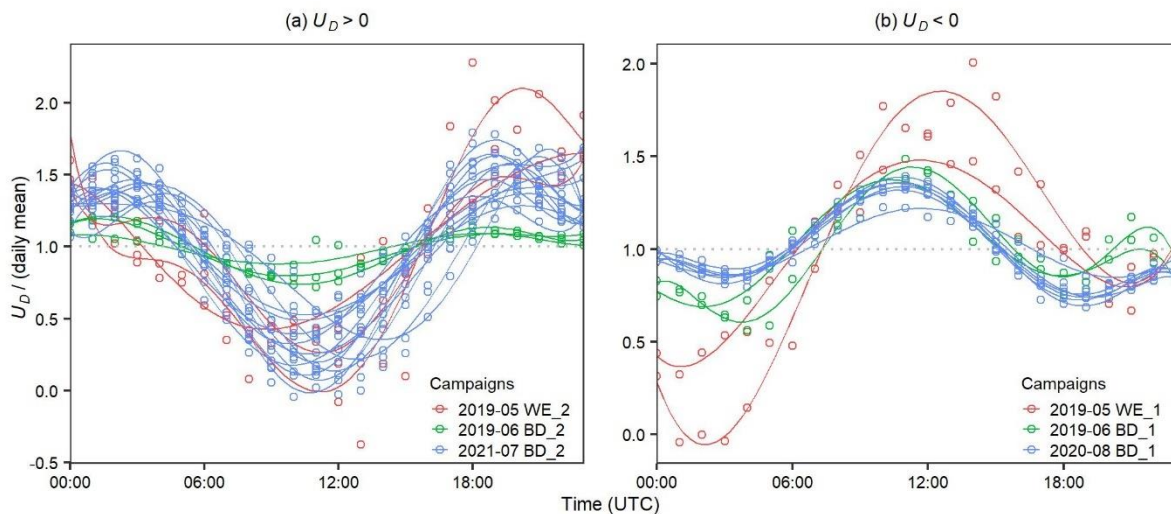


Figure 3.5. Diel patterns of the subtracted U_D . The rescaled U_D in y-axes were calculated as hourly U_D divided by the mean values in each day. Note that here we only showed campaigns exhibiting consistent heterotrophic uptake $U_D > 0$ (a) or release $U_D < 0$ (b).

3.5. Discussion

3.5.1. Stream metabolism and the informed autotrophic N assimilation

During the 11 campaigns, DO concentrations showed clear diel patterns that generally peaked near midday. At the downstream station of reaches BD_1 and BD_3, DO peaked near midnight, with a consistent time lag compared to the upstream DO peaks (Figure 3.2). Artificial channel weirs were

located ca. 700 meters downstream of both downstream stations, which might have induced impoundment effects that slowed the flow velocity and decreased the reaeration rate (Churchill et al., 1964) (see also Table 3.2). Moreover, GPP can be higher in the afternoon than in the morning with similar radiation due to higher temperatures at the cellular level (Beaulieu et al., 2013) or changes in the influence of riparian vegetation shading due to channel orientation (azimuth) (Julian et al., 2008). Moreover, complex hydraulic characteristics in high-order reaches (e.g., dispersion and transient storage) and their impacts on DO signals largely affected direct inferences of stream metabolism using two-station monitoring data (Hensley & Cohen, 2016), and future research could be oriented to further integrate high-frequency data analysis with hydraulic simulations.

The two-station inference of GPP varied largely among the 11 campaigns (ranged between 0.7 and 4.6 g O₂ m⁻² d⁻¹, Table 3.3), primarily due to combined effects of multiple stream environmental controls (e.g., radiation variations among seasons and varying riparian shading in different reaches). Based on the stoichiometric conversion (eq. 3), this directly generated the high variability of inferred NO₃⁻-N uptake by autotrophic assimilation (U_A) among our campaigns (ranged between 16.4 and 106.1 mg N m⁻² d⁻¹). Although widely applied in literature, such stoichiometric relationship needs to be cautiously verified for specific sites, especially at the sub-daily scales. We obtained C:N molar ratios from local biofilm measurements (Junge et al., 2005; Kamjunke et al., 2015), and the derived 42.9 g O₂ per gram N assimilation in the Bode River (4.57×9.4 in eq.3) was comparable with regression slopes of 38.8 and 36.6 at the Hausneindorf site (8 km south of the BD_1) where U_A was directly inferred from diel amplitudes of NO₃⁻-N concentrations during low-flows (see Rode, Halbedel Née Angelstein, et al. (2016) and Yang et al. (2019)).

3.5.2. Nitrate transport and uptake processes

Unlike the consistent diel patterns of DO, NO₃⁻-N concentrations varied greatly among campaigns. The expected diel pattern of NO₃⁻-N concentrations decreasing to minima during the daytime due to assimilation uptake U_A (Heffernan & Cohen, 2010; Rode, Halbedel Née Angelstein, et al., 2016), was rarely observed at individual stations. Compared to upstream perturbations of gaseous-based DO (here, variable tributaries and effluents), those of non-gaseous NO₃⁻ signals persist much longer due to the lack of atmospheric equilibration, which obscures the diel uptake signals using one-station inferences (Hensley & Cohen, 2016). This agrees with previous one-station based studies that observed clear diel signals mostly under steady upstream input (e.g., in spring-fed rivers (Heffernan & Cohen, 2010)) or during low-flow summer periods (Rode, Halbedel Née Angelstein, et al., 2016). Such methodological limitations can be largely relaxed using the two-station inference, as the present study, to extract diel patterns of in-stream NO₃⁻-N uptake from comparative upstream and downstream NO₃⁻-N signals.

Combined with whole-stream metabolism, estimates of NO₃⁻-N balances based on two-station measurements showed high spatiotemporal variability of different NO₃⁻-N uptake pathways at reach

scale. One reason could be differing degrees of hydro-biochemical connectivity between river channels and off-channel storage zones. Flow pathways from different sub-ecosystem compartments converge along the river network, and the varying residence times, contacting volumes and stream substrates create spatial and temporal variations in biogeochemical reactions (Anlanger et al., 2021; Harvey et al., 2019). Net NO_3^- -N uptake (U_{NET}) during the 2019-05 WE_2 campaign was among the highest, primarily due to the campaign period right after the annual wet season and the more natural stream conditions (Figure 3.1; Table 3.1). It is widely reported that more natural stream reaches can retain more nutrients than highly modified reaches (Sweeney et al., 2004; Hall et al., 2009; Hester et al., 2018). Moreover, other compartments (e.g., adjacent riparian corridors, floodplains, the hyporheic zone) could be more active along natural reaches, which could be important N sinks involving high rates of assimilation (by both autotrophs and heterotrophs) and dissimilation (e.g., denitrification) uptake (Helton et al., 2011; Mulholland et al., 2008). Notably, the heterotrophic uptake (U_D) pathway represented ca. 73% of U_{NET} during this campaign, indicating that heterotrophic uptake processes (including assimilation by heterotrophs and dissimilation via denitrification) were active during the post-wet seasons (May-June). This phenomenon was clear when comparing June 2019 and July 2021 campaigns in reach BD_2 (U_D accounted for 90% and 69% of total uptake, respectively, Figure 3.4i and k), in which the former was conducted immediately after a high-flow event receded (Figure S3.2b). The annually high discharge during the wet season can deliver large amounts of fresh organic matter to river networks, especially the labile fraction, which can increase biogeochemical activity greatly (Fellman et al., 2009; Tesi et al., 2008), and denitrification can be promoted when vertical turbulent mixing interacts with sediments in mid-size rivers (Harvey et al., 2019). Moreover, mean *Chl-a* concentration increased greatly from 15 April ($5.67 \mu\text{g l}^{-1}$) to the beginning of July 2019 ($9.85 \mu\text{g l}^{-1}$) (see Figure S3.10 for long-term in-situ monitoring data at station GGL ($52^\circ 00' 03'' \text{ N}$, $11^\circ 21' 21'' \text{ E}$) close to the upstream site of BD_3). Increasing stream water temperature was unlikely responsible for such uptake variations since it was already $> 10^\circ\text{C}$ in late spring and early summer (data from station GGL), and the temperature during all campaigns (Table 3.2) was likely sufficient to ensure active biogeochemical reactions (Dawson & Murphy, 1972).

Even with above thorough considerations, we noted that estimating the complex lateral subsurface seepage into rivers is still challenging, especially in the flat-topographic lowland regions with heavily human-altered landscapes. For instance, the consistently negative U_{NET} in BD_1 reach (Figure 3.4e and f) could have embedded substantial uncertainties, due to that (1) the DEM-derived drainage network diverted largely from the artificially modified channels in the lower part of the sub-catchment (Figure S3.3), and (2) there existed high gradients of groundwater table, indicating complex deeper groundwater dynamics (data from LHW groundwater wells, Figure S3.4). Nevertheless, there are several ways of detecting potential impacts of such lateral inputs and obtaining first estimate. Specific conductivity can indicate additional water sources other than upstream inputs. For instance, the

consistently higher values at the downstream station than the upstream station of BD_1 (Figure S3.7) directly supported above inference of substantial lateral inflows from groundwater seepage along the BD_1 reach. The two WE reaches, in contrast, showed marginal differences of specific conductivity between upstream and downstream stations, confirming that lateral inflows had negligible influence on mass balance calculations.

Notably, negative U_{NET} needs to be critically interpreted. On the one hand, the higher downstream N loading might be contributed from underestimated lateral inputs or from additional unquantified sources. This would be particularly the case for reaches exhibiting consistent negative values (e.g., the above discussed BD_1 reach). On the other hand, the negative values could be caused by actual NO_3^- release from stream organic storage with short turnover times (e.g., nitrification, N from the reduced state to a more oxidized state). These transformations depend greatly on NH_4^+ concentration, substrate types and organic carbon (Bernhardt et al., 2002; Day & Hall, 2017; Kemp & Dodds, 2002). The production of NO_3^- by nitrification could partially offset the decrease of NO_3^- concentrations and further the calculated NO_3^- -N uptake.

3.5.3. Heterogeneous diel variations in nitrate uptake pathways

We estimated assimilation uptake (U_A) from the GPP signal assuming a constant stoichiometric C:N ratio. Because of this, both the timing and magnitude of U_A is directly coupled to GPP. GPP always had a strong increasing diel pattern (i.e., diel maxima during the daytime) during all campaigns (Figure 3.4) over a variety of radiation and riparian-shading conditions. While the temporal and stoichiometric coupling of autotrophic uptake with primary production is often assumed, it has been called into question by Appling and Heffernan (2014) and confirmed by Chamberlin et al. (2019). They suggest that de-coupling occurs significantly at low nutrient concentrations, which is not the case in any of our study reaches. Moreover, we tested scenarios of U_A lagging 1-3 hours after GPP and observed that diel minima/maxima of the net uptake (U_{NET}) were indeed delaying GPP maxima for some campaigns (e.g., 2019-08 BD_3 and 2021-07 BD_2, see details in Supplementary Section 3.8). We noted that (1) the lag times were difficult to be determined (not consistent across the 11 campaigns), and moreover (2) the further disentangled NO_3^- -N uptake pathways and their variability of diel patterns remained unaltered. Therefore, we believe that the assumption of synchronous GPP and U_A was reasonable for our study. Of course, we noted that this physiological time lag should be critically evaluated and carefully determined, especially for studies focusing on the timing of diel signals.

The reason for the diel pattern in U_D is complex, involving counterbalance of inverse processes of heterotrophic NO_3^- -N uptake and NO_3^- -N release, and varying signals of multiple measurements. For campaigns with $U_{NET} > 0$, the decreasing diel signals (i.e., diel minima during the daytime) of U_D could have largely leveraged from subtracting U_A that has the opposite diel signals. However, the

directly measured U_{NET} exhibited obvious and extensive decreasing during the daytime (e.g., the majority of dates during campaigns 2019-05 WE_2 and 2021-07 BD_2, Figure 3.4c and k, respectively). This provided direct evidence that the heterotrophic NO_3^- -N uptake processes (for cases of $U_D > 0$, Figure 3.5a) could decrease significantly during the daytime and contribute to diel variations of NO_3^- -N concentration. These diel patterns in U_D are often overlooked in reach-scale nutrient-removal studies, where diel variations in nutrient concentrations are assumed to result from U_A (Heffernan & Cohen, 2010) or additionally from diurnal hydraulic variations (Hensley, et al., 2015). Denitrification can become the dominant process in total NO_3^- -N uptake as evidenced by measuring isotopes (Cohen et al., 2012). Experimental evidence has revealed that the denitrification rate can decrease at sunrise in the water column and in sediment using an open-channel N_2 method (Reisinger et al., 2016); denitrification rates show large diel variations related to temperature in the hyporheic zone, as simulated by a physical model (Zheng & Bayani Cardenas, 2018). In addition, the decreasing U_D diel pattern (Figure 3.5a) could be influenced by the increase of DO during the daytime, since DO usually inhibits denitrification but stimulates nitrification, both having the same net effect on the decrease in NO_3^- -N removal. Besides the influence of DO, the diel pattern could also have resulted from N fixation that can balance heterotrophic assimilation (Welsh et al., 2000), resulting in an overall decreasing pattern during the daytime. Although uncertainty may embed in cases with $U_{NET} < 0$ (and consequently $U_D < 0$, Figure 3.5b), the diel pattern with maxima occurring during the daytime agreed well with the inferred N releasing processes (e.g., nitrification), which may be promoted by increasing DO and water temperature during the daytime (Gammons et al., 2011).

3.5.4. Further perspectives of in-stream process monitoring and network modeling

Benefiting from the flexibility of high-frequency sensor monitoring, this study extended the two-station inferences of in-stream NO_3^- -N processes to different high-order reaches under varying environmental conditions, including thorough considerations of lateral inputs. Combining direct measurements of stream metabolism and NO_3^- -N mass balance allowed for disentangling various NO_3^- -N uptake pathways and further investigating their spatiotemporal variability. In addition to the well-explored autotrophic assimilation U_A and the more intuitive U_{NET} , one of the major novelties of this study is to quantitatively infer the reach-scale U_D , which represents the relative dominance of the inverse heterotrophic NO_3^- -N uptake (i.e., denitrification and heterotrophic assimilation) and NO_3^- -N release (i.e., nitrification/mineralization). Direct reach-scale measuring of U_D remains challenging, given its high spatiotemporal variability and diel variations at sub-daily scale as indicated in this study. Further quantifying these multiple overlapping processes would require combining different kinds of measurements and model-based estimates. For example, isotopes can be added to further disentangle denitrification and provide information on spatial stream heterogeneity (Böhlke et al., 2004; Mulholland et al., 2008). Further information of in-stream biogeochemical processes, that is not measured but informative, can be derived from model-based estimates (e.g., Jarvie et al. (2018)

obtained continuous information of dissolve inorganic carbon and CO₂ release from the THINCARB model to support the changes of microbial respiration).

The highly complex and internally convoluted in-stream processes have also induced challenges for network-scale modelling, as well as for catchment modelling that further involves terrestrial processes. Reach-scale monitoring and analysis, like this study, are encouraging in providing pathway-specific quantifications (e.g., heterotrophic uptake U_D can reach up to 230-320 mg N m⁻² d⁻¹, Table 3.3), which are still rare at larger scales. Such quantitative information can, at least, serve as invaluable reference values for verifying model estimates, which often employ highly simplified conceptualization and rely on model parameterization. For a wider implication, by cross-comparing such information obtained under various conditions (different seasons and streams), insights into environmental controls on in-stream processes can be used to further derive new approaches of process regionalization, refining current descriptions based on e.g., first-order kinetics. For example, the parsimonious approach of quantifying autotrophic NO₃⁻-N uptake by Yang et al. (2019) was derived from the contrasting seasonal patterns of GPP-related NO₃⁻-N uptake in open- and closed-canopy reaches, and further upscaled to the river-network scale.

3.6. Conclusion

High-frequency multi-parameter sensors have great potential to quantify reach-scale in-stream net NO₃⁻ uptake and to conduct detailed investigations of in-stream metabolism and coupled NO₃⁻ cycling pathways. The high-frequency data allowed to calculate different uptake pathways at an hourly time step and to explore diel variations in these NO₃⁻-N uptake pathways. The mass-balance based rates of net NO₃⁻-N uptake varied seasonally and across stream conditions, and were highest in the more natural reach and during the post-wet seasons (May-June). Compared to assimilatory uptake (U_A), heterotrophic uptake (U_D) likely dominated the net NO₃⁻-N uptake during the post-wet seasons, but its proportions largely decreased during the dry season (August-September), often becoming negative (indicating net NO₃⁻-N release). The inferred U_D also exhibited substantial diel patterns; if U_D is strictly coupled with GPP as is commonly assumed and yet no diurnal U_{NET} signal is present, it suggests that U_D must decrease during the daytime, which has long been overlooked in previous studies. Overall, our approach and findings from high-order river monitoring and analysis can provide new insights into heterogeneous dynamics of in-stream NO₃⁻ retention processes at larger scales.

Acknowledgement

Xiaolin Zhang is funded by the Chinese Scholarship Council (CSC). We thank Uwe Kiwel for his technical support during the field work. We also thank the Federal Agency for Cartography and Geodesy (BKG) and the State Agency for Flood Protection and Water Management of Saxony Anhalt, Germany (LHW) for all data support.

Open Research

The high-frequency monitoring data used are available at Zhang et al. (2022) via <https://doi.org/10.48758/ufz.12911>. The CORINE (2018) data used for identifying landscape type in the study are available at the Federal Agency for Cartography and Geodesy (BKG) (<https://gdz.bkg.bund.de/index.php/default/corine-land-cover-5-ha-stand-2018-clc5-2018.html>). The discharge, groundwater and river morphology data in the study are available at the data portal (Datenportal) of the State Agency for Flood Protection and Water Management of Saxony Anhalt, Germany (LHW, 2022) (<https://gld.lhw-sachsen-anhalt.de/>).

3.7. References

- Alberts, J. M., Beaulieu, J. J., & Buffam, I. (2017). Watershed Land Use and Seasonal Variation Constrain the Influence of Riparian Canopy Cover on Stream Ecosystem Metabolism. *Ecosystems*, 20(3), 553–567. <https://doi.org/10.1007/s10021-016-0040-9>
- Alexander, R. B., Smith, R. A., & Schwarz, G. E. (2000). Effect of stream channel size on the delivery of nitrogen to the Gulf of Mexico. *Nature*, 403(6771), 758–761. <https://doi.org/10.1038/35001562>
- Anlanger, C., Risse-Buhl, U., Schiller, D., Noss, C., Weitere, M., & Lorke, A. (2021). Hydraulic and biological controls of biofilm nitrogen uptake in gravel-bed streams. *Limnology and Oceanography*, 66(11), 3887–3900. <https://doi.org/10.1002/lno.11927>
- Appling, A. P., & Heffernan, J. B. (2014). Nutrient limitation and physiology mediate the fine-scale (de)coupling of biogeochemical cycles. *American Naturalist*, 184(3), 384–406. <https://doi.org/10.1086/677282>
- Arango, C. P., Tank, J. L., Johnson, L. T., & Hamilton, S. K. (2008). Assimilatory uptake rather than nitrification and denitrification determines nitrogen removal patterns in streams of varying land use. *Limnology and Oceanography*, 53(6), 2558–2572. <https://doi.org/10.4319/lo.2008.53.6.2558>
- Beaulieu, J. J., Arango, C. P., Balz, D. A., & Shuster, W. D. (2013). Continuous monitoring reveals multiple controls on ecosystem metabolism in a suburban stream. *Freshwater Biology*, 58(5), 918–937. <https://doi.org/10.1111/fwb.12097>
- Bernhardt, E. S., Hall, R. O., & Likens, G. E. (2002). Whole-system estimates of nitrification and nitrate uptake in streams of the Hubbard Brook Experimental Forest. *Ecosystems*, 5(5), 419–430. <https://doi.org/10.1007/s10021-002-0179-4>
- Billen, G., Garnier, J., & Lassaletta, L. (2013). The nitrogen cascade from agricultural soils to the sea: Modelling nitrogen transfers at regional watershed and global scales. *Philosophical Transactions of the Royal Society B: Biological Sciences*, 368(1621). <https://doi.org/10.1098/rstb.2013.0123>
- Böhlke, J. K., Harvey, J. W., & Voytek, M. A. (2004). Reach-scale isotope tracer experiment to quantify denitrification and related processes in a nitrate-rich stream, midcontinent United States. *Limnology and Oceanography*, 49(3), 821–838. <https://doi.org/10.4319/LO.2004.49.3.0821>
- Bott, T. L. (2007). Primary Productivity and Community Respiration. In *Methods in Stream Ecology* (2nd edition, pp. 663–690). New York: Elsevier. <https://doi.org/10.1016/B978-012332908-0.50040-1>
- Burns, D. A., Pellerin, B. A., Miller, M. P., Capel, P. D., Tesoriero, A. J., & Duncan, J. M. (2019). Monitoring the riverine pulse: Applying high-frequency nitrate data to advance integrative understanding of biogeochemical and hydrological processes. *Wiley Interdisciplinary Reviews:*

- Water*, 6(4), e1348. <https://doi.org/10.1002/wat2.1348>
- Chamberlin, C. A., Bernhardt, E. S., Rosi, E. J., & Heffernan, J. B. (2019). Stoichiometry and daily rhythms: experimental evidence shows nutrient limitation decouples N uptake from photosynthesis. *Ecology*, 100(10), e02822. <https://doi.org/10.1002/ecy.2822>
- Chamberlin, C. A., Katul, G. G., & Heffernan, J. B. (2021). A Multiscale Approach to Timescale Analysis: Isolating Diel Signals from Solute Concentration Time Series. *Environmental Science & Technology*, 55(18), 12731–12738. <https://doi.org/10.1021/acs.est.1c00498>
- Chapra, S. C., & Di Toro, D. M. (1991). Delta Method For Estimating Primary Production, Respiration, And Reaeration In Streams. *Journal of Environmental Engineering*, 117(5), 640–655. [https://doi.org/10.1061/\(asce\)0733-9372\(1991\)117:5\(640\)](https://doi.org/10.1061/(asce)0733-9372(1991)117:5(640))
- Churchill, M. A., Elmore, H. L., & Buckingham, R. A. (1964). The Prediction of Stream Reaeration Rates. *Advances in Water Pollution Research*, 89–136. <https://doi.org/10.1016/b978-1-4832-8391-3.50015-4>
- Cohen, M. J., Heffernan, J. B., Albertin, A., & Martin, J. B. (2012). Inference of riverine nitrogen processing from longitudinal and diel variation in dual nitrate isotopes. *Journal of Geophysical Research: Biogeosciences*, 117(1), 1021. <https://doi.org/10.1029/2011JG001715>
- Core Development Team, R. (2020). A Language and Environment for Statistical Computing. *R Foundation for Statistical Computing*. Vienna, Austria: R Foundation for Statistical Computing. Retrieved from <http://www.r-project.org>
- CORINE (2018). CORINE Land Cover 5 ha, Stand 2018 (CLC5-2018) [Dataset]. Federal Agency for Cartography and Geodesy (BKG). URL <https://gdz.bkg.bund.de/index.php/default/open-data/corine-land-cover-5-ha-stand-2018-clc5-2018.html> (accessed 1.19.2023)
- Covino, T. P., McGlynn, B. L., & McNamara, R. A. (2010). Tracer additions for spiraling curve characterization (TASCC): Quantifying stream nutrient uptake kinetics from ambient to saturation. *Limnology and Oceanography: Methods*, 8(SEPT), 484–498. <https://doi.org/10.4319/lom.2010.8.484>
- Dawson, R. N., & Murphy, K. L. (1972). The temperature dependency of biological denitrification. *Water Research*, 6(1), 71–83. [https://doi.org/10.1016/0043-1354\(72\)90174-1](https://doi.org/10.1016/0043-1354(72)90174-1)
- Day, N. K., & Hall, R. O. (2017). Ammonium uptake kinetics and nitrification in mountain streams. *Freshwater Science*, 36(1), 41–54. <https://doi.org/10.1086/690600>
- Demars, B. O. L., Russell Manson, J., Ólafsson, J. S., Gíslason, G. M., Gudmundsdóttir, R., Woodward, G., et al. (2011). Temperature and the metabolic balance of streams. *Freshwater Biology*, 56(6), 1106–1121. <https://doi.org/10.1111/j.1365-2427.2010.02554.x>
- Fellman, J. B., Hood, E., D'Amore, D. V., Edwards, R. T., & White, D. (2009). Seasonal changes in the chemical quality and biodegradability of dissolved organic matter exported from soils to streams in coastal temperate rainforest watersheds. *Biogeochemistry*, 95(2), 277–293. <https://doi.org/10.1007/s10533-009-9336-6>
- Fowler, D., Coyle, M., Skiba, U., Sutton, M. A., Cape, J. N., Reis, S., et al. (2013). The global nitrogen cycle in the twenty-first century. *Philosophical Transactions of the Royal Society B: Biological Sciences*, 368(1621). <https://doi.org/10.1098/rstb.2013.0164>
- Friese, K., Schultze, M., Boehrer, B., Büttner, O., Herzsprung, P., Koschorreck, M., et al. (2014). Ecological response of two hydro-morphological similar pre-dams to contrasting land-use in the Rappbode reservoir system (Germany). *International Review of Hydrobiology*, 99(5), 335–349. <https://doi.org/10.1002/iroh.201301672>
- Gammons, C. H., Babcock, J. N., Parker, S. R., & Poulson, S. R. (2011). Diel cycling and stable isotopes of dissolved oxygen, dissolved inorganic carbon, and nitrogenous species in a stream receiving treated municipal sewage. *Chemical Geology*, 283(1), 44–55. <https://doi.org/10.1016/j.chemgeo.2010.07.006>

- Gomez-Velez, J. D., Harvey, J. W., Cardenas, M. B., & Kiel, B. (2015). Denitrification in the Mississippi River network controlled by flow through river bedforms. *Nature Geoscience*, 8(12), 941–945. <https://doi.org/10.1038/ngeo2567>
- Hall, R. O., Tank, J. L., Sobota, D. J., Mulholland, P. J., O'Brien, J. M., Dodds, W. K., et al. (2009). Nitrate removal in stream ecosystems measured by ¹⁵N addition experiments: Total uptake. *Limnology and Oceanography*, 54(3), 653–665. <https://doi.org/10.4319/lo.2009.54.3.0653>
- Harvey, J., Gomez-Velez, J., Schmadel, N., Scott, D., Boyer, E., Alexander, R., et al. (2019). How Hydrologic Connectivity Regulates Water Quality in River Corridors. *Journal of the American Water Resources Association*, 55(2), 369–381. <https://doi.org/10.1111/1752-1688.12691>
- Heffernan, J. B., & Cohen, M. J. (2010). Direct and indirect coupling of primary production and diel nitrate dynamics in a subtropical spring-fed river. *Limnology and Oceanography*, 55(2), 677–688. <https://doi.org/10.4319/lo.2010.55.2.0677>
- Heffernan, J. B., Cohen, M. J., Frazer, T. K., Thomas, R. G., Rayfield, T. J., Gulley, J., et al. (2010). Hydrologic and biotic influences on nitrate removal in a subtropical spring-fed river. *Limnology and Oceanography*, 55(1), 249–263. <https://doi.org/10.4319/lo.2010.55.1.0249>
- Helton, A. M., Poole, G. C., Meyer, J. L., Wollheim, W. M., Peterson, B. J., Mulholland, P. J., et al. (2011). Thinking outside the channel: Modeling nitrogen cycling in networked river ecosystems. *Frontiers in Ecology and the Environment*, 9(4), 229–238. <https://doi.org/10.1890/080211>
- Hensley, R. T., & Cohen, M. J. (2016). On the emergence of diel solute signals in flowing waters. *Water Resources Research*, 52(2), 759–772. <https://doi.org/10.1002/2015WR017895>
- Hensley, R. T., Cohen, M. J., & Korhnak, L. V. (2015). Hydraulic effects on nitrogen removal in a tidal spring-fed river. *Water Resources Research*, 51(3), 1443–1456. <https://doi.org/10.1002/2014WR016178>
- Hester, E. T., Brooks, K. E., & Scott, D. T. (2018). Comparing reach scale hyporheic exchange and denitrification induced by instream restoration structures and natural streambed morphology. *Ecological Engineering*, 115, 105–121.
- Jarvie, H. P., Sharpley, A. N., Kresse, T., Hays, P. D., Williams, R. J., King, S. M., & Berry, L. G. (2018). Coupling High-Frequency Stream Metabolism and Nutrient Monitoring to Explore Biogeochemical Controls on Downstream Nitrate Delivery. *Environmental Science and Technology*, 52(23), 13708–13717. <https://doi.org/10.1021/acs.est.8b03074>
- Julian, J. P., Doyle, M. W., & Stanley, E. H. (2008). Empirical modeling of light availability in rivers. *Journal of Geophysical Research: Biogeosciences*, 113(3), 3022. <https://doi.org/10.1029/2007JG000601>
- Junge, F. W., Hanisch, C., Zerling, L., & Gehre, M. (2005). Geochemical signatures (C, N, $\delta^{13}\text{C}$, $\delta^{15}\text{N}$, metals) of suspended matter in the river Weiße Elster (central Germany): Their seasonal and flow-related distribution 1997-2001. *Isotopes in Environmental and Health Studies*, 41(2), 141–159. <https://doi.org/10.1080/10256010500131874>
- Kamjunke, N., Mages, M., Büttner, O., Marcus, H., & Weitere, M. (2015). Relationship between the elemental composition of stream biofilms and water chemistry—a catchment approach. *Environmental Monitoring and Assessment*, 187(7), 432. <https://doi.org/10.1007/s10661-015-4664-6>
- Kemp, M. J., & Dodds, W. K. (2002). Comparisons of nitrification and denitrification in prairie and agriculturally influenced streams. *Ecological Applications*, 12(4), 998–1009. [https://doi.org/10.1890/1051-0761\(2002\)012\[0998:CONADI\]2.0.CO;2](https://doi.org/10.1890/1051-0761(2002)012[0998:CONADI]2.0.CO;2)
- Kunz, J. V., Hensley, R., Brase, L., Borchardt, D., & Rode, M. (2017). High frequency measurements of reach scale nitrogen uptake in a fourth order river with contrasting hydromorphology and variable water chemistry (Weiße Elster, Germany). *Water Resources Research*, 53(1), 328–343. <https://doi.org/10.1002/2016WR019355>

- LHW (2022). Landesbetrieb für Hochwasserschutz und Wasserwirtschaft Sachsen-Anhalt: Datenportal des Gewässerkundlichen Landesdienstes Sachsen-Anhalt [Dataset]. URL <https://gld.lhw-sachsen-anhalt.de> (accessed 1.19.2023).
- Lupon, A., Martí, E., Sabater, F. and Bernal, S. (2016), Green light: gross primary production influences seasonal stream N export by controlling fine-scale N dynamics. *Ecology*, *97*(1), 133-144. <https://doi.org/10.1890/14-2296.1>
- Mulholland, P. J., Tank, J. L., Webster, J. R., Bowden, W. B., Dodds, W. K., Gregory, S. V., et al. (2002). Can uptake length in streams be determined by nutrient addition experiments? Results from an interbiome comparison study. *Journal of the North American Benthological Society*, *21*(4), 544–560. <https://doi.org/10.2307/1468429>
- Mulholland, P. J., Helton, A. M., Poole, G. C., Hall, R. O., Hamilton, S. K., Peterson, B. J., et al. (2008). Stream denitrification across biomes and its response to anthropogenic nitrate loading. *Nature*, *452*(7184), 202–205. <https://doi.org/10.1038/nature06686>
- Mulholland, P. J., Hall, R. O., Sobota, D. J., Dodds, W. K., Findlay, S. E. G., Grimm, N. B., et al. (2009). Nitrate removal in stream ecosystems measured by ¹⁵N addition experiments: Denitrification. *Limnology and Oceanography*, *54*(3), 666–680. <https://doi.org/10.4319/lo.2009.54.3.0666>
- Odum, H. T. (1956). Primary Production in Flowing Waters. *Limnology and Oceanography*, *1*(2), 102–117. <https://doi.org/10.4319/lo.1956.1.2.0102>
- Odum, H. T. (1957). Trophic Structure and Productivity of Silver Springs, Florida. *Ecological Monographs*, *27*(1), 55–112. <https://doi.org/10.2307/1948571>
- Pellerin, B. A., Saraceno, J. F., Shanley, J. B., Sebestyen, S. D., Aiken, G. R., Wollheim, W. M., & Bergamaschi, B. A. (2012). Taking the pulse of snowmelt: In situ sensors reveal seasonal, event and diurnal patterns of nitrate and dissolved organic matter variability in an upland forest stream. *Biogeochemistry*, *108*(1–3), 183–198. <https://doi.org/10.1007/s10533-011-9589-8>
- Reisinger, A. J., Tank, J. L., Hoellein, T. J., & Hall, R. O. (2016). Sediment, water column, and open-channel denitrification in rivers measured using membrane-inlet mass spectrometry. *Journal of Geophysical Research: Biogeosciences*, *121*(5), 1258–1274. <https://doi.org/10.1002/2015JG003261>
- Roberts, B. J., Mulholland, P. J., & Hill, W. R. (2007). Multiple scales of temporal variability in ecosystem metabolism rates: Results from 2 years of continuous monitoring in a forested headwater stream. *Ecosystems*, *10*(4), 588–606. <https://doi.org/10.1007/s10021-007-9059-2>
- Rode, M., Halbedel Née Angelstein, S., Anis, M. R., Borchardt, D., & Weitere, M. (2016). Continuous In-Stream Assimilatory Nitrate Uptake from High-Frequency Sensor Measurements. *Environmental Science and Technology*, *50*(11), 5685–5694. <https://doi.org/10.1021/acs.est.6b00943>
- Rode, M., Wade, A. J., Cohen, M. J., Hensley, R. T., Bowes, M. J., Kirchner, J. W., et al. (2016). Sensors in the Stream: The High-Frequency Wave of the Present. *Environmental Science and Technology*, *50*(19), 10297–10307. <https://doi.org/10.1021/acs.est.6b02155>
- Smith, V. H. (2003). Eutrophication of freshwater and coastal marine ecosystems: A global problem. *Environmental Science and Pollution Research*, *10*(2), 126–139. <https://doi.org/10.1065/espr2002.12.142>
- Smith, V. H., Tilman, G. D., & Nekola, J. C. (1999). Eutrophication: Impacts of excess nutrient inputs on freshwater, marine, and terrestrial ecosystems. *Environmental Pollution*, *100*(1–3), 179–196. [https://doi.org/10.1016/S0269-7491\(99\)00091-3](https://doi.org/10.1016/S0269-7491(99)00091-3)
- Sobota, D. J., Johnson, S. L., Gregory, S. V., & Ashkenas, L. R. (2012). A Stable Isotope Tracer Study of the Influences of Adjacent Land Use and Riparian Condition on Fates of Nitrate in Streams. *Ecosystems*, *15*(1), 1–17. <https://doi.org/10.1007/s10021-011-9489-8>

- Sweeney, B. W., Bott, T. L., Jackson, J. K., Kaplan, L. A., Newbold, J. D., Standley, L. J., et al. (2004). Riparian deforestation, stream narrowing, and loss of stream ecosystem services. *Proceedings of the National Academy of Sciences*, *101*(39), 14132–14137. <https://doi.org/10.1073/pnas.0405895101>
- Tank, J. L., Martí, E., Riis, T., von Schiller, D., Reisinger, A. J., Dodds, W. K., et al. (2018). Partitioning assimilatory nitrogen uptake in streams: an analysis of stable isotope tracer additions across continents. *Ecological Monographs*, *88*(1), 120–138. <https://doi.org/10.1002/ecm.1280>
- Tesi, T., Langone, L., Goñi, M. A., Miserocchi, S., & Bertasi, F. (2008). Changes in the composition of organic matter from prodeltaic sediments after a large flood event (Po River, Italy). *Geochimica et Cosmochimica Acta*, *72*(8), 2100–2114. <https://doi.org/10.1016/j.gca.2008.02.005>
- Tsivoglou, E. C., & Neal, L. A. (1976). Tracer measurement of reaeration: III. Predicting the reaeration capacity of inland streams. *Journal of the Water Pollution Control Federation*, *48*(12), 2669–2689. Retrieved from <https://www.jstor.org/stable/25040082>
- Wagenschein, D., & Rode, M. (2008). Modelling the impact of river morphology on nitrogen retention-A case study of the Weisse Elster River (Germany). *Ecological Modelling*, *211*(1–2), 224–232. <https://doi.org/10.1016/j.ecolmodel.2007.09.009>
- Welsh, D. T., Bartoli, M., Nizzoli, D., Castaldelli, G., Riou, S. A., & Viaroli, P. (2000). Denitrification, nitrogen fixation, community primary productivity and inorganic-N and oxygen fluxes in an intertidal *Zostera noltii* meadow. *Marine Ecology Progress Series*, *208*, 65–77. <https://doi.org/10.3354/meps208065>
- Wollschläger, U., Attinger, S., Borchardt, D., Brauns, M., Cuntz, M., Dietrich, P., et al. (2017). The Bode hydrological observatory: a platform for integrated, interdisciplinary hydro-ecological research within the TERENO Harz/Central German Lowland Observatory. *Environmental Earth Sciences*, *76*(1), 29. <https://doi.org/10.1007/s12665-016-6327-5>
- Yang, X., Jomaa, S., Büttner, O., & Rode, M. (2019). Autotrophic nitrate uptake in river networks: A modeling approach using continuous high-frequency data. *Water Research*, *157*, 258–268. <https://doi.org/10.1016/j.watres.2019.02.059>
- Zhang, X., Yang, X., Hensley, R., Lorke, A., Rode, M. (2022). Quantify instream metabolism and N uptake based on two-station mass balance method [Dataset]. Helmholtz-Centre for Environmental Research. <https://doi.org/10.48758/UFZ.12911>
- Zhao, Y., Xia, Y., Ti, C., Shan, J., Li, B., Xia, L., & Yan, X. (2015). Nitrogen removal capacity of the river network in a high nitrogen loading region. *Environmental Science and Technology*, *49*(3), 1427–1435. <https://doi.org/10.1021/es504316b>
- Zheng, L., & Bayani Cardenas, M. (2018). Diel Stream Temperature Effects on Nitrogen Cycling in Hyporheic Zones. *Journal of Geophysical Research: Biogeosciences*, *123*(9), 2743–2760. <https://doi.org/10.1029/2018JG004412>

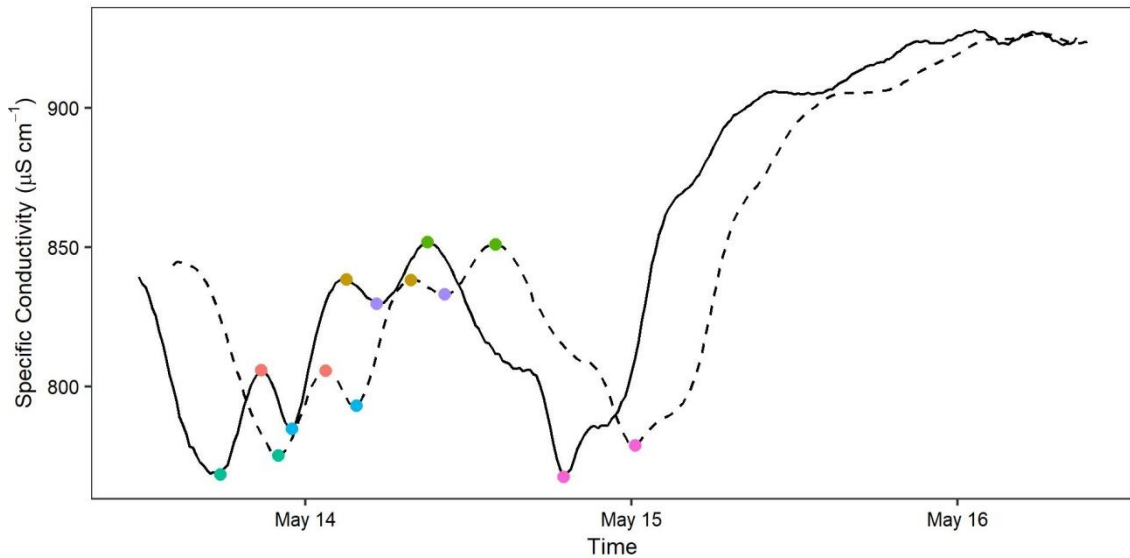
3.8. Supplementary Materials

Please check the GIF of shift between GPP and U_A via the publication website (<https://doi.org/10.1029/2022WR032329>).

Text S3.1. Method of estimating mean travel time

The 2019_05 WE_1 campaign was selected to explain how to calculate travel time using following measured specific conductivity process. First, we selected all local peak and valley values at upstream

(solid line) and downstream (dashed line) stations. Second, we put every two corresponding values into groups (with the same color). Finally, we calculated the time lag within each group and got the mean value ca. 5 hours.



No.	US_time	US_value	DS_time	DS_value	Time lag (h)
1	5/13/2019 17:45	768.43	5/13/2019 22:00	775.27	4.25
2	5/13/2019 20:45	805.80	5/14/2019 1:30	805.70	4.75
3	5/13/2019 23:00	784.87	5/14/2019 3:45	793.03	4.75
4	5/14/2019 3:00	838.37	5/14/2019 7:45	838.33	4.75
5	5/14/2019 5:15	829.77	5/14/2019 10:15	833.10	5
6	5/14/2019 9:00	851.97	5/14/2019 14:00	851.03	5
7	5/14/2019 19:00	767.53	5/15/2019 0:15	778.77	5.25

Specific conductivity for both campaigns in BD_3 were missing due to a sensor problem at the upstream station (Figure S3.7). The specific conductivity used to calculate mean travel time was converted from conductivity measurements from the sensor by the following equation (Baird et al., 2017):

$$\text{Specific conductivity} = \frac{\text{Conductivity}}{1 + 0.02 \times (\text{Temp} - 25)}$$

Text S3.2. Hydrological conditions

The hydrological year was characterized into four periods: wetting (October-December, with increasing discharge), wet (January-March, with high discharge), post-wet (April-June, with decreasing discharge) and dry (July-September, with low discharge) following the same principle in Zhang et al. (2020). Figure S3.1 shows monthly discharge conditions at the Wegeleben, Hadmersleben and Zeitz stations from 2014-2018. Figure S3.2 shows discharge of the whole year for each campaign.

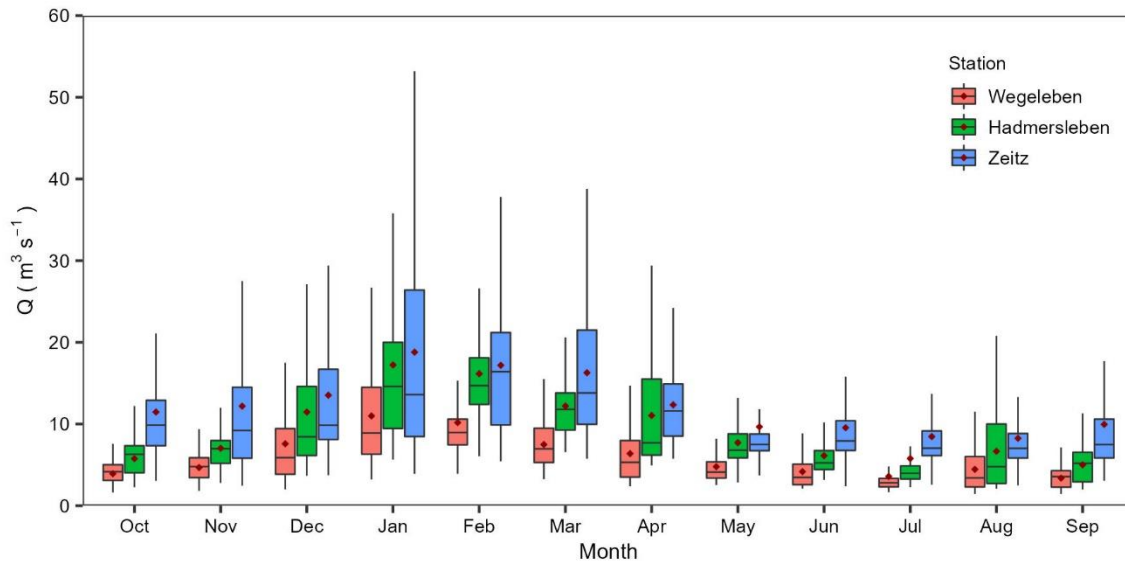


Figure S3.1. Boxplot of monthly discharge at the Wegeleben, Hadmersleben and Zeitz stations from 2014-2018. Outliers were omitted, and red diamond markers represent mean values. Whiskers represent 1.5 times the interquartile range.

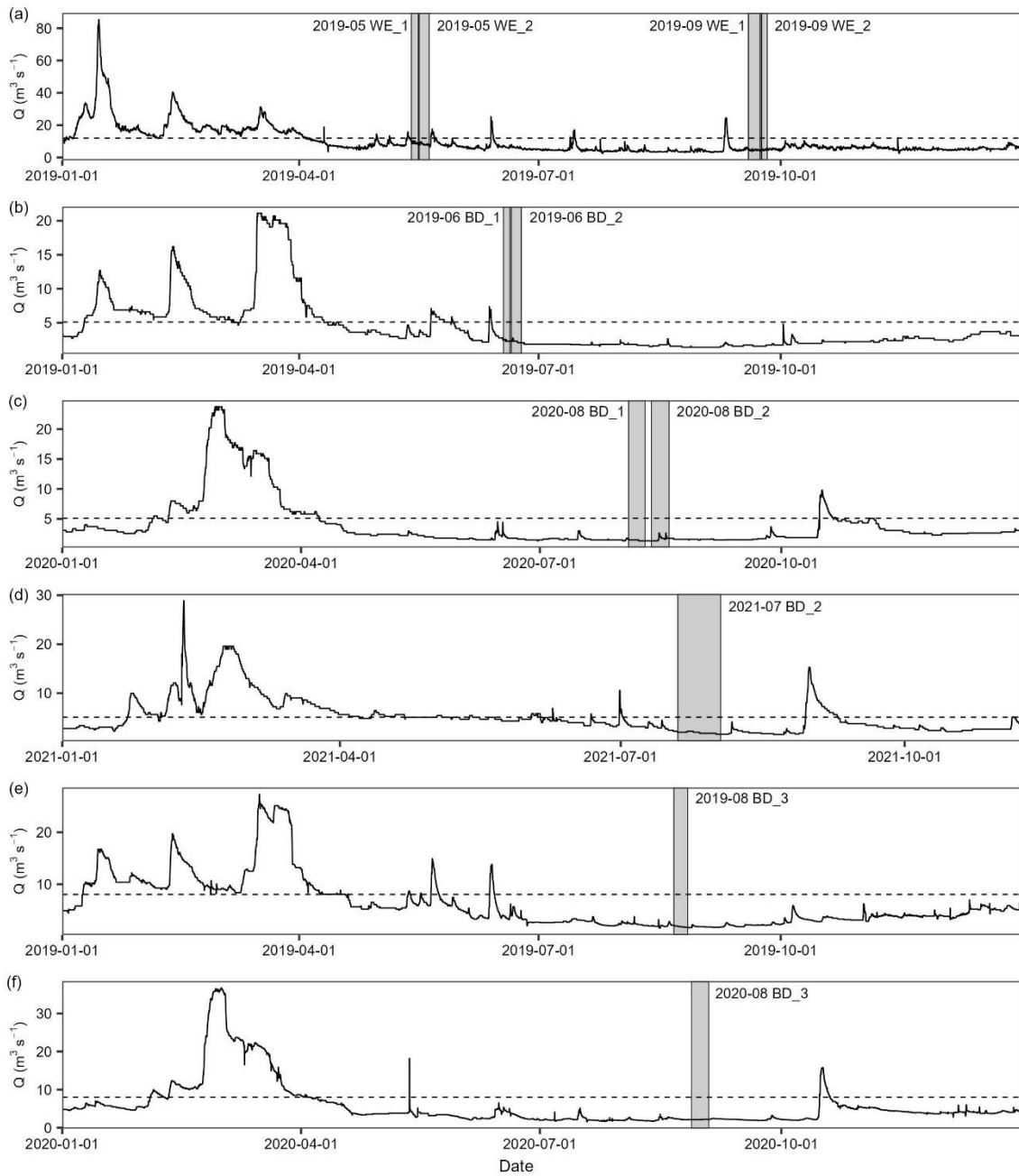


Figure S3.2. Discharge of whole year for each campaign. Dashed line means the mean value of discharge from 2016-2020 at (a) Zeitz, (b)-(d) Wegeleben and (e)-(f) Hadmersleben stations, with 11.99, 5.11 and 8.04 $\text{m}^3 \text{s}^{-1}$, respectively.

Text S3.3. Description of subcatchment for each reach

Subcatchment for each reach was divided based on DEM (Figure S3.3). For the Weiße Elster catchment, the in-between areas of WE_1 and WE_2 were only 15.2 and 7.4 km², with very low runoff generation (< 100 mm/yr annual runoff from the SWAT modelling by Guse et al. (2007)), and the groundwater table from near stream wells (from the state water authority - LHW) are much lower than stream water levels (also discussed in Kunz et al. (2017)). Therefore, we didn't consider any groundwater lateral input for the two Weiße Elster reaches.

For the Bode catchment, we have detected in-between areas as 89.1, 42.4, and 95.2 km² for BD_1, BD_2 and BD_3, respectively. For BD_1, we select the lower subcatchment as in-between area because the DEM-based flow direction is similar with the stream channel in the upper part, which means flow from the upper part could be collected by the current river channel. Lateral discharge inputs were estimated using the daily simulations from a grid-based mHM hydrological model (model structure please refer to Yang et al. (2018), the manuscript of applying this model in the Bode catchment is under review), and the associated NO₃⁻-N concentration was roughly assigned as 2 mg l⁻¹ for BD_1 and BD_2, 6.75 mg l⁻¹ for BD_3 according to the LHW measurements from several lowland tributaries. The groundwater level near BD_2 is complex (Figure S3.4), which may result in the uncertainty when considering impacts from lateral inflow.

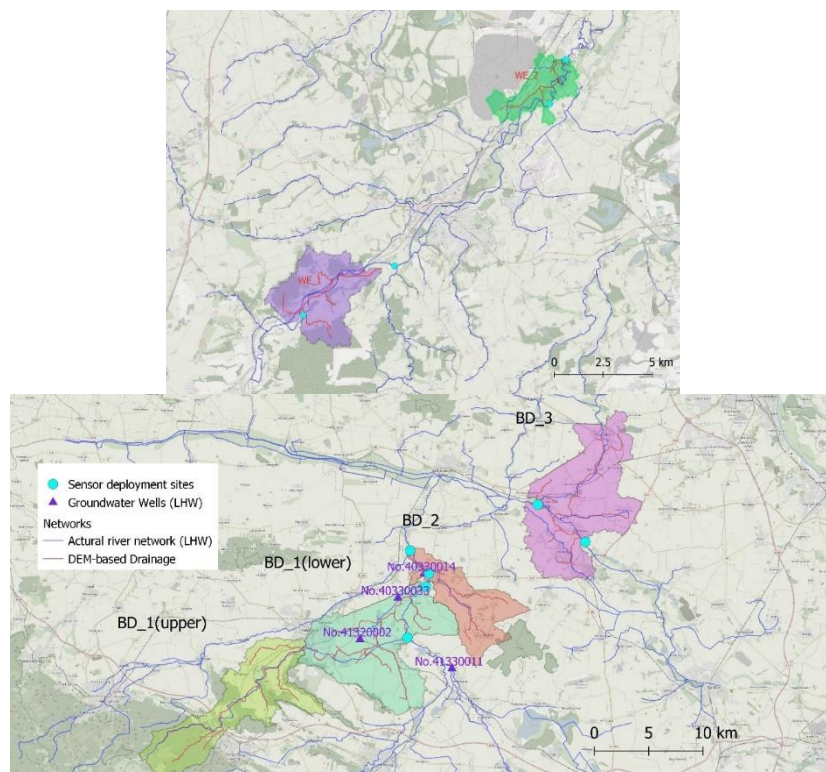


Figure S3.3. Maps of subcatchment for each reach

Table S3.1. Summary of influence from each subcatchment on discharge, N load and uptake during each campaign.

	BD_1		BD_2			BD_3		Unit
	2019-06	2020-08	2019-06	2020-08	2021-07	2019-08	2020-08	
Q_L	0.014	0.009	0.028	0.022	0.010	0.0009	0.008	$\text{m}^3 \text{s}^{-1}$
Q_L/Q	0.56	0.57	1.20	1.33	0.52	0.05	0.36	%
Load_L	0.028	0.018	0.056	0.044	0.020	0.006	0.54	g s^{-1}
L_L/L_{DS}	0.64	0.93	0.73	1.10	0.30	0.04	0.36	%
Unet, without	-121.3	-73.9	272.9	-11.8	96.1	129.5	48.6	$\text{mg N m}^{-2} \text{d}^{-1}$
Unet, with	-100.8	-61.2	357.8	53.6	130.9	133.7	86.8	$\text{mg N m}^{-2} \text{d}^{-1}$

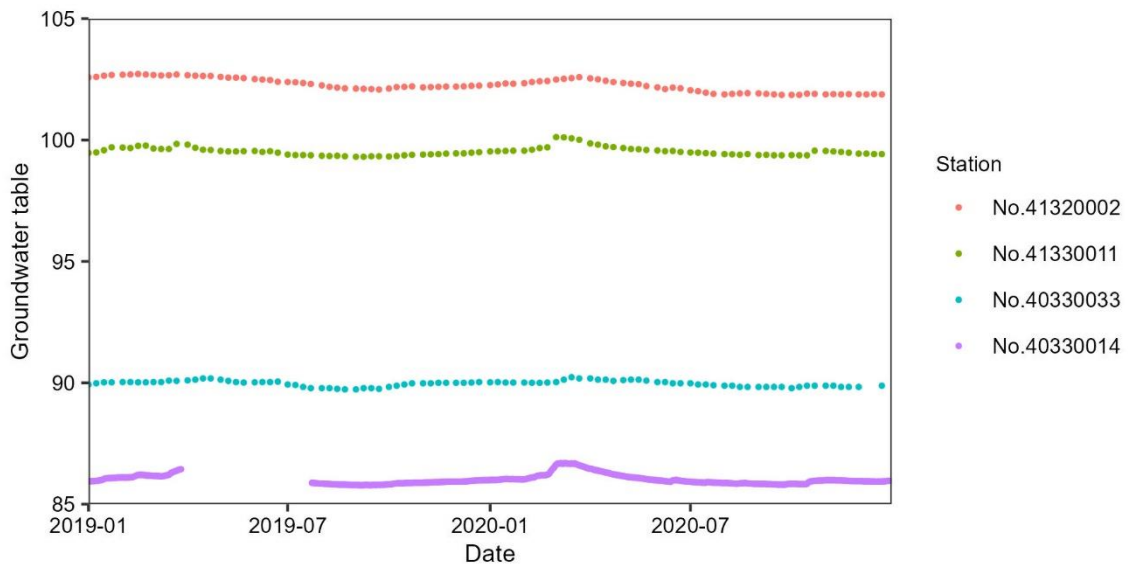


Figure S3.4. Groundwater table at the four gauging stations around the reach BD_1 (Figure S3.3).

Text S3.4. Overall of water hydrological and physiochemical processes during each campaign

Figure S3.5-S3.9 show processes and statistic values of hourly discharge and other parameters at up- (red line) and down- stream (blue line) stations during each campaign. The unit of Q, temperature, specific conductivity, turbidity and Chlorophyll a is m^3/s , $^{\circ}\text{C}$, $\mu\text{S cm}^{-1}$, FNU and $\mu\text{g l}^{-1}$, respectively. Turbidity for campaign 2019-08 BD_3 and specific conductivity for both campaigns in BD_3 were missing due to a sensor problem at the upstream station.

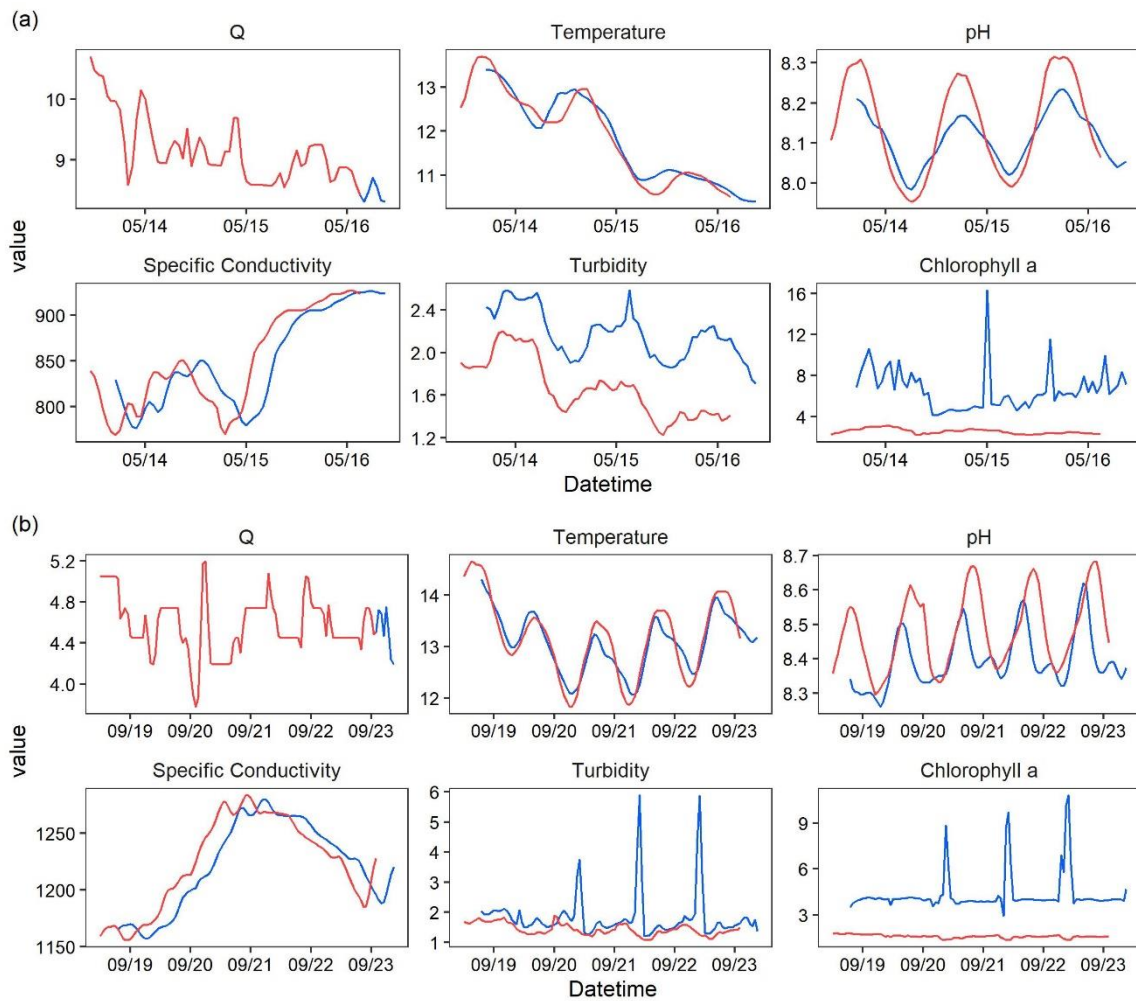


Figure S3.5. Parameter processes of study reach WE_1 in May 2019 (a) and September 2019 (b).

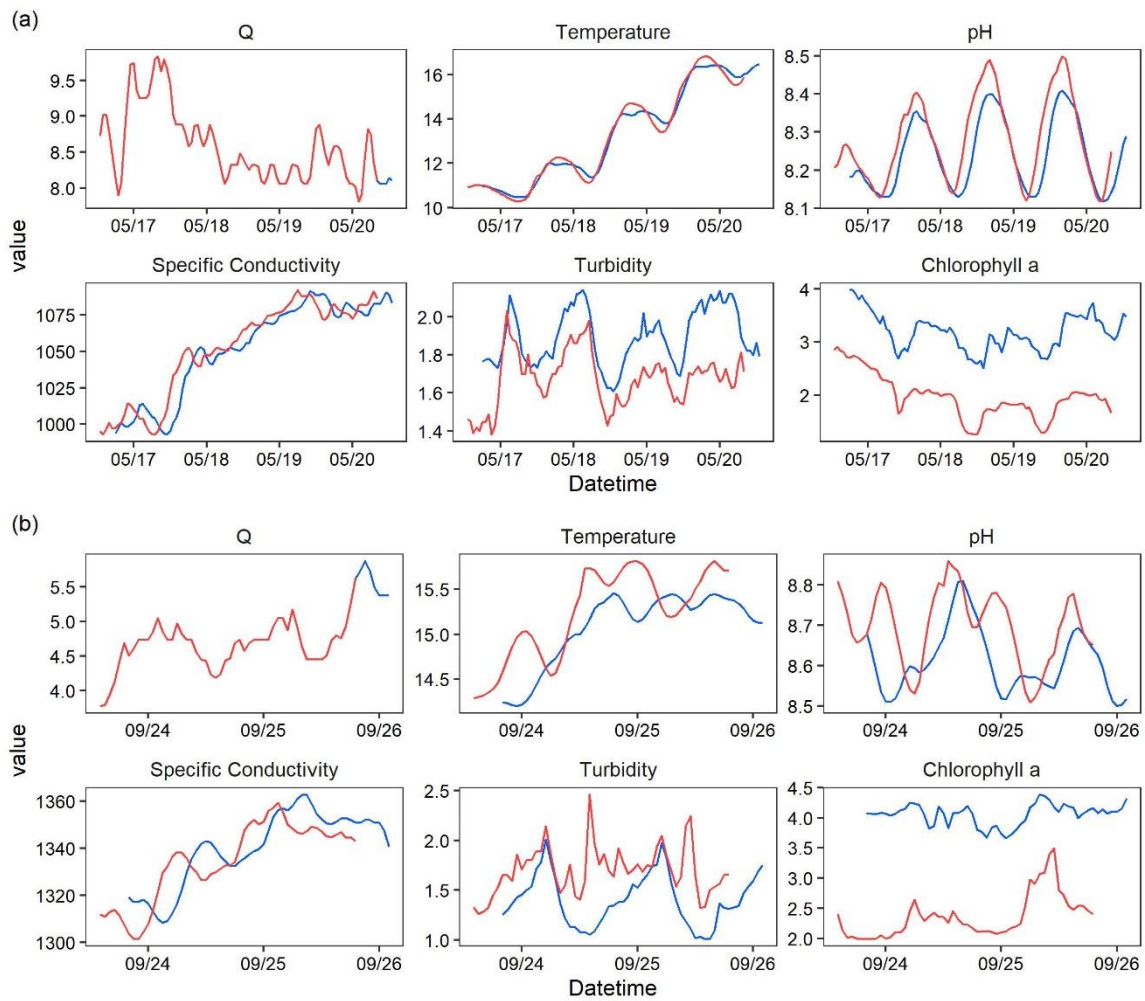


Figure S3.6. Parameter processes of study reach WE_2 in May 2019 (a) and September 2019 (b).

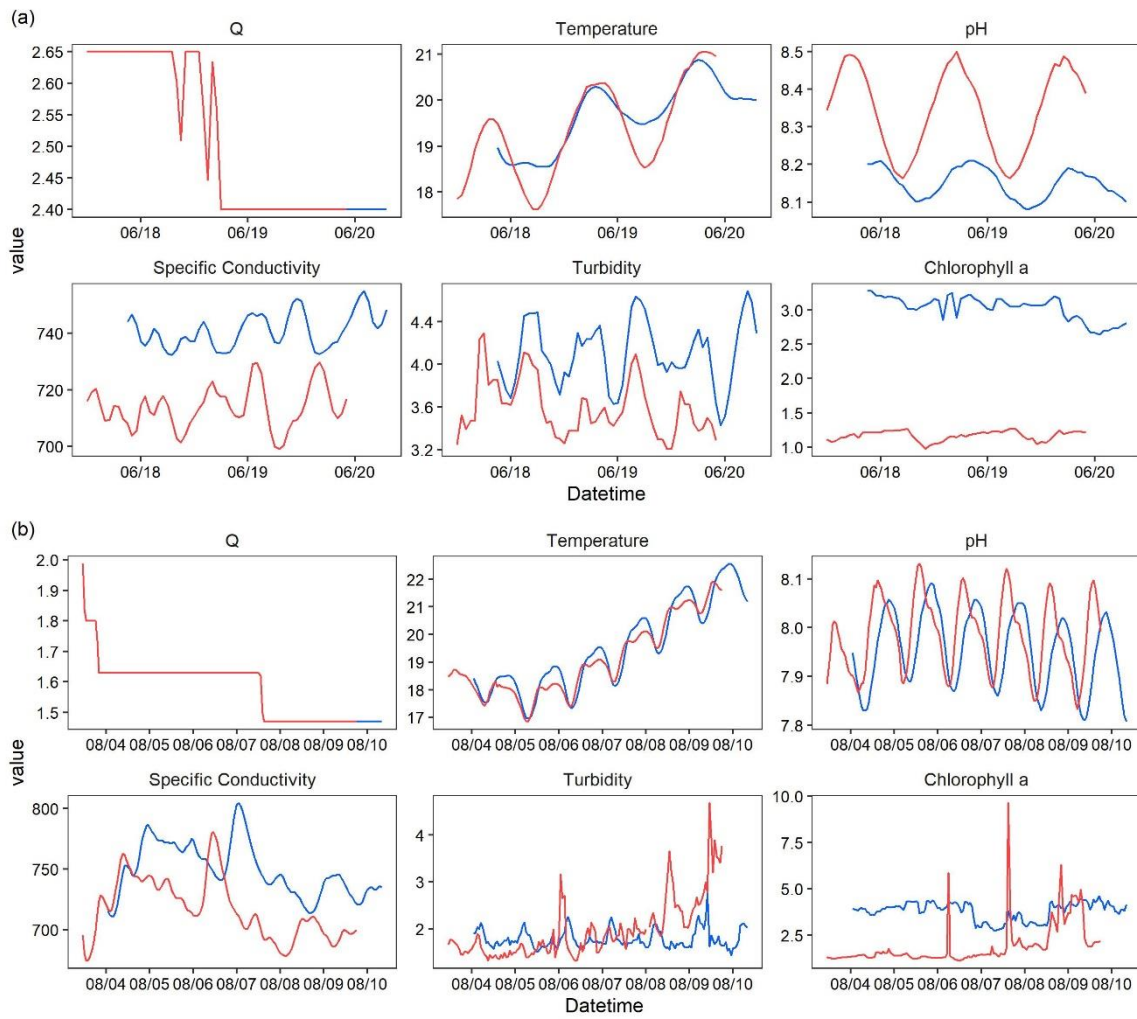


Figure S3.7. Parameter processes of study reach BD_1 in June 2019 (a) and August 2020 (b).

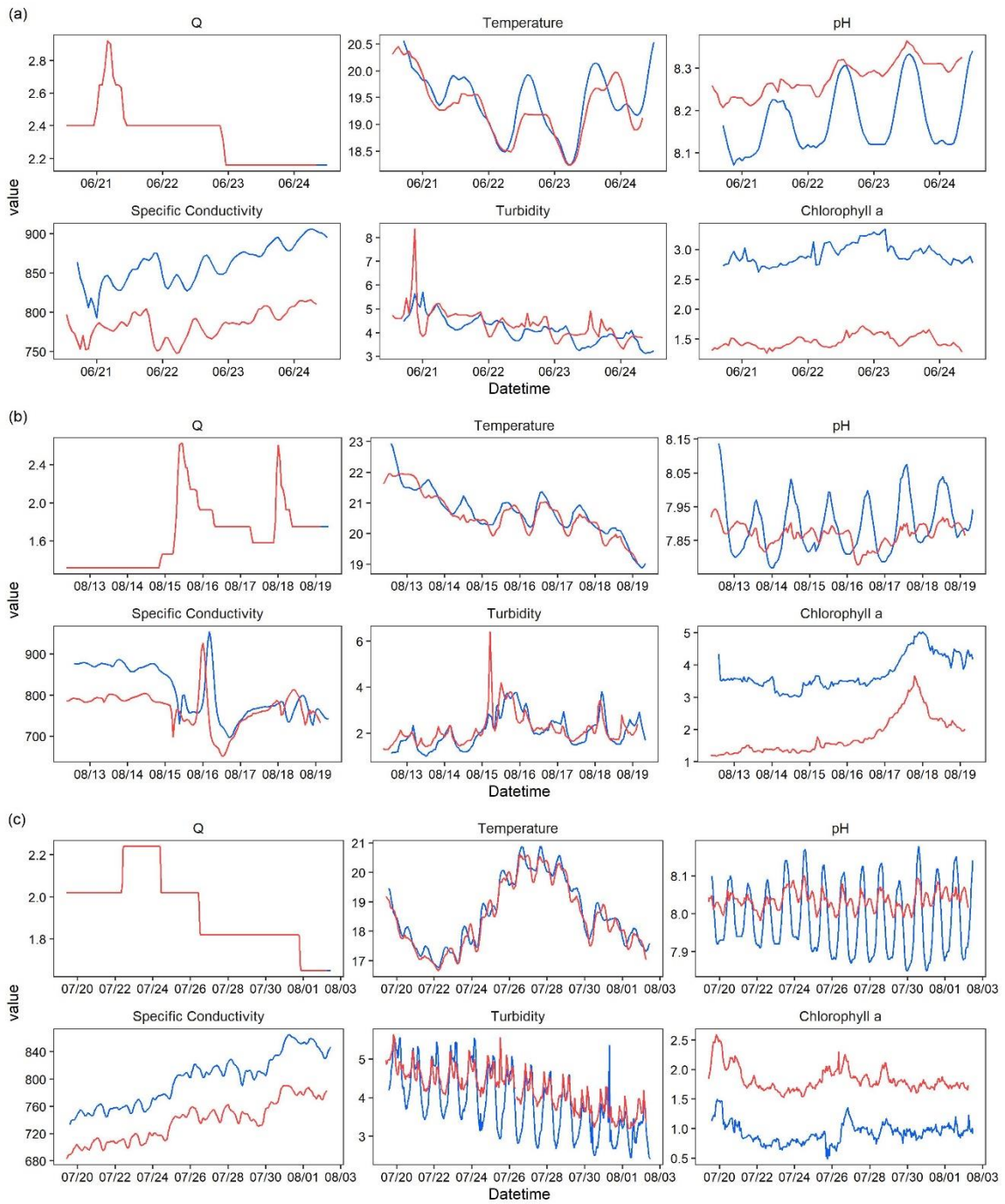


Figure S3.8. Parameter processes of study reach BD_2 in June 2019 (a), August 2020 (b) and July 2021 (c).

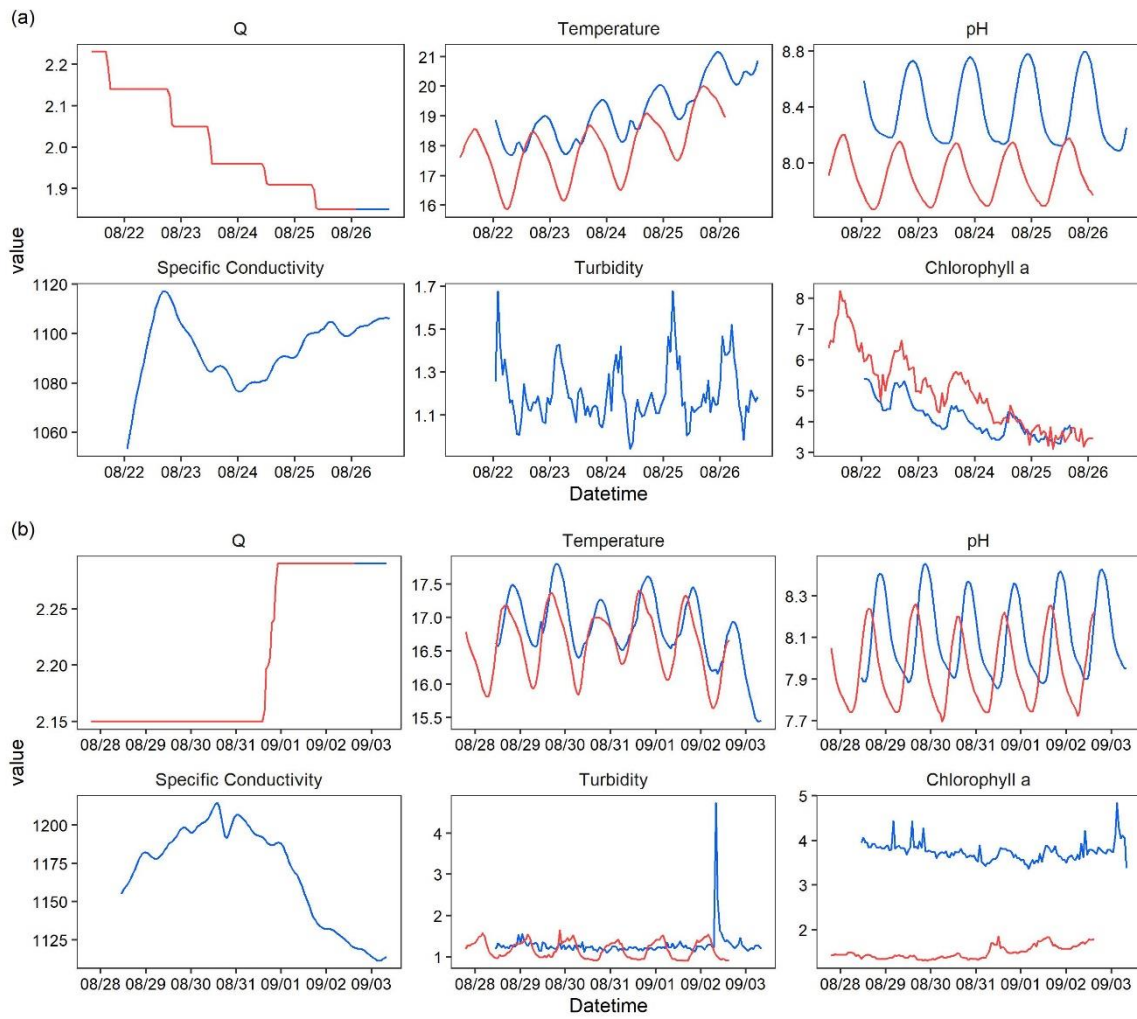


Figure S3.9. Parameter processes of study reach BD_3 in June 2019 (a) and August 2020 (b).

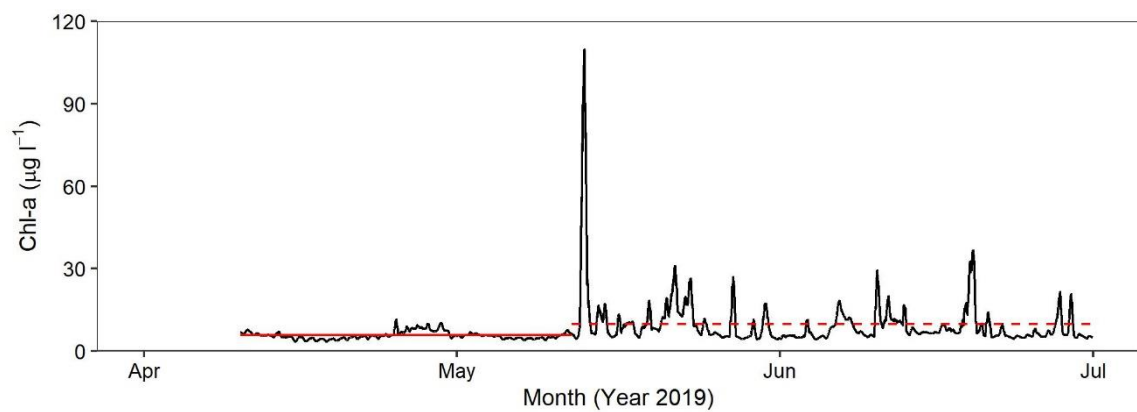


Figure S3.10. *Chlorophyll a* concentration from April to June 2019 at the GGL station. The red solid line indicates the mean value from 10 April to 11 May. The red dashed line indicates the mean value from 12 May to 30 June.

Table S3.2. Results of lab analyses for grab samples at the start and end day of each campaign (units: mg l⁻¹)

Date	Station	NO ₃ ⁻ -N	NO ₂ ⁻ -N	NH ₄ ⁺ -N	TNB	SRP	TP
5/13/2019	WE 1 US	4.012	0.045	0.096	5.22	0.089	0.140
	WE 1 DS	4.061	0.044	0.100	5.23	0.092	0.132
5/16/2019	WE 1 US	3.871	0.023	0.078	5.02	0.073	0.107
	WE 1 DS	3.862	0.023	0.051	4.89	0.073	0.126
	WE 2 US	3.497	0.021	0.086	5.31	0.072	0.140
	WE 2 DS	3.432	0.021	0.070	5.32	0.073	0.122
5/20/2019	WE 2 US	3.871	0.023	0.078	5.02	0.073	0.107
	WE 2 DS	3.432	0.021	0.070	5.32	0.073	0.122
9/18/2019	WE 1 US	3.930	0.015	0.040	5.16	0.100	0.143
	WE 1 DS	4.010	0.014	0.030	5.01	0.104	0.132
9/23/2019	WE 1 US	3.540	<0.006	0.020	4.67	0.067	0.098
	WE 1 DS	3.420	<0.006	0.020	4.57	0.065	0.106
	WE 2 US	3.480	0.008	0.073	4.47	0.068	0.108
	WE 2 DS	3.550	0.008	0.038	4.65	0.068	0.111
9/26/2019	WE 2 US	3.530	0.015	0.078	4.77	0.049	0.108
	WE 2 DS	3.480	0.015	0.057	4.68	0.048	0.106
6/17/2019	BD 1 US	1.750	0.011	0.060	2.62	0.041	0.107
	BD 1 DS	1.830	0.013	0.042	2.50	0.060	0.110
6/18/2019	BD 1 input	0.527	0.114	2.57	5.86	0.96	1.46
6/20/2019	BD 1 US	1.740	0.017	0.057	2.20	0.060	0.158
	BD 1 DS	1.960	0.017	0.067	4.98	0.054	0.103
	BD 2 US	1.890	0.017	0.057	3.13	0.054	0.126
	BD 2 DS	1.650	0.011	0.031	3.19	0.038	0.120
6/24/2019	BD 2 US	1.610	0.010	0.047	1.40	0.059	0.107
	BD 2 DS	1.620	0.009	0.030	2.22	0.060	0.108
8/3/2020	BD 1 US	1.360	0.013	0.072	2.09	0.061	0.111
	BD 1 DS	1.270	0.016	0.083	1.91	0.071	0.114
	BD 1 input	1.680	<0.006	0.350	1.96	0.003	2.4
8/10/2020	BD 1 US	1.110	0.009	0.057	1.83	0.065	0.127
	BD 1 DS	1.220	0.014	0.067	1.84	0.083	0.131
	BD 1 input	1.700	<0.006	0.031	2.01	0.005	4.0
8/12/2020	BD 2 US	1.120	0.012	0.072	1.58	0.070	0.119
	BD 2 DS	1.120	0.010	0.067	1.55	0.076	0.123
8/19/2020	BD 2 US	1.340	0.013	0.062	2.00	0.085	0.108
	BD 2 DS	1.310	0.009	0.049	1.84	0.078	0.108
7/19/2021	BD 2 US	1.800	0.010	0.053	2.38	0.059	0.094
	BD 2 DS	1.770	0.011	0.047	2.33	0.063	0.095
8/2/2021	BD 2 US	1.620	0.008	0.059	2.14	0.046	0.073
	BD 2 DS	1.580	0.007	0.058	2.28	0.044	0.104
8/21/2019	BD 3 US	1.110	0.010	0.013	1.80	0.051	0.083
	BD 3 DS	1.070	0.006	0.020	1.75	0.050	0.071
8/26/2019	BD 3 US	1.590	0.072	0.019	2.25	0.033	0.066
	BD 3 DS	1.370	0.008	0.002	2.29	0.033	0.061
8/27/2020	BD 3 US	1.130	0.022	0.073	1.73	0.078	0.121
	BD 3 DS	1.100	0.013	0.047	1.67	0.069	0.122
9/3/2020	BD 3 US	0.922	0.007	0.016	1.33	0.056	0.080
	BD 3 DS	0.931	<0.006	<0.011	1.37	0.058	0.078

Table S3.3. Several Estimated length for metabolism calculation.

	WE_1		WE_2		BD_1		BD_2		BD_3		
	2019-05	2019-09	2019-05	2019-09	2019-06	2020-08	2019-06	2020-08	2021-07	2019-08	2020-08
<i>Length (m)</i>	6280		6100		7170		3360		6150		
<i>Slope</i>	0.0005		0.00089		0.0006		0.0006		0.000359		
v (m s ⁻¹)	0.35	0.25	0.38	0.28	0.25	0.14	0.27	0.21	0.23	0.12	0.11
Q (m ³ s ⁻¹)	9.06	4.55	8.58	4.75	2.5	1.57	2.34	1.65	1.93	1.95	2.2
k ($\times 10^{-5}$ s ⁻¹)	3.84	3.85	3.62	3.51	1.76	1.23	1.65	1.22	1.73	1.23	1.01
$0.4*v/k$ (m)	4517	4517	2538	2538	3764	3764	3764	3764	3764	6291	6291
$0.7*v/k$ (m)	7906	7906	4442	4442	6588	6588	6588	6588	6588	11011	11011
v/k (m)	11294	11294	6345	6345	9412	9412	9412	9412	9412	15730	15730
$3*v/k$ (m)	33882	33882	19035	19035	28235	28235	28235	28235	28235	47190	47190

Note: k was determined following the guideline in Bott (2007), which considered the impacts of discharge and slope.

Table S3.4. Summary of high-frequency measurements for the all campaigns (i.e., statistic values of upstream and downstream measurements).

Parameters	WE_1		WE_2		BD_1		BD_2			BD_3	
	2019-05	2019-09	2019-05	2019-09	2019-06	2020-08	2019-06	2020-08	2021-07	2019-08	2020-08
Q	9.06±0.38	4.55±0.18	8.58±0.44	4.75±0.26	2.5±0.11	1.57±0.08	2.34±0.17	1.65±0.31	1.93±0.17	1.98±0.11	2.2±0.06
	[8.59,9.84]	[4.22,4.8]	[8.09,9.52]	[4.41,5.28]	[2.4,2.65]	[1.47,1.66]	[2.16,2.72]	[1.32,2.23]	[1.65,2.24]	[1.85,2.18]	[2.15,2.29]
T	11.84±0.97	13.09±0.5	13.29±2.1	15.17±0.41	19.52±0.7	19.3±1.39	19.35±0.47	20.65±0.64	18.54±1.11	18.56±0.78	16.74±0.24
	[10.57,13.37]	[12.26,13.98]	[10.54,16.5]	[14.36,15.6]	[18.45,20.52]	[17.72,21.7]	[18.53,20.15]	[19.43,21.73]	[17.04,20.36]	[17.49,20.04]	[16.18,17.03]
N	3.84±0.05	3.85±0.13	3.62±0.11	3.51±0.05	1.76±0.03	1.23±0.05	1.65±0.05	1.22±0.08	1.73±0.09	1.23±0.06	1.01±0.06
	[3.77,3.95]	[3.67,4.06]	[3.46,3.83]	[3.44,3.58]	[1.71,1.8]	[1.16,1.34]	[1.6,1.75]	[1.12,1.34]	[1.63,1.87]	[1.16,1.33]	[0.88,1.11]
DO	10.86±0.54	10.33±0.3	10.84±0.82	9.99±0.73	8.68±0.45	8.59±0.37	8.77±0.35	8.16±0.37	8.82±0.41	9.32±1.18	9.45±0.54
	[9.98,11.75]	[9.77,10.71]	[9.29,12.01]	[9.09,11.34]	[8.03,9.39]	[7.96,9.18]	[8.22,9.4]	[7.54,8.74]	[8.14,9.5]	[7.58,11.14]	[8.38,10.06]
Turb	1.91±0.23	1.53±0.16	1.78±0.11	1.52±0.17	3.84±0.17	1.8±0.22	4.21±0.44	2.11±0.58	4.05±0.61	1.2±0.14 ²	1.2±0.11
	[1.6,2.34]	[1.31,1.86]	[1.59,1.94]	[1.28,1.77]	[3.57,4.13]	[1.52,2.2]	[3.55,4.88]	[1.33,3.41]	[3.1,5.03]	[1.01,1.45]	[1.06,1.37]
pH	8.13±0.08	8.44±0.05	8.26±0.1	8.65±0.06	8.25±0.07	7.97±0.04	8.23±0.05	7.88±0.05	8.01±0.05	8.15±0.11	8.03±0.06
	[8.01,8.24]	[8.36,8.53]	[8.14,8.42]	[8.57,8.78]	[8.15,8.34]	[7.91,8.04]	[8.16,8.33]	[7.81,7.96]	[7.95,8.09]	[7.98,8.32]	[7.91,8.11]
SpCond	850.5±52.5	1224.4±39.0	1051.9±32.1	1337.6±16.1	727.5±6.5	733.0±23.5	822.6±21.6	789.0±48.6	768.6±32.9	1094.1±12.5	1169.9±31.6
	[778.6,924.2]	[1162.0,1275.0]	[996.2,1088.3]	[1307.7,1357.7]	[718.2,739.7]	[698.0,773.7]	[789.5,858.3]	[705.8,842.1]	[721.9,822.2]	[1076.6,1113.0]	[1115.1,1206.7]
<i>Chl-a</i>	4.19±0.57	2.72±0.47	2.63±0.45	3.2±0.26	2.12±0.15	2.84±0.58	2.19±0.13	2.8±0.6	1.35±0.13	4.46±0.85	2.57±0.13
	[3.47,5.18]	[1.88,3.53]	[2.09,3.78]	[2.9,3.74]	[1.92,2.21]	[2.11,4.27]	[2.02,2.46]	[2.22,4.03]	[1.17,1.6]	[3.41,6.01]	[2.38,2.71]

Note: For each parameter, the mean ± 1 standard deviation of the hourly value was shown for each campaign, followed by the 90% range (from 5% to 95%).

Q: discharge ($\text{m}^3 \text{s}^{-1}$). T: water temperature ($^{\circ}\text{C}$). N: NO_3^- -N concentration (mg l^{-1}). DO: dissolved oxygen (mg l^{-1}). Turb : turbidity (FNU). SpCond: specific conductivity ($\mu\text{S cm}^{-1}$). *Chl-a*: *chlorophyll a* ($\mu\text{g l}^{-1}$). τ : travel time from upstream to downstream stations (h). v : velocity, calculated by dividing river length by τ (m s^{-1}).

References

- Baird, R. B., Eaton, A. D., & Rice, E. W. (Eds.). (2017). *Standard Methods for the Examination of Water and Wastewater* (23rd ed.). Washington DC: American Public Health Association.
- Bott, T. L. (2007). Primary Productivity and Community Respiration. In *Methods in Stream Ecology* (pp. 663–690). New York: Elsevier. <https://doi.org/10.1016/B978-012332908-0.50040-1>
- Guse, B., Bronstert, A., Rode, M., Tetzlaff, B., & Wendland, F. (2007). Application of two phosphorus models with different complexities in a mesoscale river catchment. In *Advances in Geosciences* (Vol. 11, pp. 77–84). Copernicus GmbH. <https://doi.org/10.5194/adgeo-11-77-2007>
- Kunz, J. V., Hensley, R., Brase, L., Borchardt, D., & Rode, M. (2017). High frequency measurements of reach scale nitrogen uptake in a fourth order river with contrasting hydromorphology and variable water chemistry (Weiße Elster, Germany). *Water Resources Research*, 53(1), 328–343. <https://doi.org/10.1002/2016WR019355>
- Yang, X., Jomaa, S., Zink, M., Fleckenstein, J. H., Borchardt, D., & Rode, M. (2018). A New Fully Distributed Model of Nitrate Transport and Removal at Catchment Scale. *Water Resources Research*, 54(8), 5856–5877. <https://doi.org/10.1029/2017WR022380>
- Zhang, X., Yang, X., Jomaa, S., & Rode, M. (2020). Analyzing impacts of seasonality and landscape gradient on event-scale nitrate-discharge dynamics based on nested high-frequency monitoring. *Journal of Hydrology*, 591, 125585. <https://doi.org/10.1016/j.jhydrol.2020.125585>

Chapter 4: Large-stream nitrate retention patterns shift during droughts: seasonal to sub-daily insights from high-frequency data-model fusion

(An edited version of this paper was copyright by Elsevier Copyright (2023))

4.1. Abstract

High-frequency nitrate-N (NO_3^- -N) data are increasingly available, while accurate assessments of in-stream NO_3^- -N retention in large streams and rivers require a better capture of complex river hydrodynamic conditions. This study demonstrates a fusion framework between high-frequency water quality data and hydrological transport models, that (1) captures river hydraulics and their impacts on solute signal propagation through river hydrodynamic modeling, and (2) infers in-stream retention as the differences between conservatively traced and reactively observed NO_3^- -N signals. Using this framework, continuous 15-min estimates of NO_3^- -N retention were derived in a 6th-order reach of the lower Bode River (27.4 km, central Germany), using long-term sensor monitoring data during a period of normal flow from 2015-2017 and a period of drought from 2018-2020. The unique NO_3^- -N retention estimates, together with metabolic characteristics, revealed insightful seasonal patterns (from high net autotrophic removal in late-spring to lower rates, to net heterotrophic release during autumn) and drought-induced variations of those patterns (reduced levels of net removal and autotrophic nitrate removal largely buffered by heterotrophic release processes, including organic matter mineralization). Four clusters of diel removal patterns were identified, potentially representing changes in dominant NO_3^- -N retention processes according to seasonal and hydrological conditions. For example, dominance of autotrophic NO_3^- -N retention extended more widely across seasons during the drought years. Such cross-scale patterns and changes under droughts are likely co-determined by catchment and river environments (e.g., river primary production, dissolved organic carbon availability and its quality), which resulted in more complex responses to the sequential droughts. Inferences derived from this novel data-model fusion provide new insights into NO_3^- dynamics and ecosystem function of large streams, as well as their responses to climate variability. Moreover, this framework can be flexibly transferred across sites and scales, thereby complementing high-frequency monitoring to identify in-stream retention processes and to inform river management.

4.2. Introduction

Anthropogenically induced high nitrate (NO_3^-) levels in rivers are a pervasive threat to freshwater and coastal ecosystems, especially under the changing climate (Costa et al., 2022; Reusch et al., 2018). In addition to efforts to control point- and diffuse-sources, the “self-cleansing” capacity of river systems to retain and process NO_3^- has also been recognized (Ensign and Doyle, 2006; Jäger et al., 2017). Restoring rivers and their floodplains has been advocated as a part of “nature based” solutions to reduce NO_3^- losses to water bodies, with multiple co-benefits (EEA, 2021).

Large streams and rivers (e.g., $\geq 4^{\text{th}}$ order) receive considerable management attention, due to the impacts of nutrient pollution on water-related ecosystem services, and because in-stream biological activity likely contributes disproportionately to whole-river ecosystem function (Wollheim et al., 2022). However, current understanding of in-stream processing is mostly extrapolated from tracer-addition experiments or intensive process monitoring in small, headwater streams (Ensign and Doyle, 2006). Large streams and rivers are subject to a range of complex interactions between hydrodynamics, biological and anthropogenic activities that may limit the applicability of extrapolation from headwater measurements (Bernal et al., 2019). Moreover, owing to the practical challenges of making direct process measurements in large, deep non-wadable rivers, there is a shortage of data on whole-stream NO_3^- biochemical cycling and its constituent pathways (e.g., assimilation, denitrification, mineralization and nitrification).

Fostered by sensor technology development, high-frequency measurements are increasingly being used to infer in-stream NO_3^- retention and release in large streams and rivers (Rode et al., 2016b). Biochemical process-related information can be directly extracted from NO_3^- timeseries (Burns et al., 2019; Heffernan and Cohen, 2010). However, inferences based purely on high-frequency data are often conducted under well constrained conditions, e.g., a steady-state upstream boundary (Hensley and Cohen, 2016; Yang et al., 2019). While the more adaptive two-station approach allows a dynamic upstream boundary, the inference accuracy is still largely subject to influences of hydraulic transformation (e.g., dispersion Hensley and Cohen, (2016)) and dilution/enrichment from lateral inflow along the reach between upstream and downstream stations (Zhang et al., 2023). Consequently, in-stream process quantifications remain uncertain when extrapolating to various hydro-morphological river conditions outside the monitored reaches. As a result, while continuous high-frequency monitoring has been deployed for multiple years across river sizes and geomorphological conditions (Arndt et al., 2022; Bieroza et al., 2023; Rode et al., 2016b), inferences of in-stream processes using such invaluable long-term data, is often obscure due to dynamic flow conditions and their complex convolutions with biological activity (Hensley and Cohen, 2016; Payn et al., 2017). This complexity has hindered multi-year continuous investigations of in-stream NO_3^- retention, and the responses of in-stream processes to the changing climate, such as the severe droughts in Europe over last five years.

Conventional two-station inferences of in-stream NO_3^- biogeochemical retention along the reach were based on load ($Q \times \text{NO}_3^- - N$) differences between the upstream and downstream stations. However, purely using the monitored high-frequency data is challenging to estimate lateral inflows and transport time lags, and their inferences on the calculation require specific justifications (Jarvie et al., 2018; Zhang et al., 2023). Alternatively, high-frequency discharge (Q) and solute dataset are increasingly used to calibrate river modeling approaches, which normally include both hydraulic transport (advective and dispersive) and biogeochemical retention terms in their master equation of mass

balance (Hensley and Cohen, 2016; Huang et al., 2022). However, the simulations of biological processes are often challenged by complex hydraulic-biological convolutions and model parameterization (Rode et al., 2007). To benefit from the complementary data analysis and modelling, here we propose an innovative data-model fusion framework for in-stream process inferences in large streams and rivers. The framework is mainly based on the two-station high-frequency monitoring, but untangling impacts of hydraulic transformations along the reach using the advanced features of the Water Quality Analysis Simulation Program (WASP version 8) water and tracer simulations (Ambrose and Wool, 2017; Knightes et al., 2019). Such methodological improvements are necessary to study the nitrate retention dynamics under varying climatic and flow conditions.

Here we illustrated the analysis using six years of data from a 27.4 km 6th order reach of the lower Bode River, central Germany. The objectives of this study were: (1) to estimate continuous in-stream NO₃⁻ overall retention (net removal/release) over the normal (2015-2017) and drought (2018-2020) years based on the fusion of high-frequency data analysis and modeling; (2) to investigate responses of the in-stream processes to the droughts from sub-daily to inter-annual scales; and (3) to unravel potential environmental factors that control the in-stream processes and their pattern shifts under the drought disturbances.

4.3. Method and Materials

4.3.1. Study site and long-term high-frequency monitoring

The Bode River, ca. 169 km long with a watershed area of 3270 km², originates in the Harz Mountain area, central Germany. The studied reach of the lower Bode River (6th order) is surrounded by intensive lowland arable land (Figure 4.1a). During the study period 2015-2020, multi-parameter high-frequency monitoring equipment was deployed at two stations (27.4 km): the upstream station Groß Germersleben (GGL) and the downstream station Staßfurt (STF). The river reach mostly exhibits rectangular or trapezoidal cross-sections, due to artificial modifications in the 1970s for the purpose of agricultural activities. There are also three overflow weirs installed along the reach. The riverbed substrate consists of mostly sand and small gravel, with an average width and slope of 20 m and 0.4 ‰, respectively. Patchy bankside deciduous trees partially shade the riparian margins during summer, while the relatively open canopy allows high irradiance at the river surface and development of phytoplankton and benthic algae (Huang et al., 2022).

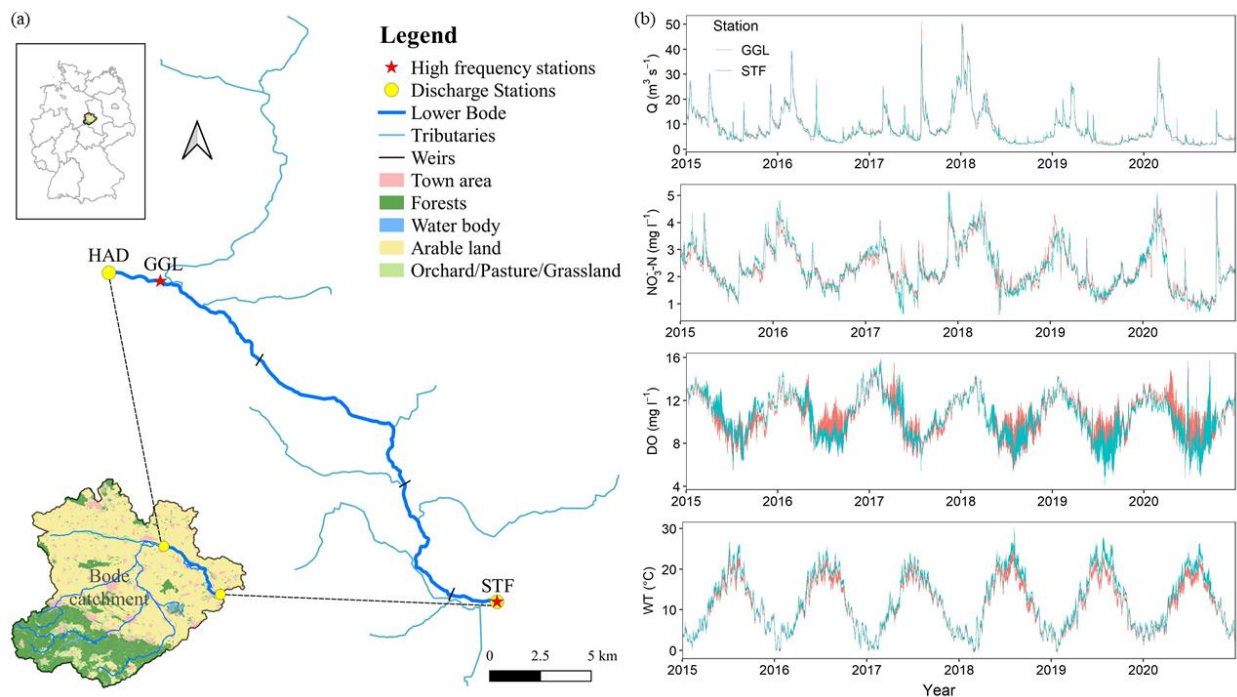


Figure 4.1. (a) The Lower Bode river reach and the multi-parameter high-frequency monitoring scheme. (b) 15-min measurements of discharge (Q), NO_3^- -N concentrations, dissolved oxygen (DO) and water temperature (WT) at the upper Groß Germersleben (GGL) and lower Staßfurt (STF) stations.

At each station, YSI 610 sensors (Yellow Springs, US) measured dissolved oxygen (DO), pH, water temperature (WT), and electric conductivity (EC) at 15-min intervals. ProPS-UV sensors (TriOS GmbH, Germany) measured spectral absorbance at 254 nm (SAC, as a proxy of dissolved organic carbon) and Nitrate-N (NO_3^- -N, precision of $0.03 \pm 2\%$ mg l^{-1}) concentrations, also at 15-min intervals. More details about sensor accuracy and maintenance were described in Rode et al. (2016a). Hourly data on photosynthetically active radiation (PAR) were collected at an eddy-covariance flux tower at Wulferstedt station (15.6 km north-west of GGL). Discharge (Q) data at 15-min intervals were obtained from the Saxony-Anhalt water authority (Water Service data portal <https://gld.lhw-sachsen-anhalt.de/>, accessed 4/27/2023) at station Hadmersleben (HAD, 2.7 km upstream of GGL without significant lateral inflows) and station STF (Figure 4.1a). According to monthly sampled analytical measurements over 2015-2020 (77 total samples, Helmholtz Centre for Environmental Research - UFZ), the total nitrogen concentrations were 3.60 ± 1.60 mg l^{-1} , of which NO_3^- -N accounts for ca. 70%; other riverine nitrogen forms were much lower, with ammonium-N concentrations of 0.175 ± 0.170 and the differences between total nitrogen and all inorganic nitrogen of 0.83 ± 0.19 mg l^{-1} (organic nitrogen is not measured directly). There are eight small tributaries along the study reach; however, total tributary inputs contributed less than 2% of total Q over 2015-2020, with NO_3^- -N concentrations of 7.67 ± 3.10 mg l^{-1} , as simulated by the catchment mHM-Nitrate model (Zhou, et. al., 2022).

The study region has experienced dramatically changing climatic conditions, especially severe summer droughts since 2018 (Zhou et al., 2022). Annual average Q at STF decreased from $9.50 \text{ m}^3 \text{ s}^{-1}$ during the “normal” years (2015-2017) to $7.21 \text{ m}^3 \text{ s}^{-1}$ during the “drought” years (2018-2020) (Figure 4.1b). Comparing normal- and drought-year summers (Jun-August), average Q decreased from 6.58 to $2.75 \text{ m}^3 \text{ s}^{-1}$, average NO_3^- -N concentration decreased from 1.79 to 1.39 mg l^{-1} , and average WT increased from 20.1 to $21.6 \text{ }^\circ\text{C}$.

4.3.2. Two-station inferences of NO_3^- retention based on the fusion of high frequency data monitoring and the WASP water and tracer simulations

The WASP model (version 8.32) has been developed by the United States Environmental Protection Agency and has been applied to different surface water systems (Wool et al., 2020). The model allows users to flexibly define and arrange control volumes (i.e., fully mixed finite segments), and resolves the mass balance over each control volume, considering material exchanges via advective and dispersive transports. WASP further distinguishes free-flowing, ponded and backwater/tidal influenced segments in a stream network, and solves them using equations of kinematic wave, weir overflow and dynamic flow, respectively (Ambrose and Wool, 2017). The tracer module implemented in WASP8 is a dummy sub-model for substances with no kinetic interactions.

In this study, we conducted 15-min interval, one-dimensional WASP8 simulations of water and tracer (i.e., virtually simulating transport of NO_3^- -N as a conservative tracer) transport in the study reach. We upgraded a prior WASP model setup in the study reach by Huang et al. (2022), with 31 segments defined as free-flowing reaches and 3 segments as ponded reaches at the locations of the weirs (Figure 4.1a). Discharge at station HAD was used as the upstream flow inputs, and the measured NO_3^- -N concentrations at GGL were taken as the virtual tracer inputs. Inputs of flow and tracer loads from the tributaries were simulated from a catchment mechanistic model mHM-Nitrate (Yang et al., 2018; Yang and Rode, 2020) (see detailed model simulations in the Bode catchment in Zhou et al. (2022)). Using the WASP hydrodynamic simulations, the upstream tracing signals of conservative NO_3^- -N concentration (N_{trck}) were transported to the downstream station STF. Thus, differences between the tracked loading (L_{trck}) predicted by the WASP virtual tracer modeling and the observed loading (L_{obs}) at STF were taken as retention along the river reach. Areal retention rates (U_T , mg N m^{-2} per time step) and efficiencies (E_{UT} , %) can be further obtained based on this data-model fusion inferences:

$$U_T = \frac{L_{trck} - L_{obs}}{A} = \frac{(N_{trck} - N_{obs}) \times Q_{STF}}{A} \quad (1)$$

$$E_{UT} = \frac{L_{trck} - L_{obs}}{L_{trck}} \times 100 \quad (2)$$

where A denotes the total river benthic area ($27400 \times 20 \text{ m}^2$) and N denotes NO_3^- -N concentrations. Note that we used observed discharge at STF (Q_{STF}) for L_{trck} to further reduce model uncertainty

leveraged from hydraulic simulations (see Section 4.4). Therefore, U_T represents overall NO_3^- net removal or net release (with positive and negative values, respectively), and E_{UT} was only analyzed in periods exhibiting net removal ($U_T > 0$).

4.3.3. Calculations of stream metabolism and in-stream autotrophic NO_3^- assimilation

Estimates of whole-stream metabolisms (i.e., gross primary production - GPP and ecosystem respiration - ER) were calculated based on the 15-min DO measurements. The hydraulic characteristics at STF were heavily disturbed by impoundment effects due to bridge piers and submerged macrophytes (field experience), and this hindered reliable estimates of stream metabolism using the data at STF. Therefore, we applied the single-station method (Odum, 1956), with reaeration coefficients from Bott (2006), using the data at the upper station GGL. We recognize that the DO signal at GGL is generated by metabolic processes occurring upstream of the study reach. However, we believe it to be more representative of average conditions in the study reach than the downstream STF station. This was verified by cross-comparisons between metabolic information available in the Bode region (see details in Text S4.1 and Table S4.1). Please also refer to Yang et al. (2019) for detailed calculation equations of the single-station approach.

We further estimated NO_3^- -N uptake via autotrophic assimilation based on the whole-stream metabolism at daily time step. Gross assimilations by autotrophs (U_A , $\text{mg N m}^{-2} \text{d}^{-1}$) can be calculated based on the measured stream metabolism and the stoichiometric C:N ratio:

$$U_A = \frac{r_a \times GPP}{2.286 \times C:N_a} \times 1000 \quad (3)$$

where autotrophic respiratory rate r_a was set as 0.5, assuming one mol of C fixed per mol of O_2 produced, and half of GPP ($\text{g O}_2 \text{m}^{-2} \text{d}^{-1}$) becomes net production (Rode et al., 2016a). The molar C:N ratio was 9.4, taken from local biofilm measurements (Kamjunke et al., 2015), and the constant 2.286 (32/14) converts the molar ratios to a mass basis.

4.3.4. Diel pattern detection and statistical analysis

The 15-min continuous NO_3^- -N retention timeseries allowed assessment of in-stream processes from sub-daily (i.e., the diel patterns) to inter-annual scales. At hourly scale, we specifically investigated diel patterns of net removal ($U_T > 0$, $\text{mg N m}^{-2} \text{h}^{-1}$). Dates for this diel pattern analysis were detected sequentially according to (1) $U_T > 0$ for all 24 hours, (2) minimal diel variations in Q (i.e., $< 50^{\text{th}}$ quantile of coefficient of variations), and (3) generally low-flow conditions (i.e., daily Q $< 25^{\text{th}}$ quantile for each year). The constraints of relative steady Q were set to avoid impacts of flow variations on NO_3^- -N signals.

The k -mean clustering method was performed to further classify them into different clusters, using the “*stat*” R package (R core team, 2022). Please refer to Text S4.2 for details of the k -mean clustering

analysis. Moreover, statistical analyses were all performed in R software, including the nonparametric Mann-Whitney U test (“*stats*” package) and the curve fitting (the GAM-based smooth function “*geom_smooth*” in “*ggplot2*” package).

4.4. Results

4.4.1. WASP simulations of discharge and traced NO_3^- dynamics

The WASP discharge simulations performed very well at the downstream station STF (i.e., Kling-Gupta Efficiency-KGE (Gupta et al., 2009) of 0.98 and percentage bias of 0.7%, Figure 4.2). This indicates that WASP captured water dynamics well in the lower Bode River, in line with Huang et al. (2022). We noted that discharge discrepancies were slightly greater during the recession and driest periods of the drought years 2018-2020, though they were negligible in terms of the general river water dynamics (Figure 4.2a).

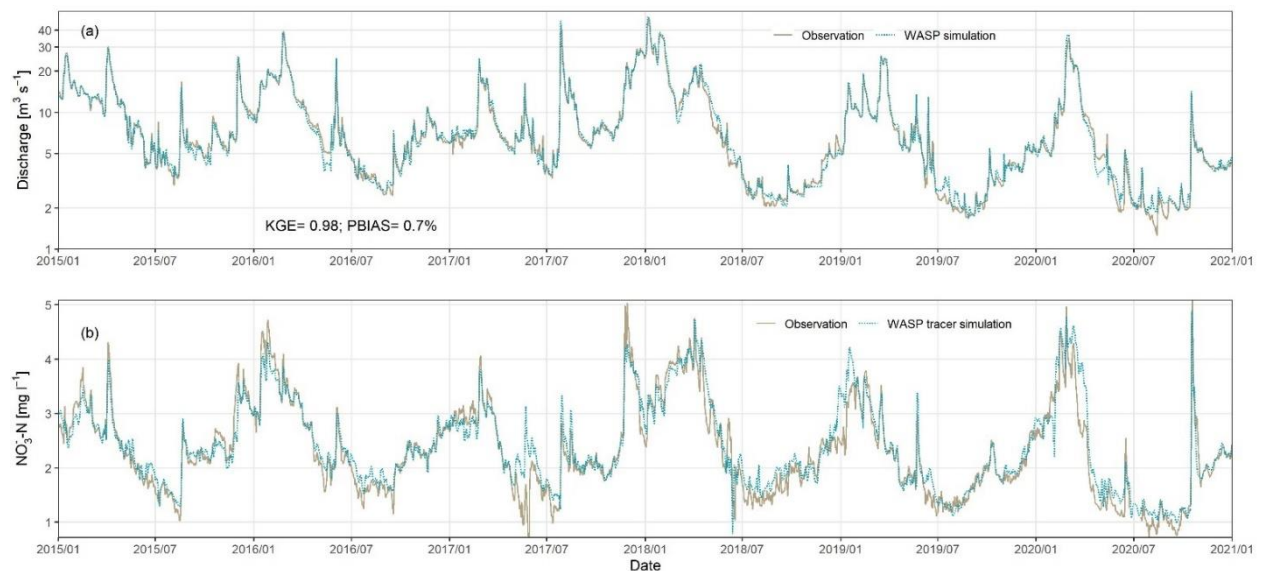


Figure 4.2. The WASP simulations of discharge (a) and NO_3^- -N tracer concentrations (b) in the reach of the lower Bode River plotted at a daily timestep. KGE–Kling-Gupta Efficiency and PBIAS–overall percentage of relative differences between discharge observations and simulations.

4.4.2. Daily overall U_T and stream metabolisms and their seasonal variations in the normal and drought years

Continuous daily retention rates U_T were estimated from the data-model fusion from 2015 to 2020 (Figure 4.3a). U_T mostly ranged between -337.8 and $419.4 \text{ mg N m}^{-2} \text{ d}^{-1}$ (i.e., 5% and 95% quantiles, respectively), while the values varied with season and across years. Apart from disturbances of annual high-flows and short-term flow events, U_T exhibited a consistent seasonal pattern in the normal period 2015-2017 (Figure 4.3a, upper panels): (1) winter and early spring seasons exhibited extensive net NO_3^- release ($U_T < 0$), though largely affected by the annual high flows; (2) general net removal ($U_T > 0$) occurred after the annual high-flow season, with significantly different retention rates in May-June

than July-September (179.5 ± 224.9 vs 104.7 ± 65.2 mg N m⁻² d⁻¹, among 123 and 230 days, respectively, with $Q <$ median value of 7.10 m³ s⁻¹; Mann-Whitney U test: Wilcoxon $W = 17453$, $p < 0.001$); (3) after October, net NO₃⁻ release occurred until the next early spring (except for the low winter Q in 2016). For the drought-impacted period 2018-2020 (Figure 4.3a, lower panels), U_T seemed to be still higher during May-June than the later months, while the pattern was heavily disturbed by the annual-high flow recessions and small- to median-size flow events. Moreover, U_T was generally reduced during the annual low-flow seasons (e.g., 68.6 ± 45.44 mg N m⁻² d⁻¹ among 206 days in July-September), and the late-autumn net release during the drought years was not as consistently present as it was during the normal years. The removal efficiency E_{UT} was higher during the drought than in normal years ($10.8 \pm 8.1\%$ vs $8.6 \pm 9.5\%$, respectively), and the drought years exhibited prolonged periods with higher E_{UT} (e.g., around 25%, Figure S4.1a).



Figure 4.3. (a) Daily total retention rate U_T in each year based on the model-data fusion framework, and monthly counts of the four clusters of diel patterns. (b) Daily ratios of whole-stream gross primary production and respiration (i.e., P/R ratio) in the normal (2015-2017) and the drought (2018-2020) years. Note that, for subplot (b), P/R ratios on dates exhibiting diel patterns are highlighted with the same cluster colors as in subplot (a).

Such varying seasonal patterns between the normal and drought years were also observed in the whole-stream metabolic characteristics (Figures 4.3b and S4.2). In spring seasons, the ratio of GPP to ER (P/R) was > 1 , indicating autotroph-dominated system. This occurred in both the normal and drought years (Figure 4.3b), though in the former it was likely driven by relatively high levels of GPP, while in the latter by relatively low ER (Figure S4.2). During the summer seasons, the P/R ratios varied largely among the normal years, often with similar levels of GPP but more variable ER (Figure S4.2). In contrast, the ratios were more consistent and relatively high in the drought years (0.77 ± 0.20).

In autumn and winter, P/R ratios were extensively less than 1, indicating a heterotroph-dominated system for both normal and drought years. Comparatively, the drought years exhibited higher P/R ratios (Figure 4.3b) primarily induced by the significantly different ERs (i.e., 2.85 ± 1.04 vs 3.65 ± 2.27 g O₂ m⁻² d⁻¹ over October-February of the drought and normal years, respectively; Mann-Whitney U test: $W = 75740$, $p < 0.001$, Figure S4.2). The GPP-informed autotrophic NO₃⁻ uptake (U_A) maintained similar in the normal and drought years (i.e., 47.92 ± 42.76 vs 51.04 ± 42.38 mg N m⁻² d⁻¹, respectively, Figure S4.1a), while its proportions to U_T were more consistently > 1 during July-October of the drought years (calculated among dates with $U_T > 0$ and below-median Q, Figure S4.1b).

4.4.3. Diel patterns of net NO₃⁻-N removal and their predominance under the normal and drought years

The high-frequency data-model fusion inference provided the unique opportunity to investigate sub-daily patterns of NO₃⁻-N removal and their variations under different hydrological conditions. Quantifiable diurnal variation in U_T was detected in a total of 178 days (90 and 88 days in the normal and drought years, respectively), and could be further grouped into four distinct clusters (Figures 4.4 and 4.3, and detailed results of the k -mean clustering in Figure S4.3). Clusters C1 and C2 exhibited increased removal during the daytime hours, with the diel maxima occur after and before 12:00, respectively (Figure 4a and b); Clusters C3 and C4 exhibited decreased removal during the daytime hours, with the diel minima occur around 12:00 for the former (Figure 4.4c) while the latter exhibited more noteworthy decreases before noon and delayed diel minima (Figure 4.4d). Meanwhile, the seasonal occurrence of the four clusters likely changed between the normal and drought years (the upper and lower panels of Figure 4.3a, respectively). Specifically, in the normal years, C1 and C2 mostly occurred before August, while C3 and C4 dominated the late summer and autumn seasons; in contrast, during drought years C1 and C2 patterns persisted into the late summer and autumn (accounting for 67% of total days detected in the drought years, compared to that of 38% in the normal years), and also more evenly distributed across summer-autumn seasons. The four diel patterns did not show substantial differences between normal and drought years, with the exception of the C1 cluster that exhibited more delayed diel maxima in the normal years than the drought years, (Figure 4.4, upper panels). However, the absolute removal rates were significantly lower under the drought conditions, except for the C3 cluster even though there existed extraordinarily high removal days in 2017 (Figure 4.4, lower panels).

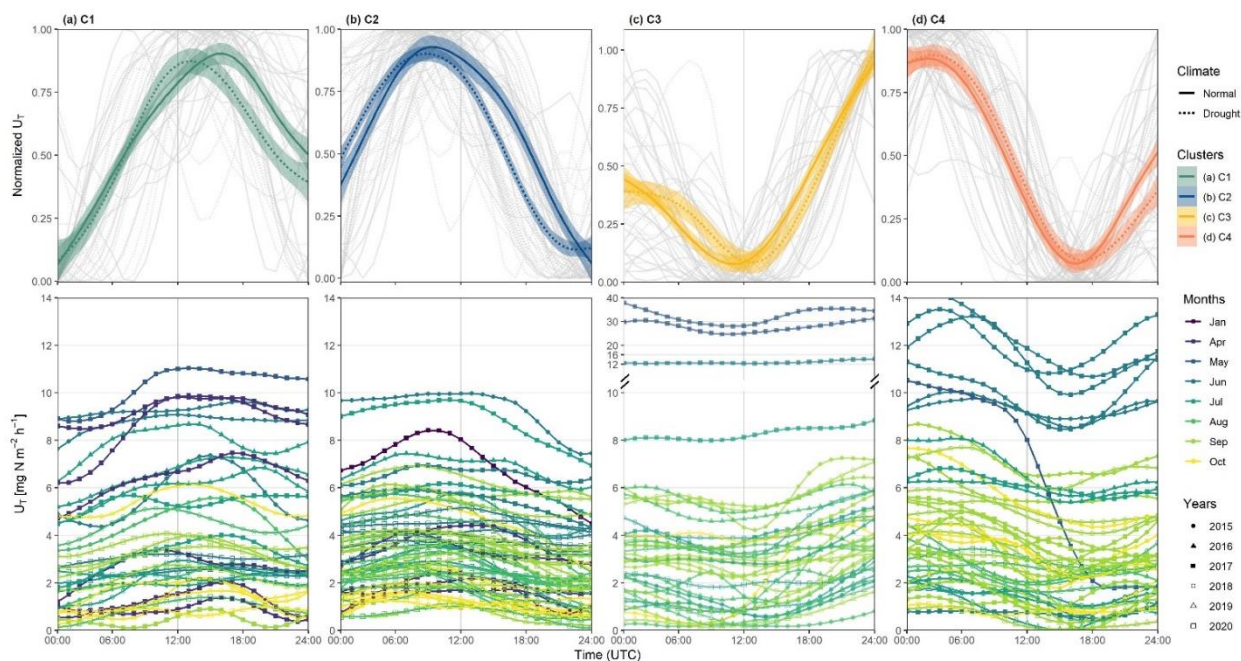


Figure 4.4. The four types of U_T diel patterns clustered among the detected 178 days and the corresponding hourly variations of retention rates (upper and lower panels, respectively). Note that the k -mean clustering was performed based on the max-min normalized U_T values.

4.5. Discussion

4.5.1. Continuous inferences of NO_3^- -N retention in complex rivers enabled by a novel high-frequency data-model fusion framework

Using a novel data-model fusion framework, we derived continuous estimates of high-frequency NO_3^- -N retention over six years in the 6th order reach of the lower Bode River. To our knowledge, this is among the first time that such in-stream inferences have been made in a large stream or river with complex flow dynamics as well as across different hydrological conditions. Importantly, the model-data fusion framework provided reasonable estimates of in-stream NO_3^- -N retention in the well-studied lower Bode region, as cross validated by previous studies using different methodologies. For example, previous work (Zhang et al., 2023) using the conventional two-station method reported a similar range and seasonal variations in net NO_3^- -N retention and release (-205 and $381 \text{ mg N m}^{-2} \text{ d}^{-1}$ as for 5th and 95th quantiles, respectively, with consistently higher values in campaigns during May-June than July-September). Huang et al. (2022) applied the WASP biogeochemical modeling in the same lower Bode River reach and calibrated model parameters using the high-frequency data (including only the first drought year 2018). They also obtained generally similar levels of net NO_3^- -N removal, and similar seasonal patterns (Huang et al., 2022).

Our estimates of in-stream retention rate and retention efficiency were also well in line with wider literature ranges (Alexander et al., 2009; Ensign and Doyle, 2006; Miller et al., 2016; Seitzinger et al.,

2002). Ensign and Doyle (2006) reported the interquartile range of 9.1 and 376.7 mg N m⁻² d⁻¹ based on 14 nutrient-addition/isotope-tracer experiments conducted in 4th order streams. This fits well with our estimated range of the NO₃⁻ removal (Figure 4.3a), which is also similar to the headwater measurements from the pioneering LINX II project (Mulholland et al., 2006). Heffernan and Cohen (2010) deployed a high-frequency monitoring in a Florida spring-fed river and revealed that U_T is two times higher in spring than in fall seasons, though the reported magnitude was relatively high due to high denitrification rates in subtropical rivers (Heffernan et al., 2010). Using E_{UT} as a more cross-comparable removal metric, Seitzinger et al. (2002) found that individual reaches generally retain < 20% of N input, and specifically for 5th- and higher-order reaches, the proportions are mostly < 10%. This is well in line with our estimated ranges (e.g., mostly < 20.8% as of the 90% quantile value over the six years).

The high-frequency data-model fusion framework allows assessment of in-stream processes to be extended across temporal and spatial scales, thereby advancing understanding of NO₃⁻ processes. First, the framework can make use of the increasingly available long-term time series of high-frequency monitoring, being collected as part of routine monitoring by water authorities. Given the logistic convenience and advances of cross-parameter analysis (Rode et al., 2016b; van Geer et al., 2016), these continuous sensor deployments are often co-located with flow gauging stations, allowing assessment of varying and complex flow regimes and their impacts on biogeochemical processes (Bieroza et al., 2023; Oldham et al., 2013). Integrating the robust in-stream hydraulic and conservative tracer modeling facilitates the extraction of biogeochemically induced nutrient signals, even with shifts between advective and dispersive flow dominance and variations in water residence/travel times (Hensley and Cohen, 2016). This, in our view, serves as a step forward in maximizing the multi-benefits of these unique datasets, especially compared to the uses of constraining synthesized in-stream water quality models at a finer temporal resolution (though still informative, see Huang et al. (2022)).

Second, the framework quantifies in-stream NO₃⁻ retention from sub-daily to inter-annual scales, providing new process understanding (see discussion in Section 4.5.2) and reference values for specific processes. For instance, the WASP modeling by Huang et al., (2022) also revealed the consistent pattern of net release after late-autumn (i.e., $U_T < 0$), while with more conservative estimates (17.4 mg N m⁻² d⁻¹ compared to our inferences of > 100 mg N m⁻² d⁻¹, Figure 4.3a). Given the well-acknowledged poor process understanding (von Schiller et al., 2015) and the simplified model conceptualization, our inferences derived more directly from high-frequency data, can be further used to validate model simulations and improve in-stream process representation in water quality models.

4.5.2. Insights into seasonal patterns of NO_3^- retention and release under the changing climate

Both net NO_3^- removal ($U_T > 0$) and net NO_3^- release ($U_T < 0$) exhibited substantial seasonality, which also differed between the normal (2015-2017) and drought (2018-2020) years. Moreover, this variation was well supported by the independent calculations of stream metabolic characteristics, which also exhibited strong seasonality (Figure 4.3 and S4.2).

Despite the flow-induced uncertainty during the high-flow periods, winter to early-spring seasons showed extensive net NO_3^- release, which was more pronounced in the normal years than the drought years. Meanwhile, the normal-year P/R $\ll 1$ and ER remained as high as that in the summer seasons, indicating higher heterotrophic microbiological activity during the normal year. Such net heterotrophy likely also reflects reduced rates of autotrophic activity (due to seasonally lower light availability and water temperature) and promoted remineralization processes (given that riverine dissolved organic carbon (DOC) is abundantly flushed from the catchment and riparian areas). The DOC in anthropogenically affected rivers is likely more labile to the microbial community than in unaffected rivers (Graeber et al., 2012; Stutter et al., 2018). Meanwhile the relatively high water temperature (i.e., interquartile range of 3.4 and 7.9 °C) may have contributed to higher rates of microbiological transformation of DOC (Lu et al., 2013). However, under sequential droughts, the recalcitrance of DOC could have been increased due to the longer exposure times of terrestrial organic matter to catchment microbiological transformations before being transported (Catalán et al., 2016). This agrees well with the observed low ERs (Figure S4.2) but with largely maintained DOC concentrations during the drought years (monthly sampled DOC measurements in Figure S4.4, although direct DOC quality information is not available). Also, the reduced levels of net NO_3^- release during winter and early-spring seasons may be ascribed to the low respiration activity.

The extensive net removal patterns during the mid-spring to early-autumn warmer seasons are well in line with general literature findings that highlight the significant nutrient “cleansing function” of lotic ecosystems, while the dominant mechanisms could vary largely under different stream and climatic conditions (Heffernan and Cohen, 2010; Jarvie et al., 2018; Jones et al., 2015). The net removal reached the highest level between mid-spring and early-summer, associated with the promoted and autotrophy-dominated ecosystem activities (the high P/R ratios and increased GPP and ER, Figures 4.3 and S4.2). The normal-year overall net removal was still greater than the autotrophic assimilation, although with increasing amount and proportions for the latter pathway. This indicates that (1) autotrophic assimilation played a dominant role in NO_3^- -N uptake, primarily due to the sufficient light availability during the season before leaf-out (Rode et al., 2016a; Yang et al., 2019) and (2) other removal pathways via heterotrophic direct assimilation and denitrification were likely substantial in the normal years, given the abundant nutrient and organic matter availability (Kamjunke et al., 2013). In contrast, the drought years exhibited relatively reduced overall net removal and ER, but a similar

level of GPP, together resulting in earlier, more consistent $U_A/U_T > 1$ (Figure S4.1b). This indicates an earlier predominance of autotrophic assimilation, which is also buffered partly by N-release processes (Jarvie et al., 2018). The reduction in other heterotrophic pathways is likely ascribed to the limited allochthonous labile DOC during the droughts, given the synchronous changes between ER and NO_3^- -N removal (Stutter et al., 2018; Sunjidmaa et al., 2022).

Nevertheless, the increasingly buffered autotrophic assimilation ($U_A/U_T \gg 1$) under dry conditions indicated that autochthonous DOC from antecedent primary production may have provided an important energy source.. This is supported by DOC measurements across the Bode River network by Kamjunke et al. (2013), that the September samples from the lower Bode River exhibited better DOC quality (i.e., lower molecular weights and lower humic content) than the headwater samples. Also, Dupas et al. (2017) demonstrated that the Bode lowland aquatic systems likely acted as a DOC source. There is a pressing and strategic need for better mechanistic understanding of the responses of river ecosystems to climate variability.

4.5.3. Insights into diel patterns of NO_3^- retention under the changing climate

The high-frequency data-model fusion framework also allowed in-depth investigations of diel patterns of NO_3^- -N removal. Here we identified four distinct clusters of diel patterns, as well as their seasonal distributions, revealing shifts in dominant NO_3^- retention processes under normal and drought conditions. We can speculate as to some of the underlying mechanisms potentially responsible for generating these patterns.

Cluster C1 represented a typical autotrophic assimilation induced diel pattern, which is correlated with the diurnal variations of GPP and related environmental factors (e.g., radiation, temperature and DO; Figures 4.4a, S4.5a and S4.6). Interestingly, the diel removal maxima were delayed relative to those of GPP, indicating physiological time lags between NO_3^- -N removal and photosynthesis. This is potentially due to photosynthesis providing additional energy to further reduce NO_3^- for assimilation and biosynthesis (Mulholland et al., 2006). The observed time-lag differences between normal and drought years are in line with the spring-fall differences reported by Heffernan and Cohen (2010), which may be related to seasonal differences of such energetic costs.

Cluster C2 also largely represented the dominance of autotrophic assimilation, given the extensive positive correlations with GPP-related factors (Figure S4.5) and their well-fitted falling limbs after 12:00 (Figure S4.6b). Besides, as a concatenation of Cluster 1 and Clusters 3/4, NO_3^- autotrophic assimilation in the afternoon might be buffered to a greater extent by release processes, resulting in apparently earlier net removal maxima. These diurnally earlier NO_3^- removal peaks are also reported in high-frequency NO_3^- data analysis, with complex, often unclear mechanisms (Aubert and Breuer, 2016; Greiwe et al., 2021; Heffernan and Cohen, 2010). Here we observed that (1) this pattern

occurred mostly after high-flow recessions in the normal years (Figure 4.3a), which is coincidentally presented by Aubert and Breuer (2016) via data mining of NO_3^- timeseries; (2) the high correlations with SAC in drought years at the diurnally normalized scale (Figures S4.5 and S4.6b). This indicates a crucial role of DOC availability, particularly its quality as aforementioned, in shaping (either promoting or constraining) the diel pattern of NO_3^- removal.

Clusters C3 and C4 revealed less-explored diel patterns with diel minima removal during the daytime. For C3, diel minima occurred nearly at mid-day hours, the timing of GPP and temperature maxima (Figure S4.6c); meanwhile, the NO_3^- removal (U_T and the U_A pathway) and metabolisms (GPP, ER and their ratios) were similar to Clusters C1 and C2, indicating high daytime photosynthesis. The exact mechanisms would need further specific investigations, while possible explanations could be: (1) this pattern occurred mostly during late summer and autumn, when diel variations of denitrification rates govern the net NO_3^- removal patterns; (2) redox controls (linked to high daytime O_2 production by photosynthesis) will likely suppress denitrification, resulting in diel minima during daytime hours. The C4 pattern was highly comparable with C3 (see Figure 4.4c-d, and the clustering results in Figure S4.3), while likely exhibited higher rates of heterotrophic-related removal like denitrification (linked to lower P/R ratios Figure 4.3b, and significantly positive correlations with SAC Figure S4.5).

In addition to specific mechanistic understanding of the four cluster types, their seasonal distributions and changes between normal and drought years (Figure 4.3a, bar-plots), also reveal shifts in river ecosystem function. In the normal years, the autotrophy-characterized C1 and C2 patterns mostly occur during earlier seasons, which are then followed by a shift to heterotrophy-dominated C3 and C4 patterns during later summer-autumn low-flow periods. However, the sequential droughts have shifted this seasonal distribution to greater persistence of C1 and C2 across seasons, extending the window of autotrophic dominance into the late summer and autumn. Such varying seasonal distributions of diel patterns are likely linked to the drought-induced changes in catchment and stream environmental factors and their contrasting impacts on in-stream NO_3^- biogeochemical processes. This also corresponds with the seasonal insights derived based on the daily timeseries (Section 4.5.2) that showed a shift to greater persistence of net autotrophy during the drought years.

4.5.4. Limitations and future work

There are several considerations of current limitations when transferring the framework to a wider context. Firstly, the estimation uncertainty may be large during high-flow seasons and short-term runoff events. This uncertainty source could be primarily induced by increased inflows from tributaries and lateral subsurface, though we have cautiously estimated tributary inputs from a process-based catchment modeling (Zhou et al., 2022). Also, hyporheic exchange might be elevated and need to be considered, especially when the process is known to be significant and sufficient data are available to constrain it (Gomez-Velez et al., 2015).

Second, the complementary stream metabolic information offered an independent evidence of the drought-induced pattern shifts of nitrate retention, therefore, its estimation uncertainty should be carefully constrained. It is unfortunate that the heavily disturbed stream hydraulics at the downstream STF have prohibited reliable metabolism estimates, and this leads to the large deviation from the general levels of the Lower Bode stream metabolism as compared to available information from other comparable reaches in the Bode region (Text S4.1 and Table S4.1). Nevertheless, GPP and ER levels obtained from the upstream station GGL have been verified through the cross-comparisons. Future implementations of the high-frequency monitoring and the fusion framework should be well aware of such issues, to make most use of the invaluable measurements and better ensuring reliable in-stream process inferences. Also, future study needs to be oriented to better quantify the autotrophic respiration rate (Hall and Beaulieu, 2013) and the seasonally varying biofilm C:N ratios to further reduce stream metabolic related uncertainty.

Third, in-stream nitrate processes are inherently related to the whole-stream ecosystem functioning, which is reliant on riverine DOC availability. In other words, information of DOC quantity and quality can directly support the reasoning of nitrate retention patterns and their shifts under changing conditions. Therefore, future work should combine simultaneous high-frequency monitoring of DOC levels, particularly with further information of the DOC quality (see, e.g., Bierzoza et al. (2023); Ruhala and Zarnetske (2017)).

4.6. Conclusion

This study proposed a data-model fusion framework that enables continuous inferences of in-stream NO_3^- biogeochemical processes in large streams and rivers, overcoming major methodological constraints of using high-frequency monitoring data under variable flow and climatic conditions. Long-term high-frequency estimates in the 6th-order lower Bode River further revealed new insights into NO_3^- dynamics in relation to river ecosystem function, from sub-daily to seasonal scales and under a range of flow conditions. These estimates of net in-stream retention and release, derived closely from direct *in-situ* measurements, provide useful reference values, e.g., for model validation or process conceptualization. Also, identifying and deconvoluting shifts in river ecosystem function (between autotrophy- and heterotrophy-dominance) are of key importance for understanding the impacts of climate change on water quality, ecological status and river function.

This high-frequency data-model fusion method can be applied across sites and scales, and provides an opportunity for scientists and river managers to capitalize on the emergent wave of high-frequency water-quality monitoring. The method can also be extended from small-streams under dynamic flow conditions, to river network scale applications coupled with catchment models. Moreover, the method can complement high-frequency monitoring for cost-effective evaluation of the effectiveness of management practices and river-restoration projects.

Acknowledgement

Xiaoqiang Yang and Xiaolin Zhang contributed equality to this work. Xiaolin Zhang is funded by the Chinese Scholarship Council (CSC). We thank Uwe Kiwel for his technical support during the field work. The authors thank Jingshui Huang for sharing the WASP7 set-up. The authors also thank the Federal Agency for Cartography and Geodesy (BKG) and the State Agency for Flood Protection and Water Management of Saxony Anhalt (LHW) for all data support.

4.7. References

- Alexander, R.B., Böhlke, J.K., Boyer, E.W., David, M.B., Harvey, J.W., Mulholland, P.J., Seitzinger, S.P., Tobias, C.R., Tonitto, C., Wollheim, W.M., 2009. Dynamic modeling of nitrogen losses in river networks unravels the coupled effects of hydrological and biogeochemical processes. *Biogeochemistry* 93, 91–116. <https://doi.org/10.1007/s10533-008-9274-8>
- Ambrose, R.B., Wool, T., 2017. WASP8 Stream Transport - Model Theory and User's Guide. U.S. Environmental Protection Agency, Office of Research and Development, Washington.
- Arndt, J., Kirchner, J.S., Jewell, K.S., Schluesener, M.P., Wick, A., Ternes, T.A., Duester, L., 2022. Making waves: Time for chemical surface water quality monitoring to catch up with its technical potential. *Water Res.* 213, 118168. <https://doi.org/10.1016/j.watres.2022.118168>
- Aubert, A.H., Breuer, L., 2016. New Seasonal Shift in In-Stream Diurnal Nitrate Cycles Identified by Mining High-Frequency Data. *PLOS ONE* 11, e0153138. <https://doi.org/10.1371/journal.pone.0153138>
- Bernal, S., Lupon, A., Wollheim, W.M., Sabater, F., Poblador, S., Martí, E., 2019. Supply, Demand, and In-Stream Retention of Dissolved Organic Carbon and Nitrate During Storms in Mediterranean Forested Headwater Streams. *Front. Environ. Sci.* 7.
- Bieroza, M., Acharya, S., Benisch, J., ter Borg, R.N., Hallberg, L., Negri, C., Pruitt, A., Pucher, M., Saavedra, F., Staniszewska, K., van't Veen, S.G.M., Vincent, A., Winter, C., Basu, N.B., Jarvie, H.P., Kirchner, J.W., 2023. Advances in Catchment Science, Hydrochemistry, and Aquatic Ecology Enabled by High-Frequency Water Quality Measurements. *Environ. Sci. Technol.* 57, 4701–4719. <https://doi.org/10.1021/acs.est.2c07798>
- Bott, T.L., 2006. Primary Productivity and Community Respiration, in: *Methods in Stream Ecology*. Elsevier, New York, pp. 663–690.
- Burns, D.A., Pellerin, B.A., Miller, M.P., Capel, P.D., Tesoriero, A.J., Duncan, J.M., 2019. Monitoring the riverine pulse: Applying high-frequency nitrate data to advance integrative understanding of biogeochemical and hydrological processes. *WIREs Water* 6, e1348. <https://doi.org/10.1002/wat2.1348>
- Catalán, N., Marcé, R., Kothawala, D.N., Tranvik, L.J., 2016. Organic carbon decomposition rates controlled by water retention time across inland waters. *Nat. Geosci.* 9, 501–504. <https://doi.org/10.1038/ngeo2720>
- Costa, D., Sutter, C., Shepherd, A., Jarvie, H., Wilson, H., Elliott, J., Liu, J., Macrae, M., 2022. Impact of climate change on catchment nutrient dynamics: insights from around the world. *Environ. Rev.* <https://doi.org/10.1139/er-2021-0109>
- Dupas, R., Musolff, A., Jawitz, J.W., Rao, P.S.C., Jäger, C.G., Fleckenstein, J.H., Rode, M., Borchardt, D., 2017. Carbon and nutrient export regimes from headwater catchments to downstream reaches. *Biogeosciences* 14, 4391–4407. <https://doi.org/10.5194/bg-14-4391-2017>

- EEA, 2021. Drivers of and pressures arising from selected key water management challenges — A European overview (Publication No. 09/2021). European Environment Agency, Copenhagen, Denmark.
- Ensign, S.H., Doyle, M.W., 2006. Nutrient spiraling in streams and river networks. *J. Geophys. Res. Biogeosciences* 111. <https://doi.org/10.1029/2005JG000114>
- Gomez-Velez, J.D., Harvey, J.W., Cardenas, M.B., Kiel, B., 2015. Denitrification in the Mississippi River network controlled by flow through river bedforms. *Nat. Geosci.* 8, 941. <https://doi.org/10.1038/ngeo2567>
- Graeber, D., Gelbrecht, J., Pusch, M.T., Anlanger, C., von Schiller, D., 2012. Agriculture has changed the amount and composition of dissolved organic matter in Central European headwater streams. *Sci. Total Environ.* 438, 435–446. <https://doi.org/10.1016/j.scitotenv.2012.08.087>
- Greiwe, J., Weiler, M., Lange, J., 2021. Diel patterns in stream nitrate concentration produced by in-stream processes. *Biogeosciences* 18, 4705–4715. <https://doi.org/10.5194/bg-18-4705-2021>
- Gupta, H.V., Kling, H., Yilmaz, K.K., Martinez, G.F., 2009. Decomposition of the mean squared error and NSE performance criteria: Implications for improving hydrological modelling. *J. Hydrol.* 377, 80–91. <https://doi.org/10.1016/j.jhydrol.2009.08.003>
- Hall, R.O., Beaulieu, J.J., 2013. Estimating autotrophic respiration in streams using daily metabolism data. *Freshw. Sci.* 32, 507–516. <https://doi.org/10.1899/12-147.1>
- Heffernan, J.B., Cohen, M.J., 2010. Direct and indirect coupling of primary production and diel nitrate dynamics in a subtropical spring-fed river. *Limnol. Oceanogr.* 55, 677–688. <https://doi.org/10.4319/lo.2010.55.2.0677>
- Heffernan, J.B., Cohen, M.J., Frazer, T.K., Thomas, R.G., Rayfield, T.J., Gulley, J., Martin, J.B., Delfino, J.J., Graham, W.D., 2010. Hydrologic and biotic influences on nitrate removal in a subtropical spring-fed river. *Limnol. Oceanogr.* 55, 249–263. <https://doi.org/10.4319/lo.2010.55.1.0249>
- Hensley, R.T., Cohen, M.J., 2016. On the emergence of diel solute signals in flowing waters. *Water Resour. Res.* 52, 759–772. <https://doi.org/10.1002/2015WR017895>
- Huang, J., Borchardt, D., Rode, M., 2022. How do inorganic nitrogen processing pathways change quantitatively at daily, seasonal and multi-annual scales in a large agricultural stream? *Hydrol. Earth Syst. Sci.* 1–23. <https://doi.org/10.5194/hess-2021-615>
- Jäger, C.G., Hagemann, J., Borchardt, D., 2017. Can nutrient pathways and biotic interactions control eutrophication in riverine ecosystems? Evidence from a model driven mesocosm experiment. *Water Res.* 115, 162–171. <https://doi.org/10.1016/j.watres.2017.02.062>
- Jarvie, H.P., Sharpley, A.N., Kresse, T., Hays, P.D., Williams, R.J., King, S.M., Berry, L.G., 2018. Coupling High-Frequency Stream Metabolism and Nutrient Monitoring to Explore Biogeochemical Controls on Downstream Nitrate Delivery. *Environ. Sci. Technol.* 52, 13708–13717. <https://doi.org/10.1021/acs.est.8b03074>
- Jones, C.N., Scott, D.T., Guth, C., Hester, E.T., Hession, W.C., 2015. Seasonal Variation in Floodplain Biogeochemical Processing in a Restored Headwater Stream. *Environ. Sci. Technol.* 49, 13190–13198. <https://doi.org/10.1021/acs.est.5b02426>
- Kamjunke, N., Büttner, O., Jäger, C.G., Marcus, H., von Tümpling, W., Halbedel, S., Norf, H., Brauns, M., Baborowski, M., Wild, R., Borchardt, D., Weitere, M., 2013. Biogeochemical patterns in a river network along a land use gradient. *Environ. Monit. Assess.* 185, 9221–9236. <https://doi.org/10.1007/s10661-013-3247-7>
- Kamjunke, N., Mages, M., Büttner, O., Marcus, H., Weitere, M., 2015. Relationship between the elemental composition of stream biofilms and water chemistry—a catchment approach. *Environ. Monit. Assess.* 187, 432. <https://doi.org/10.1007/s10661-015-4664-6>

- Knights, C.D., Ambrose, R.B., Avant, B., Han, Y., Acrey, B., Bouchard, D.C., Zepp, R., Wool, T., 2019. Modeling framework for simulating concentrations of solute chemicals, nanoparticles, and solids in surface waters and sediments: WASP8 Advanced Toxicant Module. *Environ. Model. Softw.* 111, 444–458. <https://doi.org/10.1016/j.envsoft.2018.10.012>
- Lu, Y., Bauer, J.E., Canuel, E.A., Yamashita, Y., Chambers, R.M., Jaffé, R., 2013. Photochemical and microbial alteration of dissolved organic matter in temperate headwater streams associated with different land use. *J. Geophys. Res. Biogeosciences* 118, 566–580. <https://doi.org/10.1002/jgrg.20048>
- Miller, M.P., Tesoriero, A.J., Capel, P.D., Pellerin, B.A., Hyer, K.E., Burns, D.A., 2016. Quantifying watershed-scale groundwater loading and in-stream fate of nitrate using high-frequency water quality data. *Water Resour. Res.* 52, 330–347. <https://doi.org/10.1002/2015WR017753>
- Mulholland, P.J., Thomas, S.A., Valett, H.M., Webster, J.R., Beaulieu, J., 2006. Effects of light on NO₃⁻ uptake in small forested streams: diurnal and day-to-day variations. *J. North Am. Benthol. Soc.* 25, 583–595. [https://doi.org/10.1899/0887-3593\(2006\)25\[583:EOLONU\]2.0.CO;2](https://doi.org/10.1899/0887-3593(2006)25[583:EOLONU]2.0.CO;2)
- Odum, H.T., 1956. Primary Production in Flowing Waters¹. *Limnol. Oceanogr.* 1, 102–117. <https://doi.org/10.4319/lo.1956.1.2.0102>
- Oldham, C.E., Farrow, D.E., Peiffer, S., 2013. A generalized Damköhler number for classifying material processing in hydrological systems. *Hydrol. Earth Syst. Sci.* 17, 1133–1148. <https://doi.org/10.5194/hess-17-1133-2013>
- Payn, R.A., Hall Jr., R.O., Kennedy, T.A., Poole, G.C., Marshall, L.A., 2017. A coupled metabolic-hydraulic model and calibration scheme for estimating whole-river metabolism during dynamic flow conditions. *Limnol. Oceanogr. Methods* 15, 847–866. <https://doi.org/10.1002/lom3.10204>
- Reusch, T.B.H., Dierking, J., Andersson, H.C., Bonsdorff, E., Carstensen, J., Casini, M., Czajkowski, M., Hasler, B., Hinsby, K., Hyytiäinen, K., Johannesson, K., Jomaa, S., Jormalainen, V., Kuosa, H., Kurland, S., Laikre, L., MacKenzie, B.R., Margonski, P., Melzner, F., Oesterwind, D., Ojaveer, H., Refsgaard, J.C., Sandström, A., Schwarz, G., Tonderski, K., Winder, M., Zandersen, M., 2018. The Baltic Sea as a time machine for the future coastal ocean. *Sci. Adv.* 4. <https://doi.org/10.1126/sciadv.aar8195>
- Rode, M., Halbedel née Angelstein, S., Anis, M.R., Borchardt, D., Weitere, M., 2016a. Continuous In-Stream Assimilatory Nitrate Uptake from High-Frequency Sensor Measurements. *Environ. Sci. Technol.* 50, 5685–5694. <https://doi.org/10.1021/acs.est.6b00943>
- Rode, M., Suhr, U., Wriedt, G., 2007. Multi-objective calibration of a river water quality model—Information content of calibration data. *Ecol. Model.* 204, 129–142. <https://doi.org/10.1016/j.ecolmodel.2006.12.037>
- Rode, M., Wade, A.J., Cohen, M.J., Hensley, R.T., Bowes, M.J., Kirchner, J.W., Arhonditsis, G.B., Jordan, P., Kronvang, B., Halliday, S.J., Skeffington, R.A., Rozemeijer, J.C., Aubert, A.H., Rinke, K., Jomaa, S., 2016b. Sensors in the Stream: The High-Frequency Wave of the Present. *Environ. Sci. Technol.* 50, 10297–10307. <https://doi.org/10.1021/acs.est.6b02155>
- Ruhala, S.S., Zarnetske, J.P., 2017. Using in-situ optical sensors to study dissolved organic carbon dynamics of streams and watersheds: A review. *Sci. Total Environ.* 575, 713–723. <https://doi.org/10.1016/j.scitotenv.2016.09.113>
- Seitzinger, S.P., Styles, R.V., Boyer, E.W., Alexander, R.B., Billen, G., Howarth, R.W., Mayer, B., van Breemen, N., 2002. Nitrogen retention in rivers: model development and application to watersheds in the northeastern U.S.A. *Biogeochemistry* 57, 199–237. <https://doi.org/10.1023/A:1015745629794>
- Stutter, M.I., Graeber, D., Evans, C.D., Wade, A.J., Withers, P.J.A., 2018. Balancing macronutrient stoichiometry to alleviate eutrophication. *Sci. Total Environ.* 634, 439–447. <https://doi.org/10.1016/j.scitotenv.2018.03.298>

- Sunjidmaa, N., Mendoza-Lera, C., Hille, S., Schmidt, C., Borchardt, D., Graeber, D., 2022. Carbon limitation may override fine-sediment induced alterations of hyporheic nitrogen and phosphorus dynamics. *Sci. Total Environ.* 837, 155689. <https://doi.org/10.1016/j.scitotenv.2022.155689>
- van Geer, F.C., Kronvang, B., Broers, H.P., 2016. High-resolution monitoring of nutrients in groundwater and surface waters: process understanding, quantification of loads and concentrations, and management applications. *Hydrol. Earth Syst. Sci.* 20, 3619–3629. <https://doi.org/10.5194/hess-20-3619-2016>
- von Schiller, D., Bernal, S., Sabater, F., Martí, E., 2015. A round-trip ticket: the importance of release processes for in-stream nutrient spiraling. *Freshw. Sci.* 34, 20–30. <https://doi.org/10.1086/679015>
- Wollheim, W.M., Harms, T.K., Robison, A.L., Koenig, L.E., Helton, A.M., Song, C., Bowden, W.B., Finlay, J.C., 2022. Superlinear scaling of riverine biogeochemical function with watershed size. *Nat. Commun.* 13, 1230. <https://doi.org/10.1038/s41467-022-28630-z>
- Wool, T., Ambrose, R.B., Martin, J.L., Comer, A., 2020. WASP 8: The next generation in the 50-year evolution of USEPA’s water quality model. *Water Basel* 12, 1398. <https://doi.org/10.3390/W12051398>
- Yang, X., Jomaa, S., Büttner, O., Rode, M., 2019. Autotrophic nitrate uptake in river networks: A modeling approach using continuous high-frequency data. *Water Res.* 157, 258–268. <https://doi.org/10.1016/j.watres.2019.02.059>
- Yang, X., Jomaa, S., Zink, M., Fleckenstein, J.H., Borchardt, D., Rode, M., 2018. A new fully distributed model of nitrate transport and removal at catchment scale. *Water Resour. Res.* 54, 5856–5877. <https://doi.org/10.1029/2017WR022380>
- Yang, X., Rode, M., 2020. A Fully Distributed Catchment Nitrate Model - mHM-Nitrate v2.0. <https://doi.org/10.5281/zenodo.3891629>
- Zhang, X., Yang, X., Hensley, R., Lorke, A., Rode, M., 2023. Disentangling In-Stream Nitrate Uptake Pathways Based on Two-Station High-Frequency Monitoring in High-Order Streams. *Water Resour. Res.* 59, e2022WR032329. <https://doi.org/10.1029/2022WR032329>
- Zhou, X., Jomaa, S., Yang, X., Merz, R., Wang, Y., Rode, M., 2022. Exploring the relations between sequential droughts and stream nitrogen dynamics in central Germany through catchment-scale mechanistic modelling. *J. Hydrol.* 614, 128615. <https://doi.org/10.1016/j.jhydrol.2022.128615>

4.8. Supplementary Materials

Text S4.1. Methodological justifications of using single-station based GGL stream metabolic characteristics as the representative of the Lower Bode region.

We collected and cross-compared available whole-stream metabolism information from different sites (see locations in Figure 4.1a) in the well-studied Bode catchment. The comparison dataset (Table S4.1) includes: (1) using the high-frequency dataset of this study, the single-station based daily GPP (gross primary production) and ER (ecosystem respiration) at GGL and STF continuously over 2015-2020; (2) from Yang et al., 2019, the single-station based daily GPP and ER at station Hausneindorf (the outlet of the Selke sub-catchment, located in the lower Bode agricultural region) continuously over 2011-2016; (3) from Zhang et al., 2023, the two-station based daily GPP and ER at a 6.15 km stream reach (BD_3) between GGL and STF over two periodic deployments (8/22-8/25, 2019 and 8/28-9/2, 2020). Although the information was derived from different methods and periods, it could be still valuable in informing reference levels of the lower Bode stream metabolic characteristics. At the

annual scale, GPP levels at GGL and Hausneindorf were similar (ANOVA-test, $p=0.48$), while they were both significantly higher than those at STF (ANOVA-test, $p<0.001$); ERs at STF were the lowest, although those at GGL and Hausneindorf were also significantly different. Similarly, for the periodic values, the calculated levels at STF were consistently lower than those at GGL and the BD_3 reach.

Given the complex river hydraulic conditions and hydrodynamics, it is not possible to use the conventional two-station inferences that only use monitored data, neither be the idea of adopting similar data-model fusion on dissolved oxygen (DO) transport. There might be high uncertainties in quantifying (1) DO levels of the in-between inflows (both from tributaries and groundwaters) and (2) impacts of the stream surface reaeration process.

Therefore, the single-station values from GGL were likely the best information that represents of the stream metabolic characteristics.

Text S4.2. *k*-means cluster

The *k*-means clustering partitions a given dataset into *k* groups so that the sum of squares from the dataset to the assigned cluster centers is minimized. The input dataset should be a matrix where rows represent elements to be partitioned and columns represent the dimensions of elements. In this study, the elements are selected days for diel pattern analysis and the dimensions are the time within each day ($n = 24$ at an interval of 1 hour).

The determination of *k* is somewhat subjective. Hence we tried *k* up to 20 and used function “*fviz_nbclust*” in the “*factoextra*” R package to visualize the optimal number of clusters (Kassambara and Mundt, 2020; R core team, 2022). According to the Figure S4.3a, we determine *k* by both elbow method (an assessment of explanatory benefit per cluster) and by visual verification. We finally took 4 clusters since higher values of *k* did not provide better partitioning effects. We compute *k*-means in “*stat*” R package with the algorithm by Hartigan and Wong (1979). The final cluster plot from *k*-means cluster is shown as Figure S4.3b using function “*fviz_cluster*” in the “*factoextra*” R package.

Table S4.1. Comparisons of Stream metabolism levels (mean \pm standard deviation) calculated at different stations in the Bode catchment. GPP-gross primary production ($\text{g O}_2 \text{ m}^{-2} \text{ d}^{-1}$); ER-ecosystem respiration ($\text{g O}_2 \text{ m}^{-2} \text{ d}^{-1}$).

Station/Reach	This study		Yang et al., 2019	Zhang et al., 2023
	GGL	STF	Hausneindorf	BD_3
Annual level	2015-2020		2011-2016	--
GPP	2.12 \pm 1.82	1.21 \pm 1.35	2.07 \pm 1.71	--
ER	4.16 \pm 2.22	2.57 \pm 2.57	3.19 \pm 1.71	--
Periodic level	10 days (8/22-8/25, 2019 and 8/28-9/2, 2020)			
GPP	3.63 \pm 0.20	1.65 \pm 0.22	--	4.36 \pm 0.38
ER	4.49 \pm 0.17	2.02 \pm 0.46	--	2.83 \pm 0.55

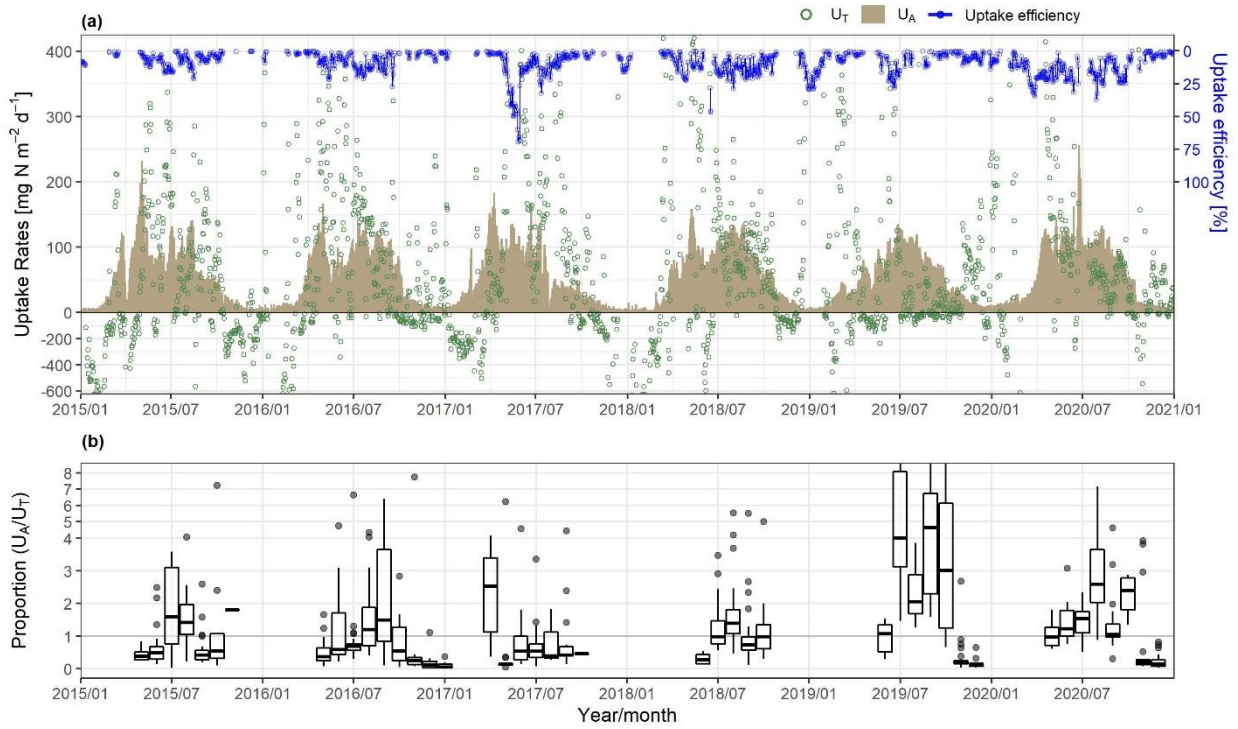


Figure S4.1. The GPP-informed daily autotrophic NO_3^- assimilation U_A over 2015-2020 (a) and its proportions to the total NO_3^- retention U_T in each month (b). Note that the proportions were considered only among dates with positive U_T and with discharge below the median values of the normal and drought years (i.e., 7.20 and $4.38 \text{ m}^3 \text{ s}^{-1}$, respectively).

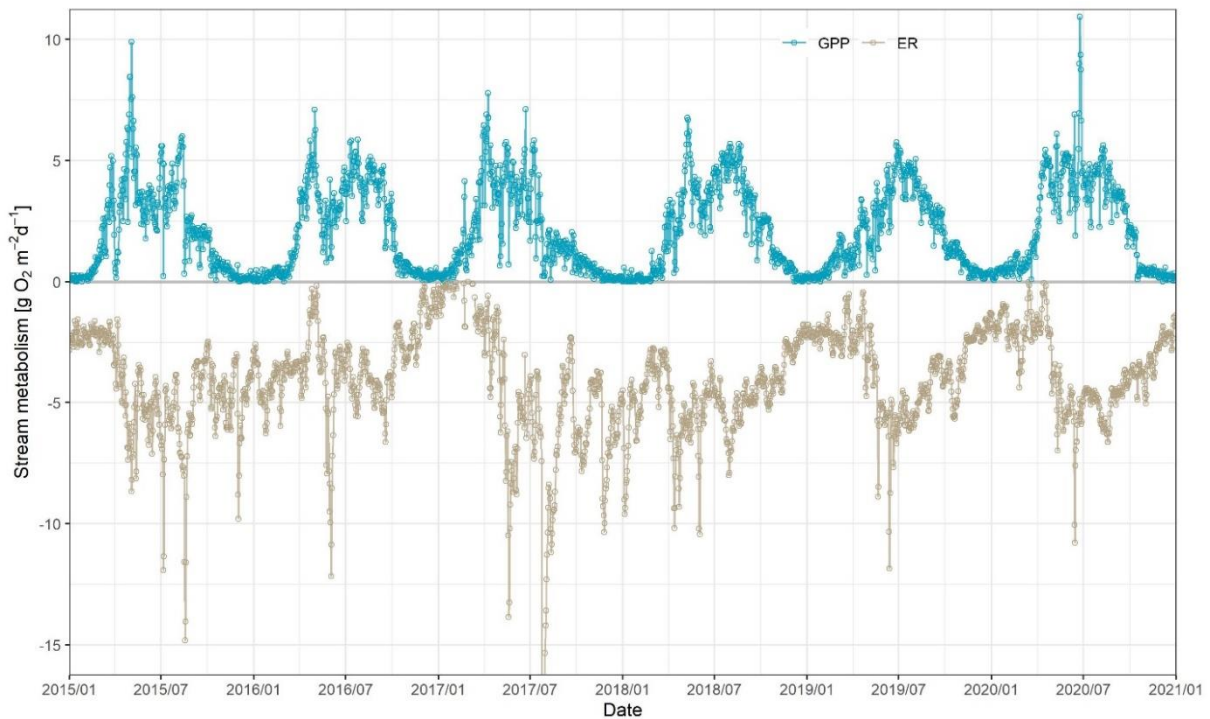


Figure S4.2. Daily whole stream metabolisms (i.e., Gross Primary Production-GPP and Ecosystem Respiration-ER) at the upstream station GGL, representing the whole lower Bode river reach.

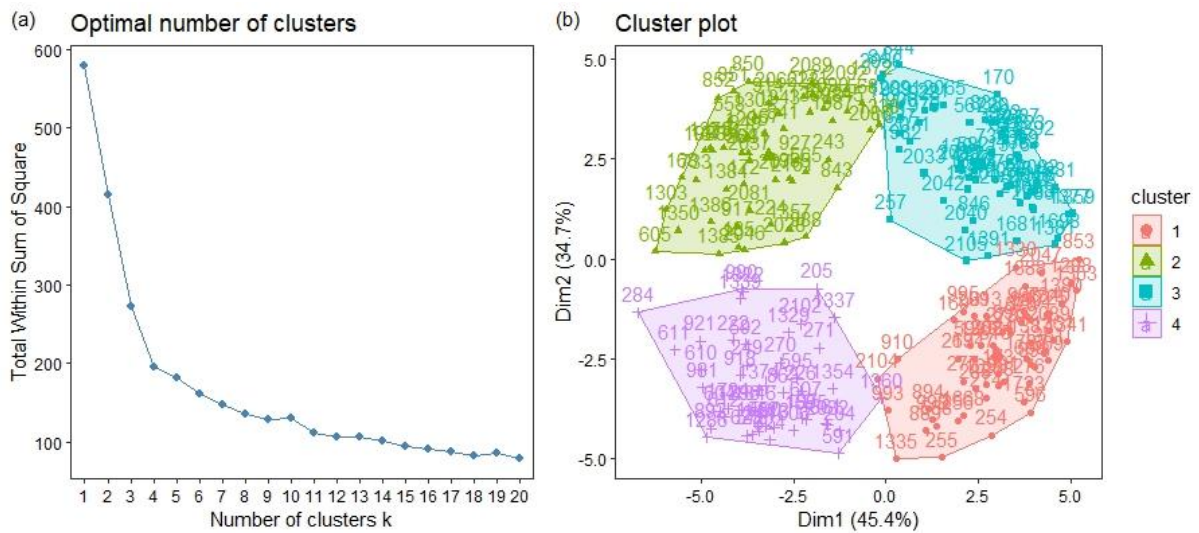


Figure S4.3. Results of the k-mean clustering analysis. (a) the determinations of the number of clusters (= 4), and (b) the differentiation of different clusters.

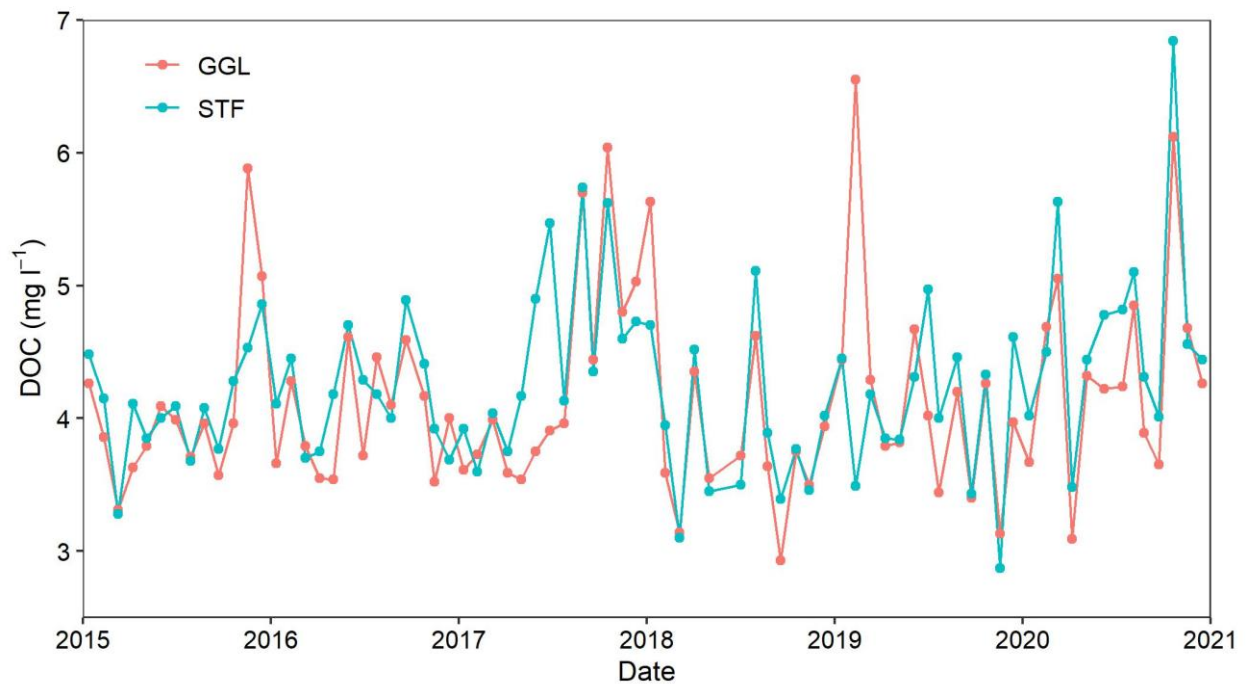


Figure S4.4. Monthly sampled DOC measurements at both upstream GGL and downstream STF stations during the study period 2015-2020.

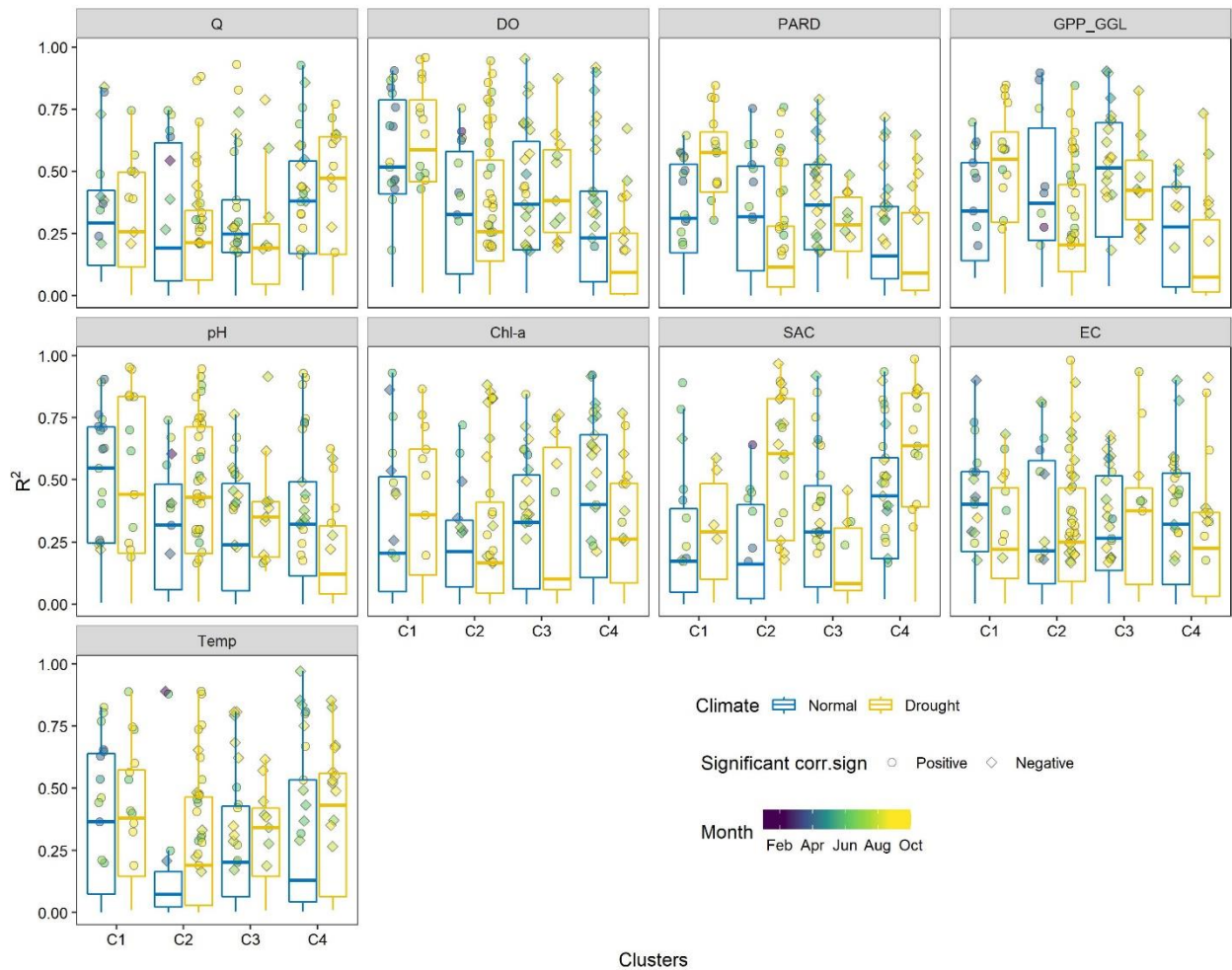


Figure S4.5. Pearson correlations between diel patterns of NO_3^- uptake and environmental factors (max-min normalized for each date) for each of the four clusters under the normal and drought climates (boxplot of the adjusted R^2). Q-discharge, DO-dissolved oxygen, PARD-photosynthetically active radiation, GPP_GGL-gross primary production at station GGL, Chl-a - concentration of *chlorophyll a*, SAC- spectral absorbance at 254 nm, EC- electric conductivity and Temp-water temperature. For the days exhibited significant correlations ($p < 0.05$), the R^2 values were further plotted with shapes and colors, representing positive/negative correlations and the occurred months, respectively.

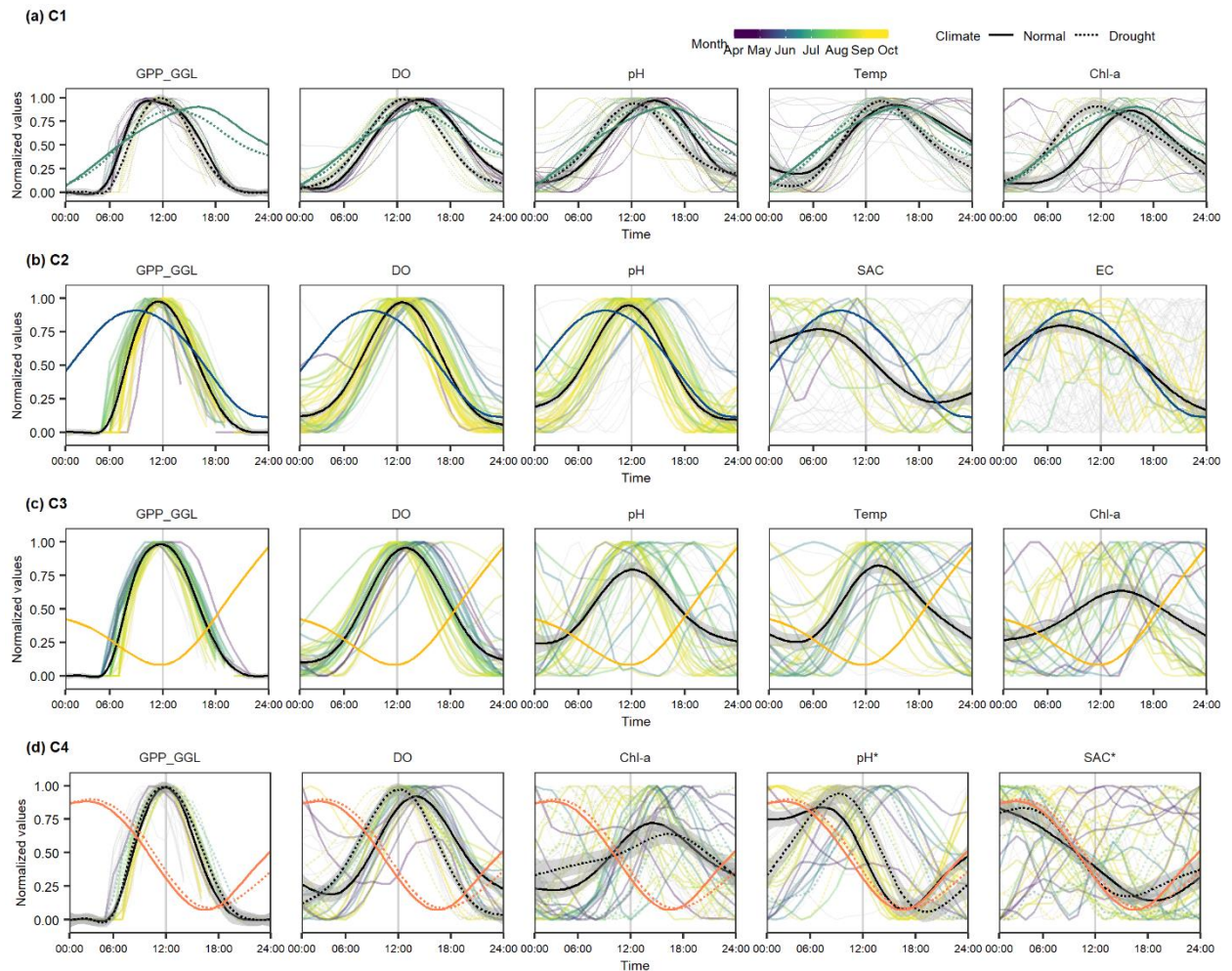


Figure S4.6. Diel patterns of plausible key environmental factors for each type of the four clusters. The NO_3^- uptake patterns were plotted as references for each cluster, using the same color as in Figure 4.4 of the main text. The fitted curves and uncertainty intervals (black-colored lines and shaded bands, respectively) were derived from the GAM-based smooth functions implemented in the “*ggplot2*” R package. Note that, in subplot (d), pH^* and SAC^* were only fitted based on dates with positive correlations.

Reference

Hartigan, J. A. and Wong, M. A. (1979). Algorithm AS 136: A K-means clustering algorithm. *Applied Statistics*, 28, 100–108. doi:10.2307/2346830.

Kassambara, A., Mundt, F., 2020. *factoextra: Extract and Visualize the Results of Multivariate Data Analyses*.

R Core Team (2022). *R: A language and environment for statistical computing*. R Foundation for Statistical Computing, Vienna, Austria. URL <https://www.R-project.org/>.

Yang, X., Jomaa, S., Büttner, O., Rode, M., 2019. Autotrophic nitrate uptake in river networks: A modeling approach using continuous high-frequency data. *Water Res.* 157, 258–268. <https://doi.org/10.1016/j.watres.2019.02.059>.

Zhang, X., Yang, X., Hensley, R., Lorke, A., Rode, M., 2022. Disentangling in-stream nitrate uptake pathways based on two-station high-frequency monitoring in high-order streams. *Water Resour. Res.* 59, e2022WR032329. <https://doi.org/10.1029/2022WR032329>.

Chapter 5: Discussion

In the foregoing chapters, we have seen successful deployments of in-situ high-frequency water quality monitoring and further data applications. Catchment-scale nitrate (NO_3^-) storage and transport dynamics are disentangled based on high-frequency nitrate and discharge data (Chapter 2). In-situ multi-parameter monitoring stations are set up in high order streams to quantify the in-stream NO_3^- uptake pathways and explore their characteristics at the sub-daily scale on the basis of mass balance methodology (Chapter 3). Then the methodology is applied to a longer reach to decipher nitrate turnover and its responses to drought disturbances from sub-daily to inter-annual scale (Chapter 4). This content is hardly achieved by low-frequency sampling (e.g., monthly or biweekly). Hence, high-frequency monitoring is becoming a powerful tool to advance our understanding of hydrological and biogeochemical processes spatiotemporally (from catchment to stream scale and from inter-annual to sub daily scale). Further discussion, inspirations and outlooks beyond that already in the preceding chapters will be described in this chapter.

5.1. Evaluation of in-situ high-frequency monitoring

5.1.1. Catchment-scale nitrate export dynamics

Catchment response on NO_3^- source and transport of internal (e.g., soil, geology and land use) and external (e.g., soil moisture and precipitation) factors can cause different C-Q relationships during the rising and falling limbs of event-scale hydrographs. Hysteresis is a common pattern to reflect such response, which can be successfully quantified with high-frequency monitoring of NO_3^- and discharge processes. In this way, event-scale hysteresis is comparable at different stations during a long period. Current research in the nested catchment, Selke, nicely shows the various combinations of hysteresis indices, *HI* and *FI* (defined as *CI* in Chapter 2), at the three gauging stations due to complex combinations of meteorological, hydrological, geographical and pedological characteristics within each subcatchment, confirming objective I-1.

Presented comprehensive understanding of active NO_3^- source areas and transport pathways by combing hysteresis and flushing indices proves objective I-2 and generally agrees with and further improve previous results. The delivery of NO_3^- can be divided into the supply- and transport-limitation. Urban area (e.g., the lowermost subcatchment) is a typical supply-limitation land use. Due to massive impermeable areas and lack of legacy NO_3^- , the in-stream NO_3^- concentration is diluted by quick surface flow and keeps decreasing later on without any addition, showing the pattern of $FI < 0$ and $HI > 0$ (Bronstert et al., 2002; Niehoff et al., 2002). Transport-limitation usually occurs under a warm and dry antecedent climatic condition with poor hydrological connectivity (Baker & Showers, 2019; Outram et al., 2014). It also happens in arable area with lower NO_3^- in the topsoil while higher NO_3^- in the deep soil due to legacy NO_3^- . After proximal NO_3^- sources being flushed out at the

beginning of an event, the deep soil NO_3^- storage cannot be transported by interflow due to poor hydrological connectivity, with the pattern of $FI > 0$ and $HI > 0$. Such two typical types both show clockwise hysteresis: few or immobilized distal nitrate sources make NO_3^- lower during the falling limbs. For cases of higher NO_3^- concentrations during the falling limb (i.e., counterclockwise hysteresis), a wet pre-condition or high precipitation intensity is necessary. In mountainous arable areas (e.g., the middle subcatchment), agricultural draining (e.g., pipes) could also cause quick flow to dilute in-stream NO_3^- concentration at the beginning of an event, but later subsurface flow could transport distal NO_3^- sources to elevate in-stream concentration on the falling limb, causing the pattern of $FI < 0$ and $HI < 0$ (Goodridge & Melack, 2012; Jacobs et al., 2018). If the proximal and distal NO_3^- sources are both plentiful (e.g., the uppermost forest area) and the hydrological connectivity is strong, the NO_3^- will keep increasing and peak after discharge, showing the pattern of $FI > 0$ and $HI < 0$. From this research, we can see how land use affects the C-Q pattern, as well as how the pattern changes under the wet-dry seasonal variations (I-3). Further analysis of shared events further proved that the uppermost subcatchment always dominated runoff volume and nitrate-N load during all periods except the dry period, when the lowermost catchment dominated (I-4). This alternation also supports I-3 that high nitrate-loaded interflow dominated in the upper mountainous subcatchments, while quick runoff (e.g., surface flow with low nitrate concentration) dominated in the lowermost subcatchment. Nitrate storage and its dominant flowing pathways change with landscape and seasonal variation.

Anthropogenic activities have changed nature intensively, e.g., urban constructions and agricultural activities. One catchment can take various social functions according to municipal planning. Hence, understanding nutrient storage and transport pathways are important to prevent pollution affecting human life. As one severe pollutant, NO_3^- raises much attention and its transport can be monitored by setting up water quality stations. Further improvement to forecast NO_3^- transport dynamics can be accompanying discharge, soil moisture and precipitation measurements in hot spots. An analysis in France concluded that biogeochemical processes dominate at low flow and hydrological processes dominate at high flow (Moatar et al., 2017). From a socio-economic point of view, floods can cause huge damage and induce large NO_3^- loads, which we should raise awareness. Hence, a well-established monitoring system is crucial for both scientific research and water management.

5.1.2. Quantification of in-stream nitrate uptake pathways in large streams

In-stream biogeochemical processes such as assimilation, denitrification and nitrification have been discovered to play an important role on the transport and fate of NO_3^- for a long time (Hill, 1979; McColl, 1974). Diel variations of NO_3^- has been well recognized before the widespread use of high-frequency monitoring and now is being extensively discussed in terms of internal mechanism and has been used to calculate assimilatory uptake based on high-frequency data (Greiwe et al., 2021; Hensley & Cohen, 2016; Mulholland, 1992; Yang et al., 2019). Two-station mass balance approach provides a

straightforward way to determine NO_3^- uptake rate within a reach by calculating the difference of NO_3^- load at the upstream and downstream station. High-frequency data helps to highly elevate the precision of nitrate retention processes compared to previous studies due to high temporal resolution (Miller et al., 2017). We applied the approach in the 4th and 6th streams (i.e., Weiße Elster and Bode river) under different environmental conditions, calculated the net NO_3^- uptake and metabolism rate in Chapter 3 and confirmed the Objective II-1. Additional multi-parameter measurements help to disentangle various pathways, but not totally (II-2). That is, autotrophic assimilation can be coupled with GPP, calculated by dissolved oxygen, discharge and stoichiometry C:N ratio. However, detailed denitrification and heterotrophic assimilation cannot be separated and hence are estimated as the remaining part (called as heterotrophic uptake in Chapter 3) by subtracting autotrophic assimilation from net NO_3^- uptake. With these assumptions, we found diel pattern of all pathways besides NO_3^- (II-3), especially for heterotrophic uptake which was seen as constant or linear change during one day (Heffernan & Cohen, 2010). Moreover, due to monitoring schemes in different seasons, net NO_3^- uptake exhibited high variations even with negative values (i.e., net NO_3^- release). Multi-parameter monitoring like chlorophyll, temperature and specific conductivity can help explain the reason (II-4). For example, the huge difference of specific conductivity between two stations may indicate unexpected inflow. The proportions of each pathway also changed: heterotrophic uptake became important during post-wet seasons (II-5).

Despite existing limitations, current research shows the potential of high-frequency sensors to assess reach-scale nutrient turnover rates. In principle, a mass balance approach can be applied to any nutrient similar to NO_3^- that can be monitored with automated high-frequency sensors. Although current use of real time sensors is restricted to fundamental aquatic attributes such as DO, pH, soluble reactive phosphorus (SRP) and NO_3^- , the sensor development is rapidly advancing due to promising prospects (Yaroshenko et al., 2020). The continuous implementation allows quantitative assessment of aquatic system and reflect sub-daily variations in biogeochemical and physical hydrologic processes.

5.1.3. Responses of nitrate uptake processes to climate change

The mass-balance inferred nitrate (NO_3^-) uptake and metabolism rate has been successfully estimated in stream reaches with length 3-8 km in Chapter 3 and other research (Jarvie et al., 2018; Kunz et al., 2017). The length is still limited due to few constrains: heterogenous river morphology conditions, the nitrate and dissolved oxygen (DO) signals with convolution processes and unexpected inflow turbulences (Demars et al., 2015). With the water quality model NO_3^- can be simulated as a non-decay tracer without biogeochemical processes (III-1). Hence, the mass balance approach for calculating net NO_3^- uptake can be upscaled to the lower Bode (27.4 km) with 6-year high-frequency monitoring. However, metabolism cannot be calculated here due to the physical characteristics of DO (e.g.,

equilibrium between air and water), one-station calculation or model simulation (e.g., streamMetabolizer) can be a better choice. With some assumption, various uptake pathways were separated, i.e., autotrophic assimilation, heterotrophic assimilation and denitrification (III-2). With such continuous long-term NO_3^- uptake pathways, we applied cutting-edge k-cluster analysis and categorized diel variations into 4 types. On the seasonal and sub-daily scales, we got obvious pattern change between normal and drought year from seasonal to sub-daily time scale using k-cluster analysis (III-3).

To our knowledge such in-stream inferences are the first time to be enabled continuously in large rivers with complex flow dynamics as well as crossing different climatic conditions. Upon such step-forward methodological advances, the long-term high-frequency estimates of in-stream nitrate retention, which further revealed insights into large-river nutrient dynamics and the functioning of river ecosystems, as well as their cross-scale temporal pattern shifts under the changing climate. Moreover, this data-model fusion approach can be applied to other large rivers with appropriate high-frequency measurements, which makes it promising to bridge the gap of in-stream nitrogen processes to large rivers.

5.2. Scientific inspirations from field experiments and future work

In this dissertation, nitrogen dynamics on the catchment scale and realistic nitrate turnover rate were evaluated on the in-stream scale based on high-frequency monitoring, showing comprehensive and cutting-edge methodology and results in understanding nitrogen cycle across biogeochemical and hydrological disciplines. There are several important points and implications raised when conducting the work, which will be discussed in this section.

Either from the catchment or from the in-stream perspective, it's important to select suitable locations for the sensor installations. Systematic monitoring of hydrology and water quality parameters can help save labor- and equipment- cost and make analysis more precise. For example, the three station in the nested Selke catchment can capture the response of NO_3^- storage and transport to land use, geological and pedological variations, from the uppermost forest to the middle forest-agriculture mixed to the lowermost agriculture-urban mixed subcatchments. In our study of reach-scale NO_3^- uptake, a suitable distance between the upstream and downstream stations is crucial for good performance of metabolism estimation (Demars et al., 2015), as well as reach morphology conditions. We carefully chose reaches based on morphological and hydrological characteristics to avoid tributaries, point source inputs and hydraulic engineering. Longitudinal profiling was also conducted because it's useful to detect spatiotemporal variations in water chemistry (Hensley et al., 2020). But we can hardly rely on longitudinal profiling to measure NO_3^- uptake because it only represents conditions at the specific sampling time (Kunz et al., 2017). Despite such careful preparation, there are still unexpected conditions happened such as groundwater conditions. Although we conducted measurements during

low-flow periods, the net NO_3^- uptake and metabolism calculated by mass balance method can be underestimated by ignoring groundwater contribution (Hall & Tank, 2005). We provided a method to quantify groundwater influence in Chapter 3 but the uncertainty behind is inevitable. Hence, it's also necessary to notice the groundwater conditions when choosing study reach.

When partitioning various NO_3^- uptake pathways, the lack of contemporary high frequency measurements of NH_4^+ or N_2 can obscure the denitrification, heterotrophic uptake and nitrification, which cause the greatest uncertainty on their turnover rates. In Chapter 3, the three pathways are together seen as 'heterotrophic uptake' (we assumed nitrification insignificant due to the low level of NH_4^+). To deal with this problem, one way is to combine other experiments with the sensor monitoring to disentangle detailed pathway rates, such as quantifying denitrification rate by isotope tracer addition (Dodds et al., 2000; P. J. Mulholland et al., 2009) or calculating nitrification rate by incubation studies (Kemp & Dodds, 2002). Although such experiments are only snap shots, the results are still valuable to fulfill the overall picture of the in-stream NO_3^- cycle with high-frequency data. Another way is to measure NH_4^+ or N_2 at the same time, which may quantify nitrification and denitrification rate.

High-frequency monitoring brings high potential to quantify NO_3^- turnover rate in large streams by using the two-station mass balance method, which can be applied to more streams worldwide with carefulness to meet certain purposes. With long-term monitoring, data mining approaches can be used and dig NO_3^- turnover response to climate change. It is reported that analysis of multiple high-frequency sensor signals from a single station can better inform understanding of dominant processes, reduce the number of potential hypotheses that may explain NO_3^- patterns, and help develop quantitative model estimates (Burns et al., 2019). If the methodology can be applied to other nutrients (e.g., SRP) with the new development of high-frequency sensors, it will help build a comprehensive and interdisciplinary understanding in aquatic ecosystem science about nutrients transport, transformation and retention across ecological, biological, biogeochemical and hydrological disciplines.

Hence, there are still promising points for future work and improve the :

- Systematic and scientific monitoring networks of hydrology, ecology and water quality. Refinement of high-frequency sensors will sure improve the precision and duration of measurements. More parameters are on the way to be measured using sensors (e.g., SRP). With combination of low-frequency grab sample measurements, the instream biogeochemical processes can be analyzed and evaluated more comprehensively.
- Measurements or modeling in key in-stream compartments. Instream nitrate process (e.g., denitrification, assimilatory uptake and remineralization) are complex. It's difficult to separate each pathway only with the in-stream monitoring. Hence, measure or model relative parameters can be

important to have quantitative analysis. Hyporheic zone is a key compartment within streams and rivers and is important for specific nitrate uptake pathways like denitrification. In-situ measurements (e.g., passive flux meter, Kunz et al., 2017) can further disentangle the convoluted processes.

- Benefit from data-model fusion approach. Current data-model fusion approach combined high-frequency data with instream water quality model, successfully upscaling two-station method to a longer and larger stream. Meanwhile, a catchment hydrological model provided discharge and nitrate data for tributaries. Such usage of multiple model can somewhat simulate processes of the whole system. In the future, considering groundwater effects on instream processes, groundwater simulations can be another research concern.

5.3. Broader outlooks for water management

The high-frequency monitoring of NO_3^- presented here not only shows the potential to improve scientific research, but also can help establish water management practices. Anthropogenic activities have altered the natural system and increased large nutrients input. Despite the high cost, authorities in Germany and other industrial countries have installed sensors at least for flux measurements and warning system (Rode, Wade, et al., 2016). Regarding to water quality parameters, current strategy is mostly regularly grab sampling (e.g., biweekly or monthly), which may miss the hot moments of NO_3^- inputs. Hence, a combination of traditional grab sampling and real-time sensor monitoring can be an optimal choice to observe environmental responses to anthropogenic activities and climatic changes, especially during certain periods. We found streams may release NO_3^- during post-wet period, which means lower amounts of the pollutant should be poured to avoid environmental burden. On the other side, during summer period, streams have stronger self-cleaning ability to remove NO_3^- . High-frequency monitoring can be set up based on such seasonal variation considering its cost and dependency on electric power.

In the dissertation, stream reaches with natural morphology have a higher NO_3^- uptake rate compared to modified ones in the Weiße Elster River. This could be another reason to restoration river banks and wetlands. During flooding periods, there will be excessive NO_3^- from catchment upstream to downstream, restored wetland can be successfully decrease the cost to remove NO_3^- . Hey et al. (2005) compared the total annual cost between restored wetlands and water reclamation plant (WRP) for treating up to 3 mg l^{-1} TN and 1 mg l^{-1} TP in a catchment (76500 ha), the former cost 63 million dollar and the latter cost 174 million dollar. In the EU, restoring rivers and floodplains has been advocated as more natural-based mitigation measures with multiple benefits (EEA, 2021a). The economic benefits are high considering current large amount of additional nutrients input due to industrial factories and agricultural activities. Current river constructions like channelization and dredging will decrease assimilatory uptake and autochthonous organic sources to fuel denitrification. In-stream and near-stream biogeochemical processes play an important role in local and global nitrogen cycles.

Adequate knowledge about how these processes respond to increasing loads and altered hydraulic conditions and changing climate is important before conducting water management projects.

Chapter 6: Summary

In this dissertation, nitrate concentration-discharge (C-Q) hysteretic relationships at three gauging stations in the 4th order Selke river are analyzed to explore nitrate storage and transport dynamics during storm events within the nested catchment. Various combinations of C-Q hysteresis (clockwise and counterclockwise, accretion and dilution) indicate various patterns of nitrate transport and its influential factors. Clockwise hysteresis occurs more during the dry period, indicating low hydrological connectivity from land to stream for export of distal nitrate sources. Dilution effects dominate in the lowermost catchment, which may have been influenced by flow propagating from upstream subcatchments during the wet period or generated by quick flow from paved areas. The alteration of dominant contribution from the uppermost to lowermost subcatchment to runoff volume and nitrate load suggests variations of dominant flowing pathways and nitrate storage zone. High nitrate-loaded interflow dominated in the upper mountainous subcatchments, while quick runoff (e.g., surface flow with low nitrate concentration) dominated in the lowermost subcatchment. This difference in nitrate export can increase during dry/hot seasons, when hydrological connectivity and biogeochemical processes change greatly. Such reliable interpretation of the fundamental mechanism of C-Q relationships can help water or agricultural management.

Further focus on in-stream nitrate dynamics, two-station mass-balance methodology is used to quantify reach-scale in-stream net nitrate cycling, metabolism and different nitrate uptake pathways. Measurements are conducted in 5 reaches (from 3-7 km) in the 4th (Weiße Elster) and 6th river (Bode). Net nitrate uptake is observed the highest in the most natural reach and during the post-wet seasons. Heterotrophic uptake predominates the net nitrate uptake during the post-wet seasons but decreases largely in dry season. With high-frequency data, diel patterns of the net nitrate uptake, assimilatory uptake and heterotrophic uptake become detectable. For cases of heterotrophic uptake, it decreases during the daytime, which has long been overlooked in previous studies. Such approach and findings from high-order river monitoring and analysis can provide new insights into heterogeneous dynamics of in-stream nitrate retention processes at larger scales.

To upscale the mass balance approach spatiotemporally, a water quality model is used to simulate nitrate as non-decay tracer. The lower Bode (ca. 27.4 km) is with more complex river morphology and hydraulic conditions, which was difficult to conduct mass balance approach to estimate in-stream nitrate uptake precisely. Current results from data-model fusion approach during 2015-2020 help to assess large-river in-stream nitrate retention and its responses to drought disturbances from seasonal to sub-daily scale. Nitrate retention (both net uptake and net release) exhibited substantial seasonality, which also differed in the investigated normal and drought years. The diel patterns of net nitrate uptake are categorized into four types with different frequency in normal and drought years. Such data-model fusion approach moves forward the usage of high-frequency monitoring data. New

statistical approaches like cluster analysis has been successfully applied to explore long-term continuous in-stream nitrate retention processes.

References

- Arango, C. P., Tank, J. L., Johnson, L. T., & Hamilton, S. K. (2008). Assimilatory uptake rather than nitrification and denitrification determines nitrogen removal patterns in streams of varying land use. *Limnology and Oceanography*, 53(6), 2558–2572.
<https://doi.org/10.4319/lo.2008.53.6.2558>
- Arle, J., Baumgarten, C., Blondzik, K., Borchardt, D., Hilliges, F., Mathan, C., et al. (2016). Water Framework Directive. Umweltbundesamt. Retrieved from
<https://www.umweltbundesamt.de/publikationen/water-framework-directive>
- Baker, E. B., & Showers, W. J. (2019). Hysteresis analysis of nitrate dynamics in the Neuse River, NC. *Science of The Total Environment*, 652, 889–899.
<https://doi.org/10.1016/j.scitotenv.2018.10.254>
- Bernhardt, E. S., Hall, R. O., & Likens, G. E. (2002). Whole-system estimates of nitrification and nitrate uptake in streams of the Hubbard Brook Experimental Forest. *Ecosystems*, 5(5), 419–430. <https://doi.org/10.1007/s10021-002-0179-4>
- Boyd, D. S., & Danson, F. M. (2005). Satellite remote sensing of forest resources: three decades of research development. *Progress in Physical Geography: Earth and Environment*, 29(1), 1–26.
<https://doi.org/10.1191/0309133305pp432ra>
- Bronstert, A., Niehoff, D., & Bürger, G. (2002). Effects of climate and land-use change on storm runoff generation: present knowledge and modelling capabilities. *Hydrological Processes*, 16(2), 509–529. <https://doi.org/10.1002/hyp.326>
- Burns, D. A. (2005). What do hydrologists mean when they use the term flushing? *Hydrological Processes*, 19(6), 1325–1327. <https://doi.org/10.1002/hyp.5860>
- Burns, D. A., Pellerin, B. A., Miller, M. P., Capel, P. D., Tesoriero, A. J., & Duncan, J. M. (2019). Monitoring the riverine pulse: Applying high-frequency nitrate data to advance integrative understanding of biogeochemical and hydrological processes. *Wiley Interdisciplinary Reviews: Water*, 6(4), e1348. <https://doi.org/10.1002/wat2.1348>
- Butturini, A., Alvarez, M., Bernal, S., Vazquez, E., & Sabater, F. (2008). Diversity and temporal sequences of forms of DOC and NO₃-discharge responses in an intermittent stream: Predictable or random succession? *Journal of Geophysical Research*, 113(G3).
<https://doi.org/10.1029/2008jg000721>
- Caraco, N. F., & Cole, J. J. (1990). Human impact on nitrate export: An analysis using major world rivers, 28(2), 167–170.
- Carey, R. O., Wollheim, W. M., Mulukutla, G. K., & Mineau, M. M. (2014). Characterizing Storm-Event Nitrate Fluxes in a Fifth Order Suburbanizing Watershed Using In Situ Sensors. *Environmental Science & Technology*, 48(14), 7756–7765. <https://doi.org/10.1021/es500252j>
- Covino, T. P., McGlynn, B. L., & McNamara, R. A. (2010). Tracer additions for spiraling curve characterization (TASCC): Quantifying stream nutrient uptake kinetics from ambient to saturation. *Limnology and Oceanography: Methods*, 8(SEPT), 484–498.
<https://doi.org/10.4319/lom.2010.8.484>
- Demars, B. O. L. L., Thompson, J., & Manson, J. R. (2015). Stream metabolism and the open diel oxygen method: Principles, practice, and perspectives. *Limnology and Oceanography: Methods*, 13(7), 356–374. <https://doi.org/10.1002/lom3.10030>

- Dodds, W. K., Evans-White, M. A., Gerlanc, N. M., Gray, L., Gudder, D. A., Kemp, M. J., et al. (2000). Quantification of the Nitrogen Cycle in a Prairie Stream. *Ecosystems*, 3(6), 574–589. <https://doi.org/10.1007/s100210000050>
- Dupas, R., Jomaa, S., Musloff, A., Borchardt, D., & Rode, M. (2016). Disentangling the influence of hydroclimatic patterns and agricultural management on river nitrate dynamics from sub-hourly to decadal time scales. *Science of The Total Environment*, 571, 791–800. <https://doi.org/10.1016/j.scitotenv.2016.07.053>
- Durum, W. H. (1953). Relationship of the mineral constituents in solution to stream flow, Saline River near Russell, Kansas. *Eos, Transactions American Geophysical Union*, 34(3), 435–442. <https://doi.org/10.1029/TR034i003p00435>
- Edwards, A. M. C. (1973). The variation of dissolved constituents with discharge in some Norfolk rivers. *Journal of Hydrology*, 18(3), 219–242. [https://doi.org/10.1016/0022-1694\(73\)90049-8](https://doi.org/10.1016/0022-1694(73)90049-8)
- EEA. (2005). Source apportionment of nitrogen and phosphorus inputs into the aquatic environment — European Environment Agency (Publication). Copenhagen, Denmark. Retrieved from https://www.eea.europa.eu/publications/eea_report_2005_7
- EEA. (2021a). Drivers of and pressures arising from selected key water management challenges — A European overview (Publication). Copenhagen, Denmark. Retrieved from <https://www.eea.europa.eu/publications/drivers-of-and-pressures-arising>
- EEA. (2021b). Water resources across Europe — confronting water stress: an updated assessment (Publication). Copenhagen, Denmark: European Environment Agency. Retrieved from <https://www.eea.europa.eu/publications/water-resources-across-europe-confronting>
- Evans, C., & Davies, T. D. (1998). Causes of concentration/discharge hysteresis and its potential as a tool for analysis of episode hydrochemistry. *Water Resources Research*, 34(1), 129–137. <https://doi.org/10.1029/97wr01881>
- Finch, M. S., Hydes, D. J., Clayson, C. H., Bernhard Weigl, Dakin, J., & Gwilliam, P. (1998). A low power ultra violet spectrophotometer for measurement of nitrate in seawater: introduction, calibration and initial sea trials. *Analytica Chimica Acta*, 377(2), 167–177. [https://doi.org/10.1016/S0003-2670\(98\)00616-3](https://doi.org/10.1016/S0003-2670(98)00616-3)
- Galloway, J. N., Dentener, F. J., Capone, D. G., Boyer, E. W., Howarth, R. W., Seitzinger, S. P., et al. (2004). Nitrogen Cycles: Past, Present, and Future. *Biogeochemistry*, 70(2), 153–226. <https://doi.org/10.1007/s10533-004-0370-0>
- Galloway, James N., & Cowling, E. B. (2002). Reactive Nitrogen and The World: 200 Years of Change. *AMBIO: A Journal of the Human Environment*, 31(2), 64–71. <https://doi.org/10.1579/0044-7447-31.2.64>
- Galloway, James N., Aber, J. D., Erisman, J. W., Seitzinger, S. P., Howarth, R. W., Cowling, E. B., & Cosby, B. J. (2003). The Nitrogen Cascade. *BioScience*, 53(4), 341–356. [https://doi.org/10.1641/0006-3568\(2003\)053\[0341:TNC\]2.0.CO;2](https://doi.org/10.1641/0006-3568(2003)053[0341:TNC]2.0.CO;2)
- Glover, B. J., & Johnson, P. (1974). Variations in the natural chemical concentration of river water during flood flows, and the lag effect. *Journal of Hydrology*, 22(3), 303–316. [https://doi.org/10.1016/0022-1694\(74\)90083-3](https://doi.org/10.1016/0022-1694(74)90083-3)
- Goff, T. L., Braven, J., Ebdon, L., Chilcott, N. P., Scholefield, D., & Wood, J. W. (2002). An accurate and stable nitrate-selective electrode for the in situ determination of nitrate in agricultural drainage waters. *Analyst*, 127(4), 507–511. <https://doi.org/10.1039/B201899N>
- Gomez-Velez, J. D., Harvey, J. W., Cardenas, M. B., & Kiel, B. (2015). Denitrification in the Mississippi River network controlled by flow through river bedforms. *Nature Geoscience*, 8(12), 941–945. <https://doi.org/10.1038/ngeo2567>

- Goodridge, B. M., & Melack, J. M. (2012). Land use control of stream nitrate concentrations in mountainous coastal California watersheds. *Journal of Geophysical Research: Biogeosciences*, 117(2), G02005. <https://doi.org/10.1029/2011JG001833>
- Greiwe, J., Weiler, M., & Lange, J. (2021). Diel patterns in stream nitrate concentration produced by in-stream processes. *Biogeosciences*, 18(16), 4705–4715. <https://doi.org/10.5194/bg-18-4705-2021>
- Grizzetti, B., Bouraoui, F., & De Marsily, G. (2008). Assessing nitrogen pressures on European surface water. *Global Biogeochemical Cycles*, 22(4). <https://doi.org/10.1029/2007GB003085>
- Hall, R. O., & Tank, J. L. (2005). Correcting whole-stream estimates of metabolism for groundwater input. *Limnology and Oceanography: Methods*, 3(4), 222–229. <https://doi.org/10.4319/lom.2005.3.222>
- Hall, R. O., Tank, J. L., Sobota, D. J., Mulholland, P. J., O'Brien, J. M., Dodds, W. K., et al. (2009). Nitrate removal in stream ecosystems measured by ¹⁵N addition experiments: Total uptake. *Limnology and Oceanography*, 54(3), 653–665. <https://doi.org/10.4319/lo.2009.54.3.0653>
- Heffernan, J. B., & Cohen, M. J. (2010). Direct and indirect coupling of primary production and diel nitrate dynamics in a subtropical spring-fed river. *Limnology and Oceanography*, 55(2), 677–688. <https://doi.org/10.4319/LO.2010.55.2.0677>
- Heffernan, J. B., Cohen, M. J., Frazer, T. K., Thomas, R. G., Rayfield, T. J., Gulley, J., et al. (2010). Hydrologic and biotic influences on nitrate removal in a subtropical spring-fed river. *Limnology and Oceanography*, 55(1), 249–263. <https://doi.org/10.4319/lo.2010.55.1.0249>
- Hem, J. D. (1948). Fluctuations in concentration of dissolved solids of some southwestern streams. *Eos, Transactions American Geophysical Union*, 29(1), 80–84. <https://doi.org/10.1029/TR029i001p00080>
- Hendrickson, G. E., & Krieger, R. A. (1964). Geochemistry of natural waters of the Blue Grass region, Kentucky (No. 1700). Water Supply Paper. U. S. Geological Survey. <https://doi.org/10.3133/wsp1700>
- Hensley, R., & Cohen, M. (2016). On the emergence of diel solute signals in flowing waters. *Water Resources Research*, 52(2), 759–772. <https://doi.org/10.1002/2015WR017895>
- Hensley, R T, Spangler, M. J., DeVito, L. F., Decker, P. H., Cohen, M. J., & Gooseff, M. N. (2020). Evaluating spatiotemporal variation in water chemistry of the upper Colorado River using longitudinal profiling. *Hydrological Processes*. <https://doi.org/10.1002/hyp.13690>
- Hensley, Robert T., Cohen, M. J., & Korhnak, L. V. (2014). Inferring nitrogen removal in large rivers from high-resolution longitudinal profiling. *Limnology and Oceanography*, 59(4), 1152–1170. <https://doi.org/10.4319/lo.2014.59.4.1152>
- Hey, D. L., Urban, L. S., & Kostel, J. A. (2005). Nutrient farming: The business of environmental management. *Ecological Engineering*, 24(4), 279–287. <https://doi.org/10.1016/j.ecoleng.2004.11.014>
- Hill, A. R. (1979). Denitrification in the nitrogen budget of a river ecosystem. *Nature*, 281(5729), 291–292. <https://doi.org/10.1038/281291a0>
- Hooper, R. P., Christophersen, N., & Peters, N. E. (1990). Modelling streamwater chemistry as a mixture of soilwater end-members — An application to the Panola Mountain catchment, Georgia, U.S.A. *Journal of Hydrology*, 116(1), 321–343. [https://doi.org/10.1016/0022-1694\(90\)90131-G](https://doi.org/10.1016/0022-1694(90)90131-G)
- Howarth, R., Swaney, D., Billen, G., Garnier, J., Hong, B., Humborg, C., et al. (2012). Nitrogen fluxes from the landscape are controlled by net anthropogenic nitrogen inputs and by climate. *Frontiers in Ecology and the Environment*, 10(1), 37–43. <https://doi.org/10.1890/100178>
- Howarth, R. W. (1988). Nutrient Limitation of Net Primary Production in Marine Ecosystems. *Annual Review of Ecology and Systematics*, 19, 89–110.

- Howarth, R. W., & Marino, R. (2006). Nitrogen as the limiting nutrient for eutrophication in coastal marine ecosystems: Evolving views over three decades. *Limnology and Oceanography*, 51(1part2), 364–376. https://doi.org/10.4319/lo.2006.51.1_part_2.0364
- Huang, J., Borchardt, D., & Rode, M. (2022). How do inorganic nitrogen processing pathways change quantitatively at daily, seasonal and multi-annual scales in a large agricultural stream? *Hydrology and Earth System Sciences Discussions*, 1–23. <https://doi.org/10.5194/hess-2021-615>
- Imssande, J., & Touraine, B. (1994). N Demand and the Regulation of Nitrate Uptake. *Plant Physiology*, 105(1), 3–7.
- Jacobs, S. R., Weeser, B., Guzha, A. C., Rufino, M. C., Butterbach-Bahl, K., Windhorst, D., & Breuer, L. (2018). Using High-Resolution Data to Assess Land Use Impact on Nitrate Dynamics in East African Tropical Montane Catchments. *Water Resources Research*, 54(3), 1812–1830. <https://doi.org/10.1002/2017WR021592>
- Jannasch, H. W., Johnson, K. S., & Sakamoto, C. M. (1994). Submersible, Osmotically Pumped Analyzer for Continuous Determination of Nitrate in situ. *Analytical Chemistry*, 66(20), 3352–3361. <https://doi.org/10.1021/ac00092a011>
- Jarvie, H. P., Neal, C., Smart, R., Owen, R., Fraser, D., Forbes, I., & Wade, A. (2001). Use of continuous water quality records for hydrograph separation and to assess short-term variability and extremes in acidity and dissolved carbon dioxide for the River Dee, Scotland. *The Science of the Total Environment*, 265(1–3), 85–98. [https://doi.org/10.1016/s0048-9697\(00\)00651-3](https://doi.org/10.1016/s0048-9697(00)00651-3)
- Jarvie, Helen P., Love, A. J., Williams, R. J., & Neal, C. (2003). Measuring in-stream productivity: the potential of continuous chlorophyll and dissolved oxygen monitoring for assessing the ecological status of surface waters. *Water Science and Technology*, 48(10), 191–198. <https://doi.org/10.2166/wst.2003.0573>
- Jarvie, Helen P., Sharpley, A. N., Kresse, T., Hays, P. D., Williams, R. J., King, S. M., & Berry, L. G. (2018). Coupling High-Frequency Stream Metabolism and Nutrient Monitoring to Explore Biogeochemical Controls on Downstream Nitrate Delivery. *Environmental Science and Technology*, 52(23), 13708–13717. <https://doi.org/10.1021/acs.est.8b03074>
- Johnson, K. S., & Coletti, L. J. (2002). In situ ultraviolet spectrophotometry for high resolution and long-term monitoring of nitrate, bromide and bisulfide in the ocean. *Deep Sea Research Part I: Oceanographic Research Papers*, 49(7), 1291–1305. [https://doi.org/10.1016/S0967-0637\(02\)00020-1](https://doi.org/10.1016/S0967-0637(02)00020-1)
- Kemp, M. J., & Dodds, W. K. (2002). Comparisons of nitrification and denitrification in prairie and agriculturally influenced streams. *Ecological Applications*, 12(4), 998–1009. [https://doi.org/10.1890/1051-0761\(2002\)012\[0998:CONADI\]2.0.CO;2](https://doi.org/10.1890/1051-0761(2002)012[0998:CONADI]2.0.CO;2)
- Kirchner, J. W., Feng, X., Neal, C., & Robson, A. J. (2004). The fine structure of water-quality dynamics: the (high-frequency) wave of the future. *Hydrological Processes*, 18(7), 1353–1359. <https://doi.org/10.1002/hyp.5537>
- Knowles, R. (1982). Denitrification. *Microbiological Reviews*, 46, 28.
- Kunz, J. V., Annable, M. D., Cho, J., Von Tümpling, W., Hatfield, K., Rao, S., et al. (2017). Quantifying nutrient fluxes with a new hyporheic passive flux meter (HPFM). *Biogeosciences*, 14(3), 631–649. <https://doi.org/10.5194/bg-14-631-2017>
- Kunz, J. V., Hensley, R., Brase, L., Borchardt, D., & Rode, M. (2017). High frequency measurements of reach scale nitrogen uptake in a fourth order river with contrasting hydromorphology and variable water chemistry (Weiße Elster, Germany). *Water Resources Research*, 53(1), 328–343. <https://doi.org/10.1002/2016WR019355>

- Lloyd, C. E. M., Freer, J. E., Johnes, P. J., & Collins, A. L. (2016). Technical Note: Testing an improved index for analysing storm discharge-concentration hysteresis. *Hydrology and Earth System Sciences*, 20(2), 625–632. <https://doi.org/10.5194/hess-20-625-2016>
- Lupon, A., Martí, E., Sabater, F., & Bernal, S. (2016). Green light: gross primary production influences seasonal stream N export by controlling fine-scale N dynamics. *Ecology*, 97(1), 133–144. <https://doi.org/10.1890/14-2296.1>
- McCull, R. H. S. (1974). Self-purification of small freshwater streams: Phosphate, Nitrate, and Ammonia removal. *New Zealand Journal of Marine and Freshwater Research*, 8(2), 375–388. <https://doi.org/10.1080/00288330.1974.9515512>
- Middelburg, J., & Nieuwenhuize, J. (2000). Nitrogen uptake by heterotrophic bacteria and phytoplankton in the nitrate-rich Thames estuary. *Marine Ecology Progress Series*, 203, 13–21. <https://doi.org/10.3354/meps203013>
- Miller, M. P., Tesoriero, A. J., Hood, K., Terziotti, S., & Wolock, D. M. (2017). Estimating Discharge and Nonpoint Source Nitrate Loading to Streams From Three End-Member Pathways Using High-Frequency Water Quality Data. *Water Resources Research*, 53(12), 10201–10216. <https://doi.org/10.1002/2017WR021654>
- Moatar, F., Abbott, B. W., Minaudo, C., Curie, F., & Pinay, G. (2017). Elemental properties, hydrology, and biology interact to shape concentration-discharge curves for carbon, nutrients, sediment, and major ions. *Water Resources Research*, 53(2), 1270–1287. <https://doi.org/10.1002/2016WR019635>
- Mulholland, P. J., Tank, J. L., Webster, J. R., Bowden, W. B., Dodds, W. K., Gregory, S. V., et al. (2002). Can uptake length in streams be determined by nutrient addition experiments? Results from an interbiome comparison study. *Journal of the North American Benthological Society*, 21(4), 544–560. <https://doi.org/10.2307/1468429>
- Mulholland, P. J., Helton, A. M., Poole, G. C., Hall, R. O., Hamilton, S. K., Peterson, B. J., et al. (2008). Stream denitrification across biomes and its response to anthropogenic nitrate loading. *Nature*, 452(7184), 202–205. <https://doi.org/10.1038/nature06686>
- Mulholland, P. J., Hall Jr., R. O., Sobota, D. J., Dodds, W. K., Findlay, S. E. G., Grimm, N. B., et al. (2009). Nitrate removal in stream ecosystems measured by ¹⁵N addition experiments: Denitrification. *Limnology and Oceanography*, 54(3), 666–680. <https://doi.org/10.4319/lo.2009.54.3.0666>
- Mulholland, Patrick J. (1992). Regulation of nutrient concentrations in a temperate forest stream: Roles of upland, riparian, and instream processes. *Limnology and Oceanography*, 37(7), 1512–1526. <https://doi.org/10.4319/lo.1992.37.7.1512>
- Munn, N. L., & Meyer, J. L. (1990). Habitat-Specific Solute Retention in Two Small Streams: An Intersite Comparison. *Ecology*, 71(6), 2069–2082. <https://doi.org/10.2307/1938621>
- Newbold, J. D., O'Neill, R. V., Elwood, J. W., & Van Winkle, W. (1982). Nutrient Spiralling in Streams: Implications for Nutrient Limitation and Invertebrate Activity. *The American Naturalist*, 120(5), 628–652. <https://doi.org/10.1086/284017>
- Newbold, J. Denis, Elwood, J. W., O'Neill, R. V., & Winkle, W. V. (1981). Measuring Nutrient Spiralling in Streams. *Canadian Journal of Fisheries and Aquatic Sciences*, 38(7), 860–863. <https://doi.org/10.1139/f81-114>
- Niehoff, D., Fritsch, U., & Bronstert, A. (2002). Land-use impacts on storm-runoff generation: scenarios of land-use change and simulation of hydrological response in a meso-scale catchment in SW-Germany. *Journal of Hydrology*, 267(1), 80–93. [https://doi.org/10.1016/S0022-1694\(02\)00142-7](https://doi.org/10.1016/S0022-1694(02)00142-7)
- Outram, F. N., Lloyd, C. E. M., Jonczyk, J., Benskin, C. M. H., Grant, F., Perks, M. T., et al. (2014). High-frequency monitoring of nitrogen and phosphorus response in three rural catchments to

- the end of the 2011–2012 drought in England. *Hydrology and Earth System Sciences*, 18(9), 3429–3448. <https://doi.org/10.5194/hess-18-3429-2014>
- Pellerin, B. A., Bergamaschi, B. A., Downing, B. D., Saraceno, J. F., Garrett, J. D., & Olsen, L. D. (2013). Optical techniques for the determination of nitrate in environmental waters: Guidelines for instrument selection, operation, deployment, maintenance, quality assurance, and data reporting (No. 1-D5). *Techniques and Methods*. U.S. Geological Survey. <https://doi.org/10.3133/tm1D5>
- Pellerin, B. A., Stauffer, B. A., Young, D. A., Sullivan, D. J., Bricker, S. B., Walbridge, M. R., et al. (2016). Emerging Tools for Continuous Nutrient Monitoring Networks: Sensors Advancing Science and Water Resources Protection. *JAWRA Journal of the American Water Resources Association*, 52(4), 993–1008. <https://doi.org/10.1111/1752-1688.12386>
- Peterson, B. J., Wollheim, W. M., Mulholland, P. J., Webster, J. R., Meyer, J. L., Tank, J. L., et al. (2001). Control of Nitrogen Export from Watersheds by Headwater Streams. *Science*, 292(5514), 86–90. <https://doi.org/10.1126/science.1056874>
- Rashleigh, B., Paulson, S., Flotemersch, J., & Pelletier, P. (2013). Biological assessment of streams and rivers in U.S. - design, methods, and analysis. *Journal of Ecology and Environment*, 36(1), 85–88. <https://doi.org/10.5141/ecoenv.2013.010>
- Reddy, K. R., & DeLaune, R. D. (2008). Chapter 8: Nitrogen. In *Biogeochemistry of Wetlands: Science and Applications* (pp. 257–323). Boca Raton: CRC Press. <https://doi.org/10.1201/9780203491454>
- Reddy, K. R., Patrick Jr., W. H., & Lindau, C. W. (1989). Nitrification-denitrification at the plant root-sediment interface in wetlands. *Limnology and Oceanography*, 34(6), 1004–1013. <https://doi.org/10.4319/lo.1989.34.6.1004>
- Robson, A., Neal, C., Smith, C. J., & Hill, S. (1992). Short-term variations in rain and stream water conductivity at a forested site in mid-Wales — implications for water movement. *Science of The Total Environment*, 119, 1–18. [https://doi.org/10.1016/0048-9697\(92\)90251-M](https://doi.org/10.1016/0048-9697(92)90251-M)
- Robson, A. J., Neal, C., Hill, S., & Smith, C. J. (1993). Linking variations in short- and medium-term stream chemistry to rainfall inputs — some observations at Plynlimon, Mid-Wales. *Journal of Hydrology*, 144(1), 291–310. [https://doi.org/10.1016/0022-1694\(93\)90177-B](https://doi.org/10.1016/0022-1694(93)90177-B)
- Rode, M., Halbedel Née Angelstein, S., Anis, M. R., Borchardt, D., & Weitere, M. (2016). Continuous In-Stream Assimilatory Nitrate Uptake from High-Frequency Sensor Measurements. *Environmental Science and Technology*, 50(11), 5685–5694. <https://doi.org/10.1021/acs.est.6b00943>
- Rode, M., Wade, A. J., Cohen, M. J., Hensley, R. T., Bowes, M. J., Kirchner, J. W., et al. (2016). Sensors in the Stream: The High-Frequency Wave of the Present. *Environmental Science and Technology*, 50(19), 10297–10307. <https://doi.org/10.1021/acs.est.6b02155>
- Scholefield, D., Le Goff, T., Braven, J., Ebdon, L., Long, T., & Butler, M. (2005). Concerted diurnal patterns in riverine nutrient concentrations and physical conditions. *Science of The Total Environment*, 344(1), 201–210. <https://doi.org/10.1016/j.scitotenv.2005.02.014>
- Seitzinger, S., Harrison, J. A., Böhlke, J. K., Bouwman, A. F., Lowrance, R., Peterson, B., et al. (2006). Denitrification Across Landscapes and Waterscapes: A Synthesis. *Ecological Applications*, 16(6), 2064–2090. [https://doi.org/10.1890/1051-0761\(2006\)016\[2064:DALAWA\]2.0.CO;2](https://doi.org/10.1890/1051-0761(2006)016[2064:DALAWA]2.0.CO;2)
- Seitzinger, S. P., Styles, R. V., Boyer, E. W., Alexander, R. B., Billen, G., Howarth, R. W., et al. (2002). Nitrogen retention in rivers: model development and application to watersheds in the northeastern U.S.A. *Biogeochemistry*, 57(1), 199–237. <https://doi.org/10.1023/A:1015745629794>

- Sharma, B., & Ahlert, R. C. (1977). Nitrification and nitrogen removal. *Water Research*, 11(10), 897–925. [https://doi.org/10.1016/0043-1354\(77\)90078-1](https://doi.org/10.1016/0043-1354(77)90078-1)
- Strauss, E. A., Mitchell, N. L., & Lamberti, G. A. (2002). Factors regulating nitrification in aquatic sediments: effects of organic carbon, nitrogen availability, and pH. *Canadian Journal of Fisheries and Aquatic Sciences*, 59(3), 554–563. <https://doi.org/10.1139/f02-032>
- Stream Solute Workshop. (1990). Concepts and Methods for Assessing Solute Dynamics in Stream Ecosystems. *Journal of the North American Benthological Society*, 9(2), 95–119. <https://doi.org/10.2307/1467445>
- Swistock, B. R., DeWalle, D. R., & Sharpe, W. E. (1989). Sources of acidic storm flow in an Appalachian Headwater Stream. *Water Resources Research*, 25(10), 2139–2147. <https://doi.org/10.1029/WR025i010p02139>
- Tank, J. L., Martí, E., Riis, T., von Schiller, D., Reisinger, A. J., Dodds, W. K., et al. (2018). Partitioning assimilatory nitrogen uptake in streams: an analysis of stable isotope tracer additions across continents. *Ecological Monographs*, 88(1), 120–138. <https://doi.org/10.1002/ecm.1280>
- Tank, Jennifer L., Meyer, J. L., Sanzone, D. M., Mulholland, P. J., Webster, J. R., Peterson, B. J., et al. (2000). Analysis of nitrogen cycling in a forest stream during autumn using a ^{15}N -tracer addition. *Limnology and Oceanography*, 45(5), 1013–1029. <https://doi.org/10.4319/lo.2000.45.5.1013>
- Tank, Jennifer L., Rosi-Marshall, E. J., Baker, M. A., & Hall, R. O. (2008). Are rivers just big streams? A pulse method to quantify nitrogen demand in a large river. *Ecology*, 89(10), 2935–2945. <https://doi.org/10.1890/07-1315.1>
- Toler, L. (1965). Relation between chemical quality and water discharge in Spring Creek, southwestern Georgia. *US Geological Survey Professional Paper*, 525, C209-13.
- Tsopanoglou, A., & Jiménez del Val, I. (2021). Moving towards an era of hybrid modelling: advantages and challenges of coupling mechanistic and data-driven models for upstream pharmaceutical bioprocesses. *Current Opinion in Chemical Engineering*, 32, 100691. <https://doi.org/10.1016/j.coche.2021.100691>
- Vaughan, M. C. H., Bowden, W. B., Shanley, J. B., Vermilyea, A., Sleeper, R., Gold, A. J., et al. (2017). High-frequency dissolved organic carbon and nitrate measurements reveal differences in storm hysteresis and loading in relation to land cover and seasonality. *Water Resources Research*, 53(7), 5345–5363. <https://doi.org/10.1002/2017WR020491>
- Wade, A. J., Palmer-Felgate, E. J., Halliday, S. J., Skeffington, R. A., Loewenthal, M., Jarvie, H. P., et al. (2012). Hydrochemical processes in lowland rivers: insights from in situ, high-resolution monitoring. *Hydrology and Earth System Sciences*, 16(11), 4323–4342. <https://doi.org/10.5194/hess-16-4323-2012>
- Walling, D. E., & Foster, I. D. L. (1975). Variations in the natural chemical concentration of river water during flood flows, and the lag effect: Some further comments. *Journal of Hydrology*, 26(3), 237–244. [https://doi.org/10.1016/0022-1694\(75\)90005-0](https://doi.org/10.1016/0022-1694(75)90005-0)
- Walling, D. E., & Teed, A. (1971). A simple pumping sampler for research into suspended sediment transport in small catchments. *Journal of Hydrology*, 13, 325–337. [https://doi.org/10.1016/0022-1694\(71\)90251-4](https://doi.org/10.1016/0022-1694(71)90251-4)
- Warwick, J. J. (1986). Diel variation of in-stream nitrification. *Water Research*, 20(10), 1325–1332. [https://doi.org/10.1016/0043-1354\(86\)90165-X](https://doi.org/10.1016/0043-1354(86)90165-X)
- Webster, J. R. (2000). An Example to Follow: Intersite Research among Stream Ecologists at LTER sites. *LTER Network News*, 13(1). Retrieved from <http://news.lternet.edu/Article942.html>

- Wollheim, W. M., Vörösmarty, C. J., Peterson, B. J., Seitzinger, S. P., & Hopkinson, C. S. (2006). Relationship between river size and nutrient removal. *Geophysical Research Letters*, 33(6). <https://doi.org/10.1029/2006GL025845>
- Wollschläger, U., Attinger, S., Borhardt, D., Brauns, M., Cuntz, M., Dietrich, P., et al. (2017). The Bode hydrological observatory: a platform for integrated, interdisciplinary hydro-ecological research within the TERENO Harz/Central German Lowland Observatory. *Environmental Earth Sciences*, 76(1), 29. <https://doi.org/10.1007/s12665-016-6327-5>
- Yang, X., Jomaa, S., Büttner, O., & Rode, M. (2019). Autotrophic nitrate uptake in river networks: A modeling approach using continuous high-frequency data. *Water Research*, 157, 258–268. <https://doi.org/10.1016/j.watres.2019.02.059>
- Yaroshenko, I., Kirsanov, D., Marjanovic, M., Lieberzeit, P. A., Korostynska, O., Mason, A., et al. (2020). Real-Time Water Quality Monitoring with Chemical Sensors. *Sensors*, 20(12), 3432. <https://doi.org/10.3390/s20123432>
- Ye, S., Covino, T., Sivapalan, M., Basu, N., Li, H., & Wang, S. (2012). Dissolved nutrient retention dynamics in river networks: A modeling investigation of transient flows and scale effects. *Water Resources Research*, 48. <https://doi.org/10.1029/2011WR010508>
- Yu, C., Huang, X., Chen, H., Godfray, H. C. J., Wright, J. S., Hall, J. W., et al. (2019). Managing nitrogen to restore water quality in China. *Nature*, 567(7749), 516–520. <https://doi.org/10.1038/s41586-019-1001-1>
- Zhang, X., Yang, X., Jomaa, S., & Rode, M. (2020). Analyzing impacts of seasonality and landscape gradient on event-scale nitrate-discharge dynamics based on nested high-frequency monitoring. *Journal of Hydrology*, 591, 125585. <https://doi.org/10.1016/j.jhydrol.2020.125585>
- Zhang, X., Yang, X., Hensley, R., Lorke, A., Rode, M., 2022. Disentangling in-stream nitrate uptake pathways based on two-station high-frequency monitoring in high-order streams. *Water Resour. Res. Rev.*
- Zimmer, M. A., Pellerin, B., Burns, D. A., & Petrochenkov, G. (2019). Temporal Variability in Nitrate-Discharge Relationships in Large Rivers as Revealed by High-Frequency Data. *Water Resources Research*, 55(2), 973–989. <https://doi.org/10.1029/2018WR023478>